EFFECT OF SOLAR RADIATION IN OFFICE SPACES

A Thesis

by

Ali Can Yelekci

Submitted to the

Graduate School of Sciences and Engineering

In Partial Fulfillment of the Requirements for

The Degree of

Master of Science

in the

Department of Mechanical Engineering

Özyeğin University

June 2021

EFFECT OF SOLAR RADIATION IN OFFICE SPACES

Approved by:

Prof. M. Pınar Mengüç

Advisor

Department of Mechanical Engineering

Özyeğin University

Dr. Altuğ Başol

Co-Advisor

Department of Mechanical Engineering

Özyeğin University

Dr. Özgür Ertunç

Department of Mechanical Engineering

Özyeğin University

Prof. Dr. Tuba Okutucu Özyurt

Energy Institute

Istanbul Technical University

Dr. Hande Öztürk

Department of Mechanical Engineering

Özyeğin University

Date Approved: 10 June 2021

DEDICATION

To My Family

ACKNOWLEDGEMENTS

Firstly, I would like to express my gratitude to my family for their full support.

I would like to sincerely thank my supervisors Prof. M. Pınar Mengüç and Dr. Altuğ Başol for their support and guidance throughout the years in both my B.Sc. and M.Sc. studies. Also, I would like to thank Dr. Cem Keskin for his help during my study.

ABSTRACT

This thesis examines the design components of an office that influences the thermal comfort of the occupants due to solar radiation, such as external solar shades, various window glasses, partitions between desks and floor materials.

The steps of solar shade design and design parameters specific to the building, along with the types of solar shades are explored. Solar shades can be integrated with photovoltaic (PV) panels to be mounted on the façade and windows to block the unnecessary solar radiation for energy efficiency and electricity generation purposes. Optical properties of window glasses are studied for a multi-band thermal radiation model and thermal radiative properties of low-iron, clear and grey soda lime silica glasses are supplied. PV panel system is examined along with various types of PV panels and losses in efficiency of PV panels due to misalignment, temperature and blockage by dust, clouds or solar shade are discussed. A detailed numerical study is conducted to couple natural convection in an office space with thermal radiation due to solar radiation. The study specifically investigates the combined effects of partitions located between desks of the office space, solar shades, window types and floor materials to develop a framework to determine the effect of windows on thermal and visual comfort of occupants. These steps of this framework can be applied to all other buildings with new analyses. Two different geometries are used due to different partition cases (according to the aspect ratio of the partition to the ceiling height, which are taken as 0.3 and 0.5) were studied. Single inlet and outlet is modeled for ventilation purposes. All walls other than the façade of the enclosure are assumed adiabatic, and the enclosure has a single window, which acts as a thermal radiative heat source. All surfaces are assumed to be gray-diffuse surfaces for calculation of thermal radiation. The solar radiation is analyzed as two band model (visible and IR spectra) with both diffuse and direct sunlight for a summer day and a winter day. Finally, an extreme winter day with only diffuse sunlight, colder temperature and higher wind speed is studied.

Based on the choice of window glass type, solar shade coverage on the window, partition geometry, floor materials, and the weather conditions, variations on the surface temperature distribution, air temperature, air velocity and thermal comfort of two manikins inside the office are analyzed based on Predicted Mean Vote (PMV) and Percentage of Dissatisfied (PPD) methods by Fanger.

Based on this study, a series of suggestions are made for the future designs of integrated solar shade systems.

ÖZETÇE

Bu tez, bir ofisin dış güneş kırıcıları, çeşitli pencere camları, masalar arası bölmeler ve zemin malzemeleri gibi güneş ışınımından dolayı bina sakinlerinin ısıl konforunu etkileyen tasarım bileşenlerini incelemektedir.

Bir binaya özgü tasarlanan güneş kırıcı tasarımı ve tasarım parametreleri aşamaları ile güneş kırıcı türleri incelenmiştir. Tasarlanan güneş kırıcıları, enerji verimliliği ve elektrik üretimi amacıyla gereksiz güneş ışınımını engellemek için cepheye ve pencerelere fotovoltaik (PV) panellerle entegre edilerek monte edilmiştir. Pencere camlarının optik özellikleri, çok bantlı bir termal radyasyon modeli için çalışılmış ve düşük demirli, şeffaf ve gri soda kireç silika camların termal ışıma özellikleri sağlanmıştır. PV panel sistemi, çeşitli PV panel türleri ile incelenmekte ve hatalı hizalama, sıcaklık ve toz, bulut veya güneş kırıcı nedeniyle gölgelenmeden kaynaklı PV panellerinin verimliliğindeki kayıplar tartışılmaktadır. Bir ofis alanındaki doğal konveksiyonu güneş radyasyonundan kaynaklanan termal radyasyonla birleştirmek için sayısal bir çalışma yapılmıştır. Çalışma, özellikle ofis alanının masaları arasına yerleştirilen bölmelerin, güneş kırıcıların, farklı pencere camlarının ve yer kaplamalarının bina sakinlerinin termal ve görsel konforu üzerindeki etkisini belirlemek için bir sistem geliştirmek için etkisini araştırmıştır. Bu sistemin adımları farklı binalar için yeni analizlerle tekrarlanabilir. İki farklı bölme yüksekliği (bölmenin boyunun tavan yüksekliğine oranına göre 0.3 ve 0.5 değerleri düşünülerek) incelenmiştir. Ofise tek giriş ve çıkış havalandırma amaçlı olarak modellenmiştir. Cephe dışındaki tüm duvarların ısı transferi olmadığı varsayılmış olup cephenin ısıl ışıma kaynağı olarak işlev gören tek bir penceresi vardır. Termal radyasyonun hesaplanması için tüm yüzeylerin gri yayınık yüzeyler olduğu varsayılmıştır. Güneş radyasyonu, bir yaz günü ve bir kış günü için hem yayınık hem de doğrudan güneş ışığına sahip iki bantlı model (görünür ve kızılötesi) olarak analiz edilir. Son olarak, sadece yayılmış güneş ışığı, daha soğuk hava sıcaklığı ve daha yüksek rüzgâr hızının olduğu sert bir kış günü incelenir.

Pencere camı seçimi, pencere üzerindeki güneş kırıcı oranı, masalar arası bölme geometrisi, zemin malzemeleri ve hava koşullarına göre, yüzey sıcaklık dağılımındaki değişimler, hava sıcaklığı, hava hızı ve ofis içindeki iki mankenin ısıl konforu analiz edilir. Isıl konfor analizi Fanger tarafından geliştirilen PMV ve PPD yöntemlerine dayanmaktadır.

Bu çalışmanın neticesinde, ilerde kullanılabilecek yenilikçi tasarım sistemleri önerilmiştir.

LIST OF TABLES

LIST OF FIGURES

TABLE OF CONTENTS

CHAPTER I

INTRODUCTION

1.1. Overview of the Problem

Buildings are responsible from a significant part of global overall energy consumption and account 40% of the CO_2 emissions according to International Energy Agency [1]. In order to reduce their negative impact on environment, it is imperative to develop new design strategies to have more energy efficient and comfortable buildings. Such design considerations should include both thermal and visual comfort and should take advantage of the natural conditions around buildings. In that sense, it is necessary to use readily available natural light instead of artificial lighting, to consider appropriate window glasses for the climate and orientation of the building, to utilize solar energy by using photovoltaic panels, to block the excessive solar irradiance by solar shades to minimize air conditioning use, among other measures to make the buildings more energy efficient.

The purpose of this thesis is to develop a framework to take advantage of the solar radiation in buildings to make them more energy efficient and comfortable. All presented analyses need to be repeated for different room configurations, with new geometries and boundary conditions including solar shade design, photovoltaic panel calculations and window glass selections, as all buildings require case specific design considerations.

Solar radiation has significant impact on apartment buildings especially if they are exposed to southern sky. They need to take advantage of this powerful heat and light source; otherwise, neither the efficient use of energy or the thermal and visual comfort of the occupants can be satisfied. An innovative design should take advantage of the Sun by blocking solar radiation during the summer with solar shades while generating electricity using PV panels, cooling the building using passive cooling such as Trombe walls as studied by Bairi et al. [2], letting solar irradiance inside during winter to heat up the building, using the natural light to light up the interiors providing visual comfort instead of relying on artificial lighting.

Figure 1.1: Image of the office room located at Academic Building 4 (AB-4) of Ozyegin University.

Figure 1.1 shows a rendered image of test office geometry to be used for numerical study of this thesis study. It is an office space located at Academic Building 4 (AB-4) of Ozyegin University in Istanbul, Turkey. There are two occupants on opposing sides of the desk, which is divided by a partition. There is a single window with external solar shade that controls the sunlight getting into the office. Various window glass types, solar shade coverages of the window, weather conditions, floor materials and partition heights will be analyzed to see their effects on office and thermal comfort of the occupants.

As seen on Figure 1.2 the global horizontal irradiation map by SOLARGIS [4] that Turkey has huge potential on solar energy compared to World. On Figure 1.3 more detailed map of Turkey's horizontal irradiation map by SOLARGIS [5] is depicted. According to Ministry of Energy of Turkey in 2018 Turkey generated only 2.6% of its electricity from solar systems [3]. Of course, it is desirable to have a higher contribution of this huge and free energy source instead of relying on scarce and environmentally-destructive fossil fuels.

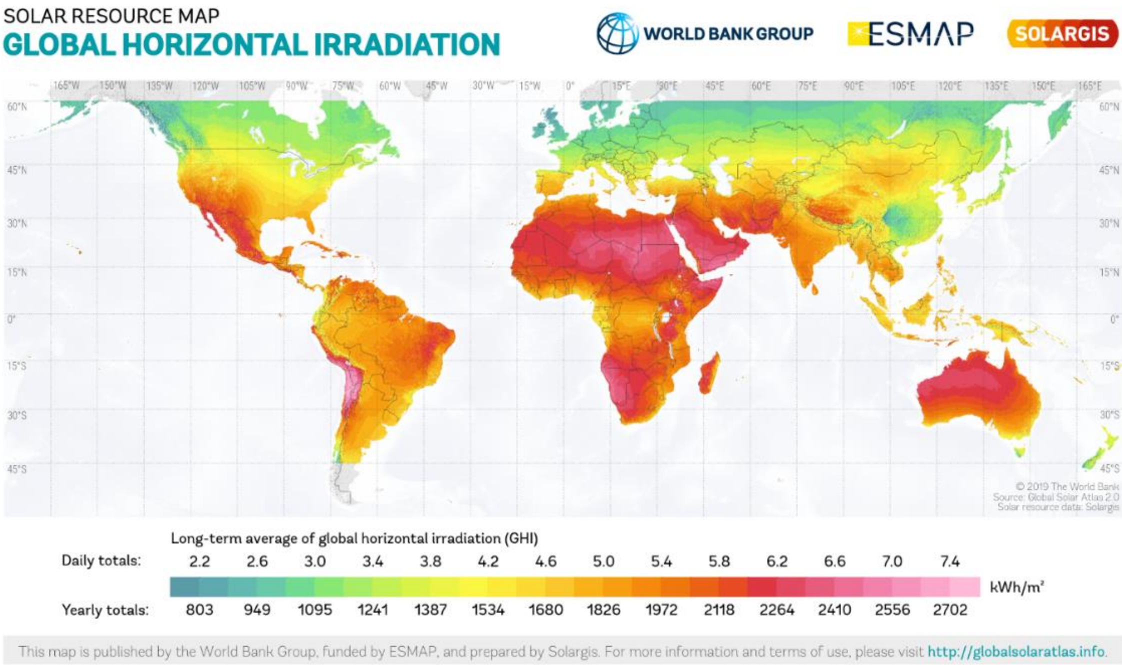

Figure 1.2: Global horizontal irradiation map by SOLARGIS [4].

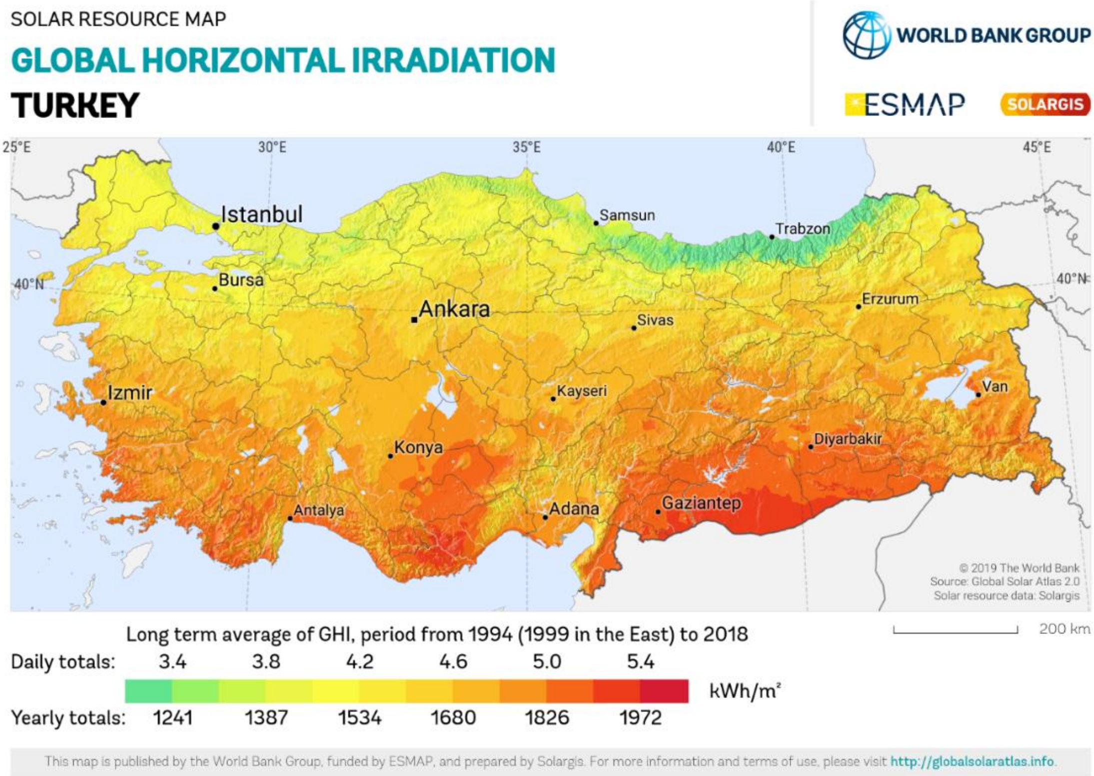

Figure 1.3: Turkey horizontal irradiation map by SOLARGIS [5].

1.2. Importance of Solar Radiation on Energy Efficiency

One of the key factors in energy efficiency on buildings is solar radiation. It can easily decrease the energy efficiency of a building if you fight it for example by building a glass southern façade without any external solar shade and trying to cool down the interior space by air conditioning or it can easily increase energy efficiency of a building for example by passive heating systems. The effects of solar radiation should be considered during the early design stages of a building and the design should be made accordingly to maximize the energy efficiency.

1.3. Importance of Solar Radiation on Thermal and Visual Comfort

Thermal comfort is dependent on temperature, air moisture content, thermal radiation, air relative velocity, personal activity, and clothing level parameters according to ASHRAE Standard 55-2017 [6]. Effects of thermal radiation on thermal comfort will be studied in this thesis by studying the main thermal radiation source, Sun. Thermal radiation is often neglected in engineering problems due to its complexity and it may not be fully understood by some of the engineers. The effects of solar radiation on both thermal and visual comfort cannot be overlooked. Solar radiation is one of the most prominent energy sources on Earth; yet we do not take its full advantage for the energy we use in buildings or industry. According to Howell et al. [7], average solar radiation incident on Earth is 1366 W/m^2, this amount of heat flux cannot be overlooked. These solar rays provide heat and light to all living things as well as the buildings around the Earth. During winter times this heat is very much needed and provides more efficient buildings, but during summer times this heat usually decreases the efficiency of the building and we waste energy to undo the effects. This solar radiation can either be blocked by solar shades before radiating through the windows and heating up the walls from outside or it can be controlled after it enters the building through windows by altering the materials and design of the indoors to provide the maximum thermal and visual comfort possible. Once the solar radiation goes through the window it starts to heat up indoors and due to greenhouse effect not all the thermal radiation can escape the enclosure through the window as it radiated inside. Therefore, during the summertime exterior solar shades is best option to block the excessive solar radiation. In terms of indoors design and placement of furniture have significant effect on temperature distributions as studied by Dominguez Espinosa and Glicksman [8]. Furnitures in an office environment also absorb and reflect the incident radiation and affect the level of thermal and visual comfort of the occupants. In a mathematical model, they can be considered as horizontal and vertical surfaces that divide the indoor environment, which make the problem a complicated one. Horizontal surfaces can be analyzed as desks and vertical surfaces can be analyzed as partitions. Partitions are known to cause temperature contrast throughout the space, and they can either be used to create hot or cold spots as well as choosing materials with various surface emissivity can help to create more thermally comfortable space according to the parameters.

In terms of solar radiation (both as heat and light), thermal comfort and visual comfort come hand in hand, one cannot be discussed without the other. We can see the visible spectrum of the solar radiation, which is between the wavelengths of 380-740 nm, as we call it natural light in buildings. More natural light that we will have at indoors results in more solar (infrared) radiation as well, which might cause thermal comfort or discomfort depending on the architectural details of a building. We need to have larger glazing surfaces to let more light in which will cause thermal discomfort at sunny summer days due to unwanted solar irradiance entering through the windows and in overcast winter days those glazing surfaces cause the indoors to lose heat to the outside environment and create radiation asymmetry. On the contrary, during the overcast summer days larger glazing surface will provide visual comfort and during the sunny winter days it provide heat, but usually (depending on the location) sunny days during the summer are much more than overcast days and overcast days during the winter are much more than sunny days. Therefore, it is important to balance the scale properly on natural light at indoors and instead of just designing bigger windows we can choose smartly placed windows to the needs of the occupants and usage of solar tubes to replace artificial lightings. For visual comfort diffuse light is desired on the surfaces at our eye comfort since direct sunlight is usually too harsh for our eyes. For the surfaces around the occupant, their reflectivity should be chosen accordingly to provide diffuse light on the occupant. For example, wood surface ($\varepsilon_{wood} \approx 0.9$) will provide more diffuse light than an aluminum sheet ($\varepsilon_{aluminum} \approx 0.1$), when light is reflected off.

1.4. Parameters on Solar Radiation Effects

This thesis will focus on both interior and exterior parameters to show how fully take advantage of the Sun in a building. The following parameters will be studied (see Figure 1.4).

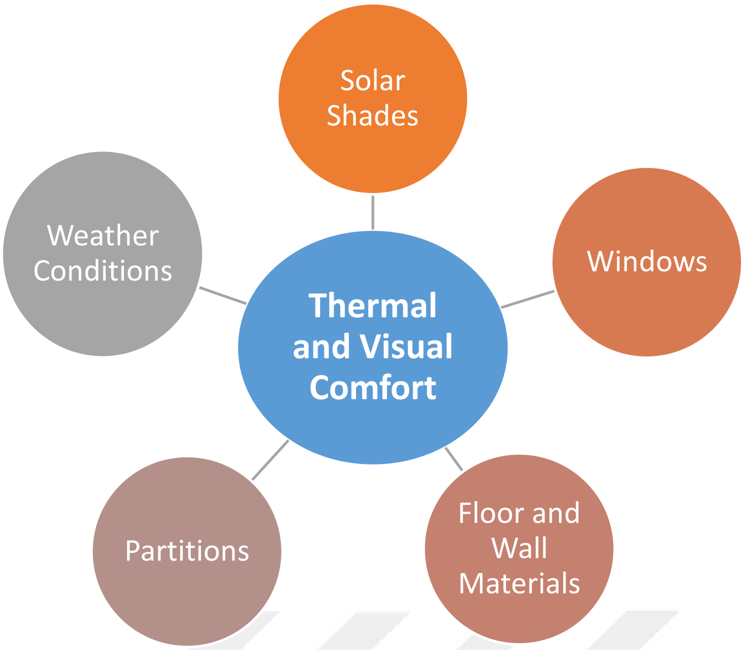

Figure 1.4: Parameters that effect thermal and visual comfort in buildings that are studied in this thesis.

- *Solar shades:* Different types of solar shades, design parameters of a solar shade and various window covering ratios will be discussed, since the solar shade is required to be design for each building.
- *Windows:* Different types of window glasses will be discussed as well as the physics behind the window glass selection.
- *Floor and wall materials:* Floor is usually the first thing that solar radiation hits once it radiates through the window and floor coverings have effect on how the radiation will be reflected and emitted inside the room.
- *Partitions:* Partitions are usually used to give privacy to occupants of an office, but they can cause both thermal and visual discomfort due to blocking the solar radiation.
- *Weather conditions:* For different weather conditions one might want to let the available solar radiation in or keep it out, therefore it is one of the most important aspects that needs to be studied.

1.5. *Literature Review*

Below, an outline of the studies conducted related to the problems that are discussed in this thesis. This literature review is divided into main subjects of heat transfer aspects, ventilation aspects, partitions in enclosure, solar shades, window types, photovoltaic panels, thermal comfort considerations, visual comfort considerations, validation studies, and studies based on modelling the manikin.

Heat transfer aspects

Cavazutti and Corticelli [9] developed an algorithm for solving steady state conduction heat transfer through complex planar walls, where the conduction is temperature dependent. The algorithm utilizes the walls as thermal networks that are connected either in series or parallel. Sartori [10] compared convective heat transfer coefficient correlations for forced air over flat plate from the literature. The study concludes that convective heat transfer coefficient should be calculated with different correlations for laminar, turbulent and mixed flows. Vincent [11] modelled thermal comfort in an open workspace using CFD tools. Where he modelled the convection coefficient due to winds on the outside of the façade by a correlation between wind speed and convective heat transfer coefficient. Moreno and Hernandez [12] analytically studied the overheating due to solar radiation at indoor environment with glazing. These analytical calculations were validated by a numerical model. The outcomes of their study can be listed as: (i) the diffuse reflections inside the room increases the absorbed energy by the surfaces and therefore increasing the indoor temperature, (ii) the solar radiation transmitted through the glazing is reflected diffusely and some of the diffuse radiation is absorbed by the walls and some by the glazing after few reflections inside the room that results in increase of the indoor temperature, and (iii) changing the color of the walls from black (total absorptivity α=1) to white (α=0) does not affect the indoor temperature because for the white wall case window absorbed the thermal radiation that has not been absorbed by the walls.

Ventilation aspects

Rees and Haves [13] conducted an experimental study and a CFD analysis of a test room with displacement ventilation and chilled ceiling. They concluded that chilled ceiling had no significant effect on the thermal characteristics of lower part of the room. Even though the ceiling was getting colder air temperature near the floor remained hotter due to heat loads and that evened out the loss of heat with radiative heat transfer between the floor and ceiling. They have found out that due to increased number of heat loads and furniture floor and ceiling are less coupled in terms of radiative heat transfer.

Vitale et al. [14] modeled the ventilation of a historical building in Rome to optimize the thermal comfort of the visitors by Fanger's thermal comfort parameters. There were three options for the ventilation which are just HVAC for 24 hours, HVAC during the day and natural ventilation during the night, and just natural ventilation for 24 hours. The results from CFD showed that cooling down the building with natural ventilation during the nighttime and utilizing the HVAC during the day when the visitors are present was the best solution to the problem.

Karimipanah et al. [15] studied the air quality in a test classroom due to impact of air quality on learning. The study was done both experimentally and by CFD analysis to compare confluent jet systems and displacement system. They concluded that the confluent jet system performed better for most cases than the displacement system both on experimental and CFD results. In addition, the standard k-ε turbulence model was not accurate on strong buoyant flows and k-ε RNG model gave better results for the buoyant flows, but it still was not accurate due to high number of heat sources when compared to experimental results.

Effects of partitions in enclosure

Partitions are vertical dividers which are mostly used in office spaces to create personal spaces for the occupants where they cannot be disturbed by other occupants (see Figure 1). There is a large body of literature on the effect of radiation to indoor thermal environment, although only a few have explored the impact of partitions. Martyushev et al. [16] numerically studied a cubical enclosure with heat source as a floor, by coupling natural convection and thermal radiation. They concluded that average convective heat transfer (based on dimensionless Nusselt number) is a decreasing, and average radiative Nusselt number is an increasing function of emissivity. Both are increasing function of Rayleigh number (another dimensionless number about the medium convective heat transfer modalities and properties). An analytical and numerical model of configuration factors and illumination parameters for a L-shaped room with opaque walls and clear windows was developed [17]. Cubical enclosure was numerically studied by Parmananda et al. [18] with partitions on opposing walls while the other opposing walls were at temperature difference. They obtained that the partitions had little effect on convective Nusselt number but had considerable effect on radiative Nusselt number. Moreover, partitions are observed to cause local temperature differences near them. Baïri et al. [2] studied Trombe wall with an experimental setup. The passive space was divided into five spaces with glass walls to be compared to no partitions. The results showed that the Trombe wall performance was improved with partitions, by improvement at natural convection and by improvement at low velocities (i.e., for low Rayleigh numbers (defined by Equation 13 below)), ratio of buoyancy and viscosity forces multiplied by the ratio of momentum and thermal diffusivities, values corresponding to low solar heat flux.

Dominguez Espinosa and Glicksman [8] studied effects of desks and partitions on surface temperatures due to ventilation and solar heat gains from the ceiling. They modeled an office space with desks, partitions and occupants. The surface areas of the desks and partitions varied between each case. The model room consisted of ventilation, and lights acting as radiative heat source. Archimedes number (see Equation 15 below), ratio of gravitational forces to viscous forces, was utilized to analyze some of the results. In their study, Prandtl number (see Equation 12 below), ratio of momentum diffusivity to thermal diffusivity, and Reynolds numbers (see Equation 10 below), ratio of inertial forces to viscous forces, were not utilized due to minimal change in them in typical room conditions. They concluded that most of the heat transfer from the ceiling is by radiation heat transfer since air cannot rise any higher, which restrains the convective heat transfer. Adding partitions caused the air temperature to change near floor and ceiling. Addition of horizontal surfaces, such as desks, to the enclosure blocked the heat transfer in between the ceiling and the floor, but because the view factors in between the ceiling and the desks are larger compared to the floor, desks heated up more. This caused higher temperature near the desks due to convective heat transfer, addition of desks and partitions moderately changed the air temperature near the occupants. The average surface temperatures inside the enclosure depend on the Archimedes number, not on the orientation or position of added surfaces. The surface temperatures decreased with the increasing Archimedes number, because increasing Archimedes number means increasing air velocity and lower air temperature at the stagnation point.

Nansteel and Greif [19] did experiments on a test room with a vertical partial division. The test room consisted of heated and chilled opposing walls. The working fluid is water and Rayleigh number (see Equation 13 below) is 10^{11}, which means the flow is turbulent. At this setup, the domain had an inactive core region, a weak recirculation due to the opposing walls at different temperatures and a peripheral boundary layer flow. The partition is found to be blocking the transitional flow and heat transfer in the enclosure, especially when the partition is non-conducting. Olson et al. [20] did an experimental study on an enclosure with hot and cold walls containing a vertical partition covering half of the area from floor to ceiling. They have concluded that the partition slightly decreased the heat transfer between hot and cold walls, but it altered the core temperature of the enclosure and flow pattern considerably.

Effects of solar shades

Bellia et al. [21] did an overview study on studies done on solar shades and pointed out the missing aspects on literature of this subject and nonuniformity of the studies. There is a need in literature for a study considering thermal, lighting, energy and comfort in buildings due to solar shades. There are some studies on these topics combined but Bellia et al. [21] states that they are not analyzed thoroughly and result in either incomplete or misleading outcomes. According to Bellia et al. [21] thermal and visual comfort should be taken into consideration in the early stages of building designs. David et al. [22] mentioned that when using solar shades, the building may become more energy efficient due to lack of need of cooling but at the same time the efficiency may drop down due to increased cost of lighting. They compared four solar shade designs in terms of both thermal and visual efficacy. The study concluded that best solar shade design for blocking solar irradiance is overhang.

Khamporn and Chaiyapinunt [23] did an experimental study on the curved venetian blinds installed on the interior part of a window and evaluated the solar radiation, temperature, mean radiant temperature, transmitted solar radiation and PPD. They concluded that when slats allowed solar radiation to pass through solar radiation is the main source of thermal discomfort and when they block the solar radiation with the venetian slats the surface temperature becomes the main source of thermal discomfort. Kim et al. [24] studied thermal performance of exterior shading device for residential buildings and concluded that “the external shading is clearly much more efficient than internal shading, since internal devices absorb heat and reradiates them to the interior” [24]. They also concluded that interior shading could decrease the cooling energy by 10% at best and exterior shading device they designed can decrease by 11% at its worst. Their design is a horizontal slat type solar shade system where the whole system is adjusted to an angle from the window and each individual slat is adjustable. Sun et al. [25] studied performance of BIPV materials on Hong Kong buildings. They concluded that BIPV that provides shading has increased the energy savings compared to PV modules. They also provided simulation data for future BIPV designs.

Effects of window types

Double and triple glazed windows were analyzed by Vincent [11] for the thermal comfort of occupants at an office space being constructed in Canada with curtain walls. They were analyzed for a winter and a summer day cases. The office space was modelled with 14 part human models for the thermal comfort. They concluded to use low-e triple glazed windows over double glazed windows for a thermally comfortable office space during the winter. The static solar shades provided too cold environment, so manually adjustable solar shades were chosen for the design. Arıcı and Karabay [26] focused their research on double glazed windows and they studied the optimum air layer thicknesses for four cities in Turkey (Ardahan, Ankara, Kocaeli, İskenderun) with various climates and five different fuel types (LPG, electricity, fuel oil, coal, natural gas) for heating systems. They concluded that fuel type had no significant effect on optimum air layer thickness for colder climates. For base temperature of 18°C optimum air layer thickness varies from 12.2-14.6 mm and for base temperature of 22°C optimum air layer thickness varies from 13.5-14.7 mm. Maximum energy saving can be achieved by using LPG. Finally, 60% of energy can be saved with window air layer thickness optimization [26].

Moreno et al. [27] studied various combinations of ethylene tetrafluoroethylene (ETFE) foils and organic photovoltaics (OPV) for window to wall ratios (WWR) of 0.25-0.95 at Barcelona and Paris, which have different climates. ETFE is considered as "light, flexible, transparent, self-cleaning, mechanically adequate, stable, thermally insulating, and environmentally friendly" [27] and OPV is "light, semitransparent, free-form, flexible, cost-effective, performant under low-light and diffuse light illuminations, and one of the eco-friendliest photovoltaic (PV) technologies". Study concluded that in Barcelona WWR of 0.25-0.45 have similar effect, but after 0.55 cooling demand outruns the electricity production and in Paris best WWR is 0.85 due to higher heating demand. High OPV coverage on ETFE foil is useful for Barcelona with hotter climate, but for Paris with cooler climate it has negative effects. Xamán et al. [28] developed a numerical model for a two-dimensional square cavity with a window. They achieved a correlation between the total Nusselt number and the Rayleigh number. The same numerical model was utilized for a study with various window sizes and locations by Olazo-Gómez et al. [29]. They concluded that the radiative heat transfer became lower than the convective heat transfer at higher values of solar irradiance, and the Nusselt numbers for convection and radiation transfer were lower at laminar flow than turbulent flow. Heltzel et al. [30] designed a metamaterial (MTM) window glass to obtain a "MTM window glass that is capable of reflecting the near-infrared and far-infrared energy from the sun in its summer configuration, while selectively absorbing solar near-infrared energy in the winter configuration" [30] by adding SiO_2 and Ag on a window glass. The design harvested more energy in winter configuration than an existing low-e glass, while high visible transmission. They concluded that the designed window glass "should improve the energy efficiency of a windowed structure with heating requirements" [30].

Lee and Tavil [31] studied electrochromic windows with overhang type exterior solar shade. They compared the electrochromic window to low-e glasses in terms of visual comfort and energy at test cases located in Chicago and Houston. The window was divided into upper and lower apertures and the overhang solar shade was located either on the top or between two apertures. The study concluded that the overhang helped with blocking the direct solar irradiance and electrochromic window decreased both daylight glare index (DGI) and annual energy use (ATE) for both climates at large window sizes. Lowest DGI was achieved when "lower aperture was modulated for solar radiation and upper aperture was modulated for daylight and the overhang was located in between two apertures" [31]. This combination lacked the required illuminance levels. However, the peak electric demand decrease for moderate and large area windows at both climates and ATE was decrease for large area windows on both climates. According to Lee and Tavil [31] the effect of electrochromic window would be more observable when compared to low-e glasses if there were no external solar shade present.

Photovoltaic panels

Roumpakias et al. [32] developed a correlation to determine the actual efficiency of photovoltaic (PV) panels with air mass. They concluded that actual efficiencies of PV panels for solar irradiance levels below of 400 W/m^2 are lower than PV panels promised. There is a nonlinear decrease in efficiency between 0 and 400 W/m^2 of solar irradiance. Gan and Riffat [33] did CFD study of an atrium with PV panels located on top. They analyzed the air flow under the glass roof of the atrium due to an opening and cooling of the PV panels. They concluded that they could decrease the temperature of PV panels and increase their performance according to their CFD results. Peng et al. [34] states that with the current development of the PV panel technology the panels could become outdated in 10 years but buildings last 50 years or longer, so they have provided a PV panel mount design for easier maintenance and replacement of the PV panels.

Thermal comfort considerations

Critical review on thermal radiation effects on thermal comfort was presented by Halawa et al. [35]. They emphasized the possible use of mean radiant temperature. There are only a few studies available which explores the effect of thermal radiation coupled with natural convection in an enclosure. Even then, a detailed study of, surface temperature distribution due to solar thermal radiation within a three-dimensional office environment is missing. Purpose of this study is to shed light on thermal radiation effects of partitions in office spaces to provide better designed offices with better thermal comfort, and to develop more energy efficient spaces. Based on the results obtained, a series of conclusions are listed to achieve these goals. Zhang et al. [36] claims that Predicted Mean Vote (PMV) by Fanger [37] does not work well when direct solar radiation is present. They back their claim with an experiment from China with 998 thermal responses from occupants on the Thermal Sensation Vote (TSV), which aligns with PMV poorly. They propose Corrected Predicted Mean Vote (CPMV), by including the solar radiation to PMV and as a result better agreement with TSV was observed when solar radiation was taken into calculations.

Bessoudo et al. [38] did an experimental study on a building at winter. They have found out that solar radiation on clear weather can cause thermal discomfort even at winter and on cloudy winter days shading device in front of the window such as venetian blinds (at 45° angle) decreased the heat loss through window. Buratti et al. [39] did a CFD study of a classroom in University of Perugia by validating with experimental data. The study pointed out the need of CFD for local thermal comfort calculations at large spaces, where you can calculate the local thermal anywhere in the space, but many sensors are required for experimental measurements at such environments. Hajdukiewicz et al. [40] did a CFD study of a naturally ventilated meeting room in Galway, Ireland with two glazing walls to assess the thermal comfort. They concluded that even only the diffuse solar radiation had significant effect on the room. Marino et al. [41] studies the effect of solar radiation on thermal comfort by calculating Mean Radiant Temperature (MRT) annually with time step of an hour and the results were reviewed by Predicted Percentage Dissatisfied (PPD), also considering the Environmental Quality Index (EQI). Outcomes of the study includes the designed solar shade for the case being “less effective than changing the cooling temperature” and rising the heating costs accordingly, therefore study suggests that comfort and energy should be analyzed together.

Cannistraro et al. [42] points out the need of using local conditions for local thermal comfort evaluations instead of using average parameters which would mislead the thermal comfort evaluations of a space. Tzempelikos et al. [43] studied thermal comfort near glazing elements. Study suggests that cloudy winter days provide stable indoor thermal conditions and the with right choice of window the thermal comfort inside can be maintained. Also, on cloudy winter days shade can decrease the radiant temperature asymmetry and increase thermal comfort.

Alwetaishi [44] states in the thermal comfort literature review that with the current PMV and PPD parameters "two users could be setting in the same internal condition, at the same time, but they might have completely different thermal comfort" feelings, due to difference in perceiving the thermal state of the environment by different occupants. It has been concluded that the air temperature is the most effective parameter among all environmental parameters. Alwetaishi [44] also states that due to usage of large glazing surfaces in office spaces makes "quite difficult to cool the space with minimum reliance on mechanical equipment such as heating and cooling."

For these reasons, thermal comfort should be specific to a person, and should be measure in an daptable manner. Studies on such efforts have been discussed by Keskin [45], and Keskin and Mengüç [46][47].

Visual comfort considerations

Modest [17] has provided one of the earliest discussions for calculation of daylight illumination on a working surface. According to his formulation, the radiative flux consists of three components: the direct sunlight illuminating from the sky, diffuse sunlight illuminating from the outside objects and diffuse sunlight illuminating from the indoor surfaces of the environment. Carlucci et al. [48] did a literature review on visual comfort and dealt with "(i) the amount of light, (ii) the uniformity of light, (iii) the quality of light, and (iv) the rendering quality of light" [48] apart from other reviews. “Spatial Daylight Autonomy (sDA) can be associated to different light situations with different spatial and temporal conditions” [48]. Useful Daylight Illuminance (UDI) deals with over-lit and under-lit conditions, useful levels of daylight, glare and excessive solar gain for long term [49]. Discomfort Glare Probability (DGP) is best approach for just glare. There is no international agreement on color rendering standard. Bakmohammadi and Noorzai [50] analyzed a primary school classroom to improve both thermal and visual comfort of the occupants while improving the energy and daylight performances as well. Study concluded that when modeling for visual comfort modeling the indoor environment as multiple zones for each occupant and supplying the required illuminance level for each occupant increased the visual comfort and decreased the lighting costs by 48% for the case study. Visual comfort is not studied extensively in this thesis study, it should be studied separately.

Validation studies

Li et al. [51] did an experimental study on a controlled test room at laboratory conditions with displacement ventilation and a cube mesh inside the room containing light bulbs as heat source. The walls were either covered with aluminum or completely black according to the case. There are various studies on literature that used this experimental study as a validation case such as Gilani et al. [52], Li et al. [31] and Khalesi et al. [53]. Gilani et al. [52] studied validation of the experimental study done by Li et al. [51] by CFD. Their results are utilized in this thesis for validation study for the flow inside the enclosure, natural convection and thermal radiation. Li et al. [31] numerically studied the experimental study done by Li et al. [51] to compare various radiation models (Monte Carlo model, Discrete transfer model, Modest model and Heat-Flux-Split approach) to a pure convection case. They concluded that for the pure convection case floor temperature was underpredicted and heat source surface was overpredicted. Monte Carlo and Discrete Transfer models had same order of accuracy, but Discrete Transfer method was more efficient in terms of computational time. Khalesi et al. [53] modelled a room with smart window by using the experimental data by Li et al. [51] and moved the study further.

Studies based on manikin modelling

Martinho et al. [54] compared k-ε, k-ω and combined k-ε and k-ω turbulence models on modeling of a manikin. The combined turbulence model solves k-ω near solid regions because it performs better than k-ε for turbulence modelling at near wall regions according to Martinho et al. [54] and k-ε turbulence model is used for the rest of the domain. They compared CFD results with experimental results that they conducted on a manikin. Outcomes of this study includes that the k-ω SST gives much closer results to the experimental data compared to k-ε turbulence model for wall heat fluxes on the manikin. They concluded that best approach for that study is to use the combination of k-ε and k-ω SST turbulence models, which gives the closest results to experimental measurements done on the manikin. Sorensen and Voigt [55] analyzed a seated human manikin on CFD for the flow and heat transfer around it. The analyzed manikin was an exact copy of a manikin from experimental setup for validation purposes. They have chosen k-ε turbulence model on contrary to the study by Martinho et al. [54] and surface to surface radiation model was chosen. According to their CFD results “43% of heat loss was due to convection and 57% due to radiation”. This is a significant percentage and shows the importance of the present study in including radiation transfer calculations for buildings.

CHAPTER II

PHYSICAL AND MATHEMATICAL MODELS

The physical model considered in this thesis is based on Figure 1.1, which is an office at Center for Energy, Environment and Economy (CEEE) located at AB-4 building of Ozyegin University. The office space is currently being used by two people. It is modelled with its actual dimensions to numerically analyze the temperature distributions, air flow and thermal comfort of the occupants under specific conditions in the Chapter 6 Numerical Modelling Studies.

2.1. Geometry

The test geometry considered for this study is an office at Center for Energy, Environment and Economy (CEEE) located at AB-4 building of Ozyegin University. The office (see Figure 2.1 for the schematics) consists of a desk with partition that hosts two occupants on opposite sides. The window from floor to ceiling lets solar radiation inside. Floor, ceiling and all the walls other than the façade are interior walls of the faculty and the heat transfer from those walls are neglected. There is a single inlet and outlet located on the ceiling for the ventilation.

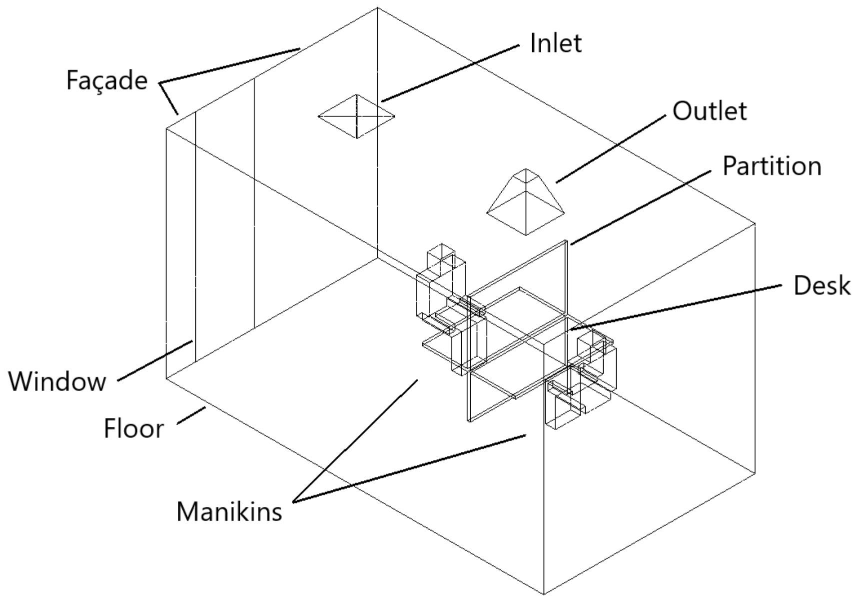

Figure 2.1: Test geometry: An office with desks and partitions; window is allowing solar radiation in.

Dimensions of the office are 3.25 m x 5.8 m x 3.36 m, window is 0.45 m away from the side wall. Partition and desk are in the middle of the adjacent wall, both have thickness of 0.04 m. Height of the desk is 0.7 m. Inlet is located 1 m away from the façade and at middle of the ceiling, outlet is 2 m away from the inlet. Both inlet and outlet are 0.6 m x 0.6 m. More detailed information on geometry will be discussed on Chapter 6.3.1 Geometry and Mesh Selection.

2.2. Governing Equations

The fluid flow coupled with heat transfer inside the office space need to be solved numerically to determine the effects of solar radiation on the office space and thermal comfort of the occupants. ANSYS Fluent 19.2, a computational fluid dynamics (CFD) tool, is used for this computation process. For the fluid flow three dimensional continuity and momentum equations need to be solved to model the fluid flow. They are both discretized for CFD computation. Under relaxation factors and CFL number are used to achieve convergence. The Shear-Stress Transport (SST) k-ω turbulence model is utilized for modeling the turbulence in the office space.

Energy equation needs to be solved for the heat transfer. Convective heat transfer is analyzed by using Grashof and Reynolds numbers whether it is natural or forced convection. Rayleigh number is used to determine the characteristics of natural convection and Reynolds number is used for the forced convection. The radiative transport equation does not need to be solved for the nonparticipating media of the office. Surface to surface (S2S) radiation model is utilized which uses view factors. According to these calculated view factors radiative heat transfer is occurred between surfaces in the office enclosure. Incident solar radiation is calculated by the air mass for the solar load model coupled with the surface to surface radiation model. Two band model (visible and IR) is used with the solar load model and weight of each band is given to solar load model by the spectral fraction.

Thermal comfort is analyzed according to the ASHRAEs Standard 55-2017 [6]. Thermal comfort is dependent on six parameters according to ASHRAE Standard 55 [6]: air (dry-bulb) temperature, mean radiant temperature, air speed, relative humidity, metabolic rate and clothing level.

2.2.1. Fluid Flow Analysis

For all CFD analysis' containing fluid flow continuity and conservation of momentum equations need to be solved and energy equation is also required if the problem involves heat transfer. The three dimensional continuity equation by Çengel and Ghajar [56].

$$\frac{\partial \rho}{\partial t}+\frac{\partial(\rho u)}{\partial x}+\frac{\partial(\rho v)}{\partial y}+\frac{\partial(\rho w)}{\partial z}=0 \tag{1}$$

The three dimensional conservation of momentum equations by Çengel and Ghajar [56].

$$\begin{aligned}\frac{\partial(\rho u)}{\partial t}+\frac{\partial(\rho u^2)}{\partial x}+\frac{\partial(\rho u v)}{\partial y}+\frac{\partial(\rho u w)}{\partial z}\\ =-\frac{\partial p}{\partial x}+\frac{1}{Re}\left[\frac{\partial \tau_{xx}}{\partial x}+\frac{\partial \tau_{xy}}{\partial y}+\frac{\partial \tau_{xz}}{\partial z}\right]+\rho g_x\end{aligned} \tag{2}$$

$$\frac{\partial(\rho v)}{\partial t}+\frac{\partial(\rho uv)}{\partial x}+\frac{\partial(\rho v^2)}{\partial y}+\frac{\partial(\rho vw)}{\partial z} = -\frac{\partial p}{\partial y}+\frac{1}{Re}\left[\frac{\partial \tau_{xy}}{\partial x}+\frac{\partial \tau_{yy}}{\partial y}+\frac{\partial \tau_{yz}}{\partial z}\right]+\rho g_y \tag{3}$$

$$\frac{\partial(\rho w)}{\partial t}+\frac{\partial(\rho uw)}{\partial x}+\frac{\partial(\rho vw)}{\partial y}+\frac{\partial(\rho w^2)}{\partial z} = -\frac{\partial p}{\partial z}+\frac{1}{Re}\left[\frac{\partial \tau_{xz}}{\partial x}+\frac{\partial \tau_{yz}}{\partial y}+\frac{\partial \tau_{zz}}{\partial z}\right]+\rho g_z \tag{4}$$

Conservation of momentum equation is discretized for the CFD

$$a_p u = \sum_{nb} a_{nb} u_{nb} + \sum p_f A \cdot i + S \tag{5}$$

ANSYS Fluent has five pressure interpolation schemes, which are Linear, Standard, Second Order, Body Force Weighted and PRESTO! (PRessure STaggering Option). The latter two pressure interpolation schemes are used to model the natural convection. In this study PRESTO! is utilized as in the validation study by Gilani et al. (2016). According to the ANSYS Fluent 19.2 Theory Guide [57] section 28.4.1 “PRESTO! scheme uses the discrete continuity balance for a “staggered” control volume about the face to compute the “staggered” pressure.” and PRESTO! scheme can be used with all types of meshes.

Continuity equation is discretized for the CFD, where the is mass flux through face.

$$\sum_{f}^{N_{faces}} J_f A_f = 0 \tag{6}$$

Available density interpolation schemes in ANSYS Fluent are first-order upwind, second-order upwind, QUICK, MUSCL, central differencing and bounded central differencing. This study utilizes both first and second-order upwind schemes as discussed at Chapter 6 Results Based on Numerical Modeling Studies.

Pressure-velocity coupling of the fluid flow can be done by following algorithms; SIMPLE, SIMPLEC, PISO and Coupled. First three of these algorithms use staggered approach while Coupled algorithm uses coupled approach. Staggered approach generates separate grids for pressure and velocity. On these separate grids corresponding pressure and velocity equations are solved separately and corrected by pressure and velocity correctors. According to the ANSYS Fluent 19.2 Theory Guide [57] they are faster than coupled approach, but coupled approach is a superior algorithm for steady state problems. Natural convection causes the analysis to converge harder or even not converge at all. Due to the convergence issues of SIMPLE algorithm on this study, coupled algorithm is used to achieve convergence. Although coupled algorithm provides slower convergence than staggered methods due to semi-implicit method utilized, it provides convergence. Momentum and continuity equations are solved together when the Coupled algorithm is utilized.

The under relaxation of equations is used to ensure the convergence stabilization in pressure-based solvers. Change of value φ at each iteration is updated by adding the difference to the previous value of φ, but if the change is too large this might cause the solution to diverge. Therefore, the difference is multiplied with under-relaxation factor (α) to stabilize the convergence.

$$\varphi = \varphi_{old} + \alpha \Delta\varphi \tag{7}$$

The Coupled algorithm utilizes CFL number for the under-relaxation. Under-relaxation factors and CFL number will be discussed on Chapter 6 Results Based on Numerical Modeling Studies.

$$\frac{1-\alpha}{\alpha} = \frac{1}{CFL} \tag{8}$$

The Shear-Stress Transport (SST) k-ω turbulence model is utilized for this study. It is chosen over k-ε turbulence model because of the better capability of modelling flow on walls, especially the superior prediction of onset and amount of flow separation on smooth surfaces. Also, the validation study by Gilani et al. [52] utilized the k-ω over k-ε turbulence model. No further discussion will be made on the turbulence model, since it is not the scope of this thesis.

2.2.2. Heat Transfer Analysis

Energy equation needs to be solved for determining heat transfer to the surfaces. According to ANSYS Fluent Theory Guide [57] Section 5.2.1 ANSYS Fluent solves the energy equation in the following form

$$\frac{\partial}{\partial t}(\rho E) + \nabla \cdot \big(\vec{v}(\rho E + p)\big) = \nabla \cdot \left(k_{eff} \nabla T - \sum_j h_j \vec{J}_j + (\bar{\bar{\tau}}_{eff} \cdot \vec{v}) \right) + S_h \tag{9}$$

Convection in office space can be either forced or natural convection. If the HVAC system is on, forced convection analysis needs to be carried out. In such analysis, a series of dimensionless numbers are used. They are used at correlations formed for various situations, such as Nusselt number correlations that are used to calculate the heat transfer coefficient for convective heat transfer by utilizing the Reynold's and Prandtl numbers. Since all cases studied will have various physical dimensions and values, these correlations are formulated with dimensionless numbers. They are usually not required for the CFD analysis', for example the heat transfer coefficient in the interior walls are computed from the flow on the wall in the CFD code.

- Reynold's number

$$Re = \frac{\rho v L}{\mu} = \frac{\text{inertia force}}{\text{viscous force}} \tag{10}$$

- Grashof number

$$Gr = \frac{g\beta(T_{wall} - T_{\infty})L^3}{v^2} = \frac{\text{buoyancy force}}{\text{viscous force}} \tag{11}$$

- Prandtl number

$$Pr = \frac{v}{\alpha} = \frac{\text{viscous diffusion rate}}{\text{thermal diffusion rate}} \tag{12}$$

- Rayleigh number

$$Ra = \frac{g\beta(T_{wall} - T_{\infty})L^3}{v \cdot \alpha} \tag{13}$$

- Nusselt number

$$Nu = \frac{hL}{k} = \frac{\text{convective heat transfer}}{\text{conductive heat transfer}} \tag{14}$$

- Archimedes number

$$Ar = \frac{gL^3\rho_f(\rho - \rho_f)}{\mu^2} = \frac{\text{gravitational forces}}{\text{viscous forces}} \tag{15}$$

Natural convection is a buoyancy driven flow due to the change in density of the fluid due to temperature difference. It is determined according to the ratio of Gr/Re^2 if $Gr/Re^2>>1$ natural convection takes place and if $Gr/Re^2<<1$ forced convection takes place.

$$\frac{Gr}{Re^2} = \frac{g\beta\Delta TL}{v^2} \tag{16}$$

If the flow is purely natural convection, Rayleigh number determines the strength of the flow. $Ra<10^8$ for laminar flow and $10^8<Ra<10^{10}$ for turbulent flow.

$$Ra = Gr \cdot Pr \tag{17}$$

Where g is gravitational acceleration, ρ is density, μ is dynamic viscosity, β is thermal expansion coefficient and α is thermal diffusivity

$$\beta = -\frac{1}{\rho}\left(\frac{\partial \rho}{\partial T}\right)_p \tag{18}$$

$$\alpha = \frac{k}{\rho c_p} \tag{19}$$

If the flow is purely forced Reynolds number determines the flow characteristics. Below the critical Reynolds number (Re_{cr}) flow is laminar and above the critical Reynolds number flow is turbulent.

$$Re_{cr} = \frac{\rho V x_{cr}}{\mu} = 5 \times 10^5 \tag{20}$$

2.2.3. Radiative Heat Transfer Analysis

In this thesis it is assumed that the air in the room is nonparticipating (no absorption, emission and scattering by the media), therefore the radiative energy is transferred from one surface to another without losing energy to the media. In this case radiative transport equation is not required to be solved. Instead, equations shown under Surface to Surface Radiation Model are solved for the radiative heat transfer and the radiative heat transfer is added to the energy equation in Equation 9 as S_h term. Radiative transport equation and definition of each term by Howell et al. [7]:

Change in radiative energy = gain due to emission – loss due to absorption
– loss due to out-scattering + gain due to in-scattering

$$\begin{aligned} I_\lambda(S+dS,\Omega,t+dt) - I_\lambda(S,\Omega,t) \\ = \kappa_\lambda I_{\lambda b}(S,t)dS - \kappa_\lambda I_\lambda(S,\Omega,t)dS - \sigma_{S,\lambda} I_\lambda(S,\Omega,t)dS \\ + \frac{1}{4\pi}\int_{\Omega_i=4\pi} \sigma_{S,\lambda} I_\lambda(S,\Omega,t)\Phi_\lambda(\Omega_i,\Omega)d\Omega_i \end{aligned} \tag{21}$$

Surface to Surface Radiation Model

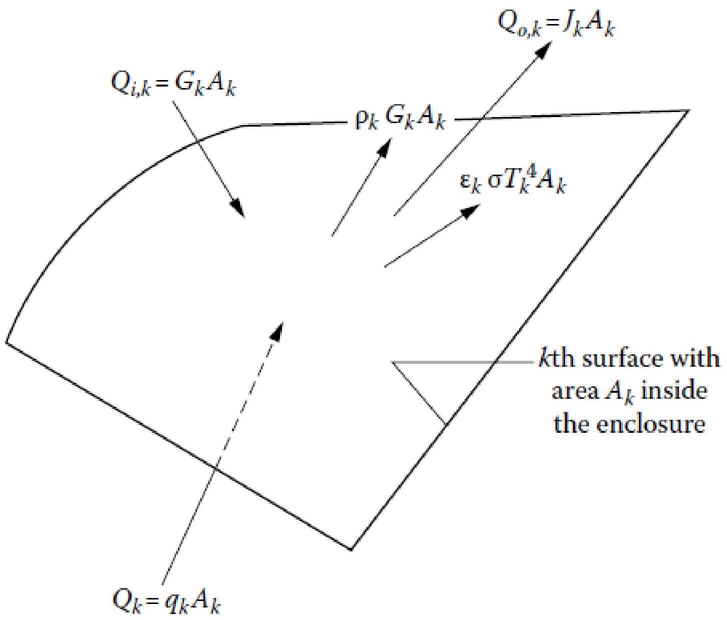

Figure 2.2: Energy quantities incident upon and leaving typical surface inside enclosure from Howell et al. [7].

Surface to surface (S2S) radiation model models radiative heat transfer in between surfaces as the name indicates, it takes the environment as non-participating media. Furthermore, gray and diffuse assumptions are made for the surfaces by the S2S radiation model. Gray body assumption is assuming the spectral emissivity and spectral absorptivity is independent from the wavelength. Diffuse assumption is directional emissivity and directional absorptivity is independent from the direction (Howell et al., 2016). By these assumptions' emissivity is equal to absorptivity ($\varepsilon = \alpha$). For surfaces chosen as opaque in S2S radiation model emissivity and reflectivity are proportionalities of the incident radiation which adds up to 100% ($\varepsilon + \rho = \alpha + \rho = 1$) and for surfaces chosen as semi-transparent emissivity, reflectivity and transmissivity are proportionalities of the incident radiation (I) which adds up to 100% ($\varepsilon + \rho + \tau = \alpha + \rho + \tau = 1$).

$$I = \tau I + \alpha I + \rho I \tag{22}$$

S2S radiation model utilizes view factors for the thermal radiation heat transfer in between surfaces. View factor from surface i to surface j (F_{ij}) is

$$F_{ij} = \frac{1}{A_i} \iint_{A_i A_j} \frac{cos\theta_i cos\theta_j}{\pi r^2} \delta_{ij} dA_i dA_j \tag{23}$$

View factors are reciprocal with the area (A) of the surfaces

$$A_j F_{jk} = A_k F_{kj} \tag{24}$$

According to the ANSYS Fluent 19.2 Theory Guide [57], mathematical model behind the S2S radiation model is as follows. The energy leaving the surface k ($q_{out,k}$) is

$$q_{out,k} = \varepsilon_k \sigma T_k^4 + \rho_k q_{in,k} \tag{25}$$

Where σ is Stefan-Boltzmann constant ($\sigma = 5.67 \times 10^{-8}\ Wm^{-2}K^{-4}$)

$$A_k q_{in,k} = \sum_{j=1}^{N} A_j q_{out,j} F_{jk} \tag{26}$$

Energy incident on a surface k ($q_{in,k}$) is

$$q_{in,k} = \sum_{j=1}^{N} F_{kj} q_{out,j} \tag{27}$$

Therefore

$$q_{out,k} = \varepsilon_k \sigma T_k^4 + \rho_k \sum_{j=1}^{N} F_{kj} q_{out,j} \tag{28}$$

Radiosity (J) is out going radiation from a surface and E is the emissive power of a surface therefore it can be written as

$$J_k = E_k + \rho_k \sum_{j=1}^{N} F_{kj} J_j \tag{29}$$

S2S radiation model is a computationally expensive model and to decrease the computational time surface clusters are formed from faces. Radiosity is calculated for these surface clusters and then distributed to faces. According to section 5.3.7 of ANSYS Fluent Theory Guide, surface cluster temperature (T_{sc}) is calculated by

$$T_{sc} = \left(\frac{\sum_f A_f T_f^4}{\sum A_f} \right)^{1/4} \tag{30}$$

Solar Load Model

Solar irradiance is the power coming from the Sun as electromagnetic radiation. It is calculated to acquire the heat flux due to solar load on a location at a date and time. The solar irradiance reaching the upper atmosphere from the Sun is 1366 W/m^2 according to Howell et al. [7].

To calculate solar irradiance at a specific location on Earth, first Sun's angle of incidence should be obtained. Horizontal coordinate system is used to define the Sun's angle of incidence, which divides the sky into two as upper and lower hemisphere. Upper hemisphere is visible to the observer on the surface of Earth and the angle of incidence is calculated using the azimuth angle and altitude angle. The upper hemisphere pole is called zenith and the lower hemisphere pole is nadir. Sum of zenith and altitude angle is equal to 90 degrees, so both can be used in the calculations.

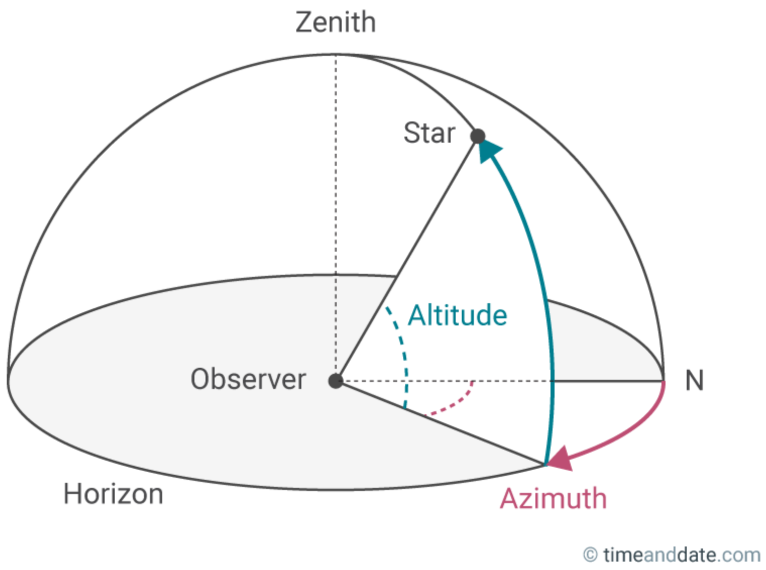

Figure 2.3: Horizontal coordinate system [58].

The azimuth angle changes throughout the day due to the Earth's rotation around its own axis. As the Earth rotates around the Sun zenith angle changes with period of one year, due to Earth's declination angle.

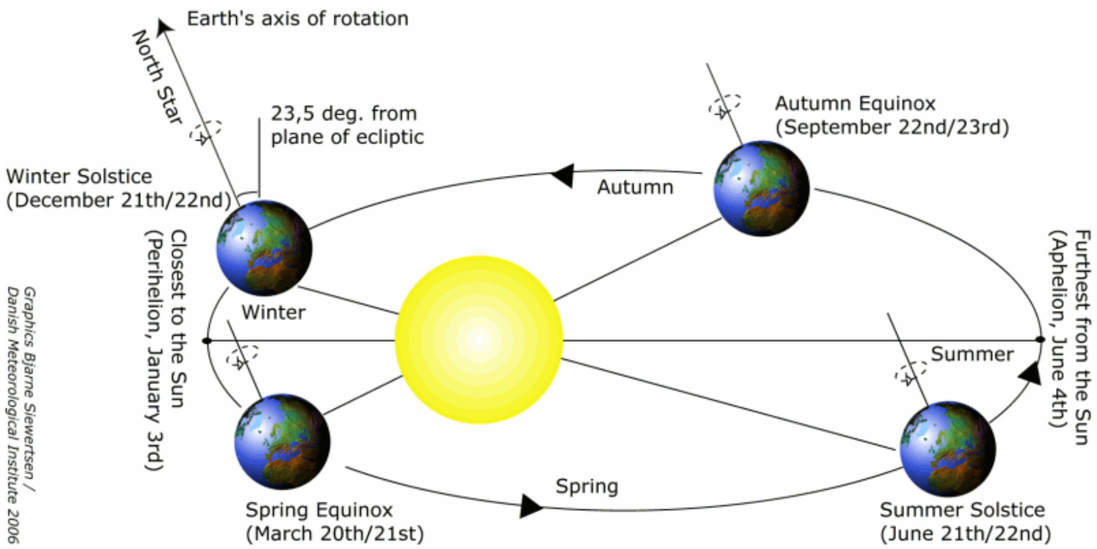

Figure 2.4: Earth's declination angle [59].

Air mass (AM) and zenith angle (θ_s) are utilized for the calculation of solar irradiance on a surface on the Earth (see Equation 31). Air mass represents the distance solar rays coming from sun travel after entering the atmosphere and until reaching the ground.

$$AM = \frac{1}{cos\theta_s + 0.050572(96.07995 - \theta_s)^{-1.6364}} \tag{31}$$

The solar radiation reaching the ground can be calculated with the direct solar irradiance (I_D) equation, which utilizes the air mass [32].

$$I_D = 1366 \cdot 0.7^{AM^{0.678}} \tag{32}$$

The calculated direct solar irradiance is the heat flux on a horizontal surface on the ground with no diffuse radiation. If the surface is angled the calculations must be modified. As seen from the equations above the azimuth angle has no effect on the direct solar irradiance calculations on horizontal surfaces.

Solar load is calculated by the solar load model integrated to ANSYS Fluent. Location of the Sun can either be entered as a vector or can be calculated by the "Solar Calculator", which takes orientation, coordinates of the geometry, cloud coverage and the time of the day as input. Either solar ray tracing or discrete ordinated irradiation can be utilized for the solar load calculations.

Solar ray tracing algorithm is used for prediction of direct illumination due to incident solar radiation. Computed heat fluxes are added as a source term to the energy equation. Solar ray tracing algorithm takes direct solar irradiation as a two-band spectral model for visible and infrared (IR) bands. Opaque surfaces take two absorptivity inputs for visible and infrared bands, semi-transparent surfaces take two transmissivity and absorptivity values. These values are for incident radiation normal to the surface. ANSYS Fluent computes corresponding values for the angle of incidence. Solar ray tracing distributes the reflected solar load to all surfaces instead of applying the reflected load to reflected surfaces only. According to ANSYS Fluent 19.2 User's Guide [60] a radiation model is used to for this implementation in conjunction with the solar ray tracing model. If a ray is intersected by a surface than shading occurs. Glazing materials are modelled with solar ray tracing, this subject is further explained at the Chapter 4 Window Glasses.

Solar ray tracing algorithm can take the following inputs into its calculations:

- Sun direction vector
- Direct solar irradiation
- Diffuse solar irradiation
- Spectral fraction
- Direct and IR absorptivity (opaque wall)
- Direct and IR absorptivity (semi-transparent wall)
- Diffuse hemispherical absorptivity and transmissivity (semi-transparent wall)
- Solar transmissivity factor
- Scattering fraction
- Ground reflectivity

Further information on surface to surface radiation model, discrete ordinates radiation model and solar load model can be found on ANSYS Fluent 19.2 User's Guide [60] and ANSYS Fluent 19.2 Theory Guide [57].

Solar Load Model enables the S2S radiation model to be two-band spectral radiation model which are visible and infrared bands. Radiation model becomes no longer gray after enabling this two-band model. It asks for spectral fraction (see Equation 33) while setting the solar load model, which is the fraction of visible light. For semi-transparent boundary conditions, it asks for both visible and infrared absorptivity and transmissivity.

$$Spectral\ Fraction = \frac{Visible\ Fraction}{(Visible\ Fraction + Infrared\ Fraction)} \tag{33}$$

Solar irradiance spectrum is approximately 4% ultraviolet, 38% visible and 58% infrared [61]. Therefore, spectral fraction will be chosen as 0.4 for this study.

2.3. Thermal Comfort

According to ASHRAE "Thermal comfort is that condition of mind that expresses satisfaction with the thermal environment." and ASHRAE Standard 55-2017 [6] subjectivizes this satisfaction with thermal environment. Thermal comfort is dependent on six parameters in ASHRAE Standard 55: air (dry-bulb) temperature, mean radiant temperature, air speed, relative humidity, metabolic rate and clothing level. Air temperature is average air temperature surrounding the occupant. Mean radiant temperature is dependent on the radiation heat transfer between the occupant and surroundings. It is dependent on the temperatures of surrounding surfaces and view factors from the occupant to surroundings. Sum of view factors multiplied by the fourth power of surface temperature gives the fourth power of mean radiant temperature as seen on Equation 34. Increasing the surface number increases the accuracy of the mean radiant temperature.

$$T_{mr}^4 = T_1^4 F_{p-1} + T_2^4 F_{p-2} + \cdots + T_N^4 F_{p-N} \tag{34}$$

Where mean radiant temperature (T_{mr}) and surface temperature (T_N) are in Kelvin. It can be measured with a black globe thermometer. Air speed is average air speed around the occupant regardless of the direction. Relative humidity is amount of water vapor in the air. Relative humidity does not have direct effects on thermal comfort. Indoor relative humidity should be kept between 30-60% in air conditioned environments according to Wolkoff et al. [62]. Metabolic rate is amount of energy our bodies burn. It depends on the activity that is being done, some of the metabolic rates can be seen on Table 2.1 and further activities can be found on ASHRAE Standard 55 [6]. It has unit of met and one met is equal to 58.2 W/m^2. Clothing level is amount of thermal insulation clothes create on our bodies. Various clothes and outfits are standardized by ASHRAE Standard 55 [6] and some outfits can be seen on Table 2.2. It has unit of clo and one clo is equal to 0.155 m^2.K/W in SI units.

Table 2.1: Metabolic rates on various activities for thermal comfort calculations according to ASHRAE Standard 55-2017 [6].

Activity	Metabolic Rate [met]
Sleeping	0.8
Reading or writing, seated	1.0
Filing, standing	1.2
Walking about	1.7
Walking 3.2 km/h	2.0
Housecleaning	2.7
Dancing	3.4
Heavy machine work	4.0

Table 2.2: Clothing levels on various outfits for thermal comfort calculations according to ASHRAE Standard 55-2017 [6].

Outfit	Clothing Level [clo]
Walking shorts, short-sleeve shirt	0.36
Typical summer indoor clothing	0.50
Knee-length skirt, short-sleeve shirt, sandals, underwear	0.54
trousers, short-sleeve shirt, socks, shoes, underwear	0.57
Trousers, long-sleeve shirt	0.61
Knee-length skirt, long-sleeve shirt, full slip	0.67
Sweatpants, long-sleeve sweatshirt	0.74
Jacket, trousers, long-sleeve shirt	0.96
Typical winter indoor clothing	1.00

Operative temperature combines dry bulb temperature and mean radiant temperature into one parameter according to ASHRAE Standard 55-2017 [6], where T_o is operative temperature, T_{mr} is mean radiant temperature, T_{db} is dry bulb temperature, h_r is radiative heat transfer coefficient and h_c is convective heat transfer coefficient.

$$T_o = (h_r T_{mr} + h_c T_{db})/(h_r + h_c) \tag{35}$$

Operative temperature (T_o) can used in its simplest form as below according to ASHRAE Standard 55-2017 [6], which will be the case for this study due to modelling of the manikins will be hollow therefore there will not be heat transfer coefficient on surfaces of manikins. This operative temperature can be determined as the average of the mean radiant temperature (T_{mr}) and the dry bulb temperature (T_{db}):

$$T_o = (T_{mr} + T_{db})/2 \tag{36}$$

There are two types of thermal comfort models, which are static and adaptive models [6]. Static models are focused on predicted mean vote and percentage of dissatisfied models, and adaptive models are focused on the body adapting to different thermal conditions psychologically, physiologically, and behaviorally. Adaptive models suggest that indoor thermal comfort expectations of occupants can change with changing outdoor climates.

Predicted Mean Vote (PMV) and Percentage of Dissatisfied (PPD) models were developed by P.O. Fanger [37] to define thermal comfort according to the skin temperature. Fanger's PMV equations calculate the thermal comfort from air temperature, mean radiant temperature, air speed, relative humidity, metabolic rate, and clothing level according to thermal comfort surveys that has scale from -3 to 3, which represents very cold to very hot and 0 is thermal neutrality. Recommended PMV limit is from -0.5 to 0.5. ASHRAE Standard 55 [6] uses PMV and PPD models for indoor thermal comfort standards, where PPD should be below 80%. Figure 2.5 shows the relationship between PMV and PPD parameters.

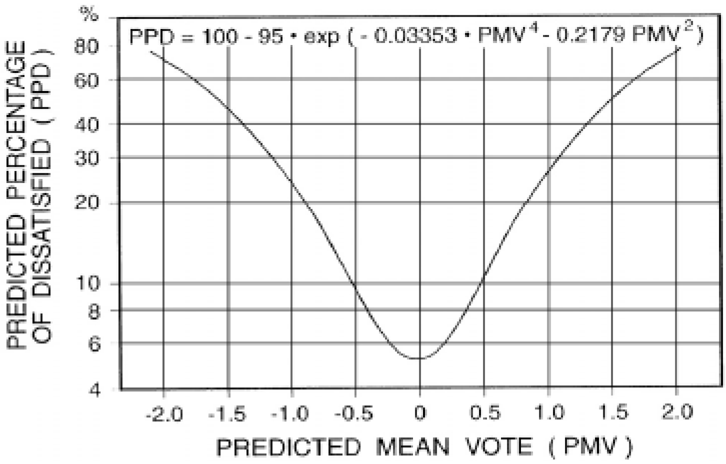

Figure 2.5: Relationship between the Predicted Mean Vote (PMV) and Percentage of Dissatisfied (PPD) according to ASHRAE Standard 55-2017 [6].

Thermal comfort can be calculated using the six parameters of thermal comfort and operative temperature by the CBE Thermal Comfort Tool for ASHRAE Standard 55 [6] by Berkeley (https://comfort.cbe.berkeley.edu/).

Formulated PMV calculations according to ISO 7730 [63]:

$$\begin{aligned} PMV = {} & [0.303 \cdot \exp(-0.036 \cdot M + 0.028)] \\ & \cdot \{(M - W) - 3.05 \cdot 10^{-3} \cdot [5.733 - 6.99 \cdot (M - Q) - p_a] \\ & - 0.42 \cdot [(M - W) - 58.15] - 1.7 \cdot 10^{-5} \cdot M \cdot (5867 - p_a) \\ & - 0.0014 \cdot M \cdot (34 - t_a) - 3.96 \cdot 10^{-8} \cdot f_{cl} \\ & \cdot [(t_{cl} + 273)^4 - (\overline{t_r} + 273)^4] - f_{cl} \cdot h_c \cdot (t_{cl} - t_a)\} \end{aligned} \tag{37}$$

$$\begin{aligned} t_{cl} = {} & 35.7 - 0.028 \cdot (M - W) - I_{cl} \\ & \cdot \{3.96 \cdot 10^{-8} \cdot f_{cl} \cdot [(t_{cl} + 273)^4 - (\overline{t_r} + 273)^4] + f_{cl} \cdot h_c \\ & \cdot (t_{cl} - t_a)\} \end{aligned} \tag{38}$$

$$h_c = \begin{cases} 2.38 \cdot |t_{cl} - t_a|^{0.25} & for \quad 2.38 \cdot |t_{cl} - t_a|^{0.25} > 12.1 \cdot \sqrt{v_{ar}} \\ 12.1 \cdot \sqrt{v_{ar}} & for \quad 2.38 \cdot |t_{cl} - t_a|^{0.25} < 12.1 \cdot \sqrt{v_{ar}} \end{cases} \tag{39}$$

$$f_{cl} = \begin{cases} 1.00 + 1.290 I_{cl} & for \quad I_{cl} \leq 0.078\, m^2 \cdot K/W \\ 1.05 + 0.645 I_{cl} & for \quad I_{cl} > 0.078\, m^2 \cdot K/W \end{cases} \tag{40}$$

Where

M	is the metabolic rate in W/m^2
W	is the effective mechanical power in W/m^2
I_{cl}	is the clothing insulation in m^2.K/W
f_{cl}	is the clothing surface area factor
t_a	is the air temperature in °C
$\overline{t_r}$	is the mean radiant temperature in °C
v_{ar}	is the relative air velocity in m/s
p_a	is the water vapor partial pressure in Pa
h_c	is the convective heat transfer coefficient in W/(m^2.K)
t_{cl}	is the clothing surface temperature in °C

Draft is defined as the unwanted air movement around a person, and it is related to local convective cooling. It can cause thermal comfort or discomfort depending on the situation, cool draft on cold weather can cause local thermal discomfort on uncovered or under covered body parts.

Radiant temperature asymmetry is large thermal radiation differences in between various surfaces and occupants. Due to different effects of various surfaces each surface have different limitations (see Figure 2.6). This limitation allows warm ceiling to have least amount of temperature difference and warm wall to have most amount of temperature difference.

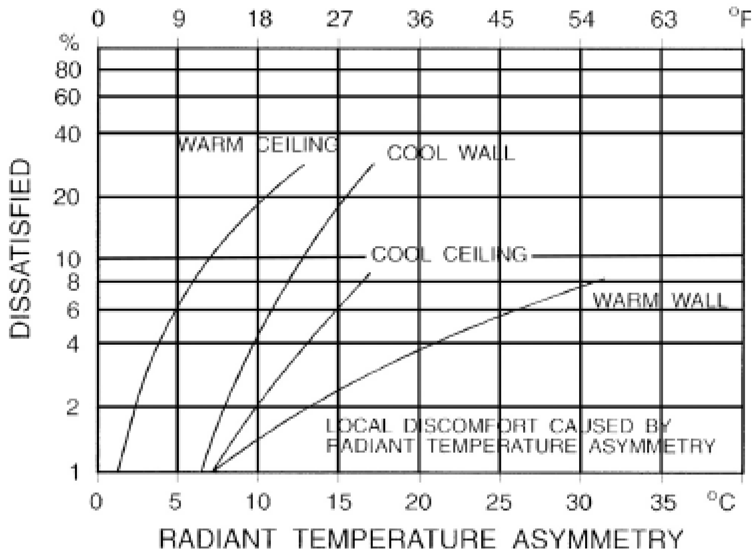

Figure 2.6: Local thermal discomfort caused by radiant asymmetry plot of ASHRAE Standard 55-2017 [6].

According to ASHRAE Standard 55-2017 [6] higher air temperature around head than ankle can cause thermal discomfort and vertical temperature difference between the ankle and head of an occupant should not exceed 3°C for seated and 4°C for standing occupants to provide thermal comfort.

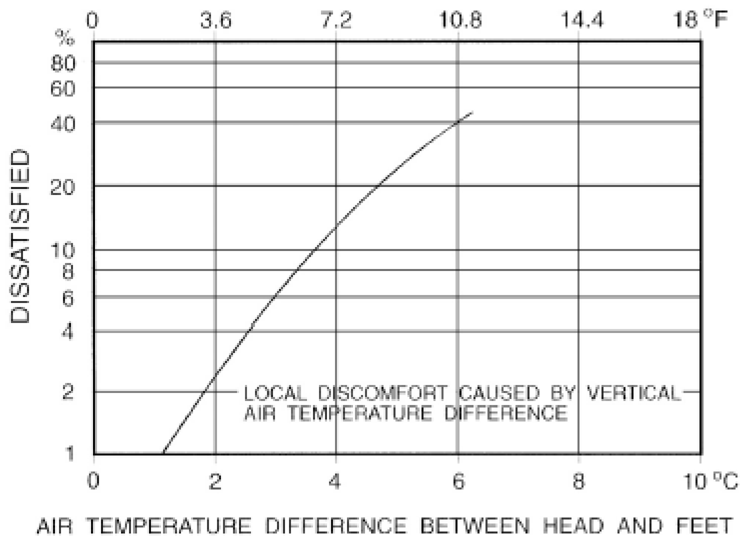

Figure 2.7: Local thermal discomfort caused by vertical temperature differences plot of ASHRAE Standard 55-2017 [6].

Floor surface temperature should be between 19-29°C to provide thermal comfort according to ASHRAE Standard 55-2017 [6], while wearing lightweight shoes. Below 19°C or above 29°C can increase the percentage of dissatisfied significantly as can be seen on Figure 2.8.

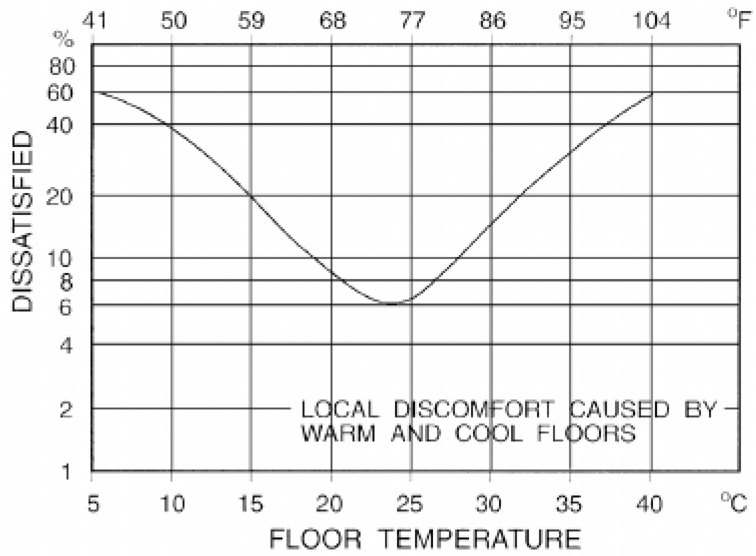

Figure 2.8: Local thermal discomfort caused by warm and cool floors plot of ASHRAE Standard 55-2017 [6].

CHAPTER III

EXTERNAL SOLAR SHADES

Solar shade is a piece of equipment used on buildings to block the solar irradiance. They come in various shapes and sizes depending on the design parameters of the building, therefore they need to be designed specifically for each building according to design parameters at early stages of building design [21]. Solar shades are mainly used to block the solar irradiance from hitting the windows but can also be used for blocking solar irradiance on walls and outside areas as well.

Solar shades also help create a buffer layer between the façade or window and the environment as seen on study of Varughese and John [64]. At summertime there will be a buffer layer of colder air in between the window or façade and solar shade, which will help keep the indoor temperature down by convection heat transfer aside from blocking the thermal radiation.

3.1. Solar Shade Design

3.1.1. Design Types

Solar shades are usually designed as a part of the building, so there are vast amount of solar shade designs available. Below are some widely utilized types (see Figure 3.1 – Figure 3.5) of solar shades, which are window shutters, horizontal slat, vertical slat, overhang and mesh type solar shades. Window shutters have been used for a long time, but they block most of the available natural light as well. Other designs are more modern approaches to the solar shades, and they can have custom sizes according to the natural light required inside the building, which results in a more energy efficient solution.

Figure 3.1: Window shutters [65].

Figure 3.2: Horizontal slat solar shades [66].

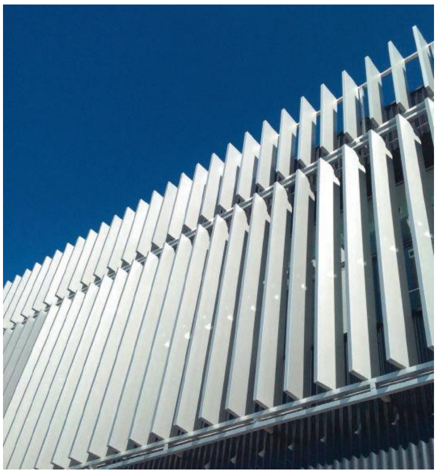

Figure 3.3: Vertical slat solar shades [67].

Figure 3.4: Overhang solar shade [68].

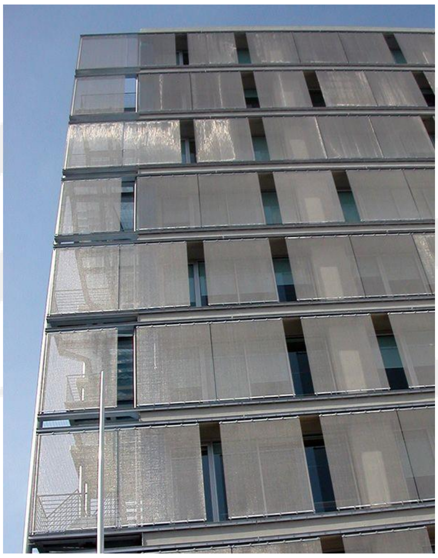

Figure 3.5: Mesh solar shade [69].

For mounting photovoltaic (PV) panels on top of solar shades; mesh type solar shades cannot be used because lack of space available on them for this process, window shutters can have small flexible PV panels mounted on them, and rest of the design can support all types of solar shades available on the market (comparison of PV panel types are done on the Chapter 5.1 Photovoltaic Panel System).

3.1.2. Design Parameters

Design parameters will be discussed on the horizontal slat solar shade because it is the best design for blocking solar irradiance according to the study by David et al. [22]

and the most efficient design for mounting PV panels on top. Design parameters are given on the following sketches (see Figure 3.6 and Figure 3.7).

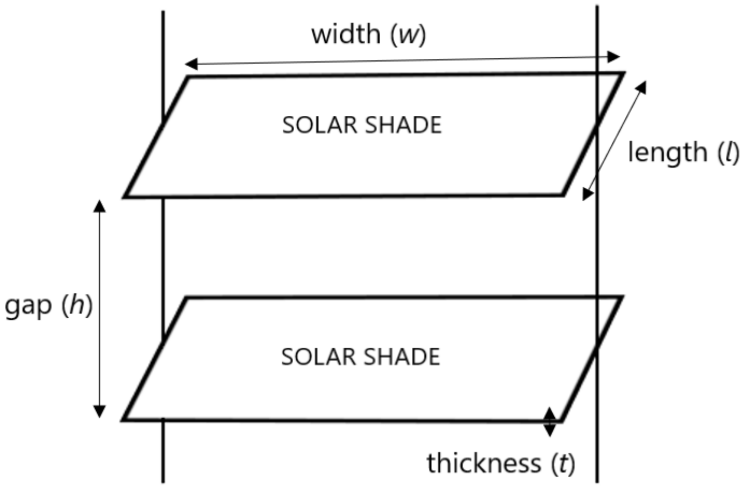

Figure 3.6: Solar shade design parameters sketch.

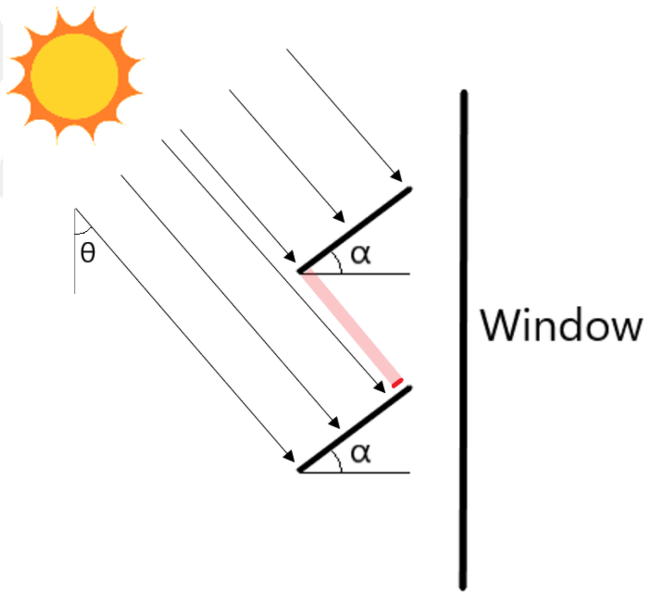

Figure 3.7: Solar shade design parameters sketch from side view.

Effects of each parameter on their own are listed below:

- *Thickness (t):* Thickness of the solar shade effects the weight of the overall system. Therefore, thinner PV panels can provide thinner solar shades and eventually a lighter system. System should be as light as possible so that the walls can support the weight. When calculating the weight of the overall system; weight of the PV panels, wind load on the panels and possible weight due to snow coverage should be considered. Other than weight, thickness of a solar shade can be neglected in the geometrical design process, because it will have relatively small thickness in any case.

- *Width (w):* Has no direct effect to the design process other than the fact that it needs to have at least the width of the window to cover it all. It can also be wider than the window if desired to block the solar irradiance from hitting the façade, which will decrease the amount of heat transferred inside the building through the outer walls.
- *Length (l):* Increasing length decreases the direct solar irradiance transmitting inside through the windows but increasing it too much will block the direct solar irradiance from reaching the lower solar shade and will decrease the performance of the PV panel located on the solar shade. Regardless of the PV panel if one solar shade blocks the lower one it is unnecessarily long and will add unnecessary amount of weight to the overall system.
- *Gap (h):* Gap in between solar shades effect the amount of direct solar irradiance incident on the window. Increasing the gap will increase the amount of solar irradiance incident on the window.
- *Angle of solar shade (α):* Angle of solar shade effects the amount of solar irradiance incident on the window, increasing it decreases the natural light inside. It is also the parameter that interferes with the angle of solar irradiance (zenith angle), which changes throughout the day and year. Therefore, α should be chosen according to the amount of direct solar irradiance desired to be incident on the window throughout the year for a stationary system. For a dynamic system, this value can be adjusted after the design process.
- *Zenith angle (θ):* This is the angle of the solar irradiance and this parameter effects the design directly, since we cannot change this parameter, we must do the design accordingly.

This design process focuses on dynamic systems rather than stationary systems, which allows the angle of solar shade to be adjusted to the desired angle. Mechanical system with a simple crank system will be more convenient than an electrical system with motors and controllers. Electric system will require more maintenance, will be more expensive as both in initial cost and maintenance and be more prone to fail due to complexity of the system in long term usage. Also, the motors will require electricity to operate which will decrease the efficiency of the overall system as solar shades combined with PV panels. Finally, dynamic system will give freedom to adjust the solar shade instantly to block more Sun light or let more Sun light in according to the desired thermal and visual comforts of occupants at that moment.

On the contrary side stationary system will be the most convenient design, but due to lack of ability to adjust the angle of solar shade according to the Sun's location will decrease the efficiency of both the solar shade and PV panels. This is discussed further under Chapter 5.3 Financial Considerations of Photovoltaic Panels.

Design process of dynamic system takes zenith angle as an input according to the location and orientation of the façade. Then length of the solar shade, gap in between solar shades and angle of the solar shade should be adjusted accordingly. To adjust these three parameters following steps can be followed:

1. Angle of solar shade can be adjusted according to the zenith angle of the Sun on that instance to maximize the energy generation by PV panels. This will not be an ideal scenario, so the zenith angle can be adjusted with longer periods to an average angle such as weekly or monthly.
2. Length (also width) of the solar shade can be decided according to the available PV panel sizes since custom building PV panels to the desired solar shade size will significantly increase the cost of the overall system.
3. Gap in between the solar shades should be chosen to minimize the blockage on lower solar shades (see Figure 3.7, at lower solar shade red mark indicates the direct solar irradiance blocked by the upper solar shade slat). This value should be chosen according to the other two parameters and considering the Sun at the average zenith angle location in the sky throughout the year.

These steps will provide a dynamic system with maximum possible electricity generation from PV panels, but the parameters can be altered as the gap can be increased to let more solar irradiance incident in the building or decreased to block more. For zenith angles other than the yearly average for the location, solar shade system will either block the lower solar shade or let irradiance through the window and this will result in the decrease of efficiency of the overall system.

CHAPTER IV

WINDOW GLASSES

4.1. Window Glass Optical Properties

There are three main optical properties of semi-transparent surfaces which need to be accounted for radiative transfer analysis of windows; they are transmissivity (τ), absorptivity (α) and reflectivity (ρ). These radiative properties depend on composition, surface finish, temperature, radiation wavelength, angle of incidence and spectral distribution of the incident radiation according to Howell et al. [7]. Absorptivity is the fraction of irradiation absorbed by the medium, transmissivity is the fraction of irradiation transmitted through the medium to the other side and reflectivity is the fraction of irradiation reflected from the surface at the change of medium. All these properties are expressed as proportionalities add up to 100% ($\tau + \alpha + \rho = 1$ as mentioned in the Chapter 2.2.3 Radiative Heat Transfer Analysis and under Surface to Surface (S2S) Radiation Model).

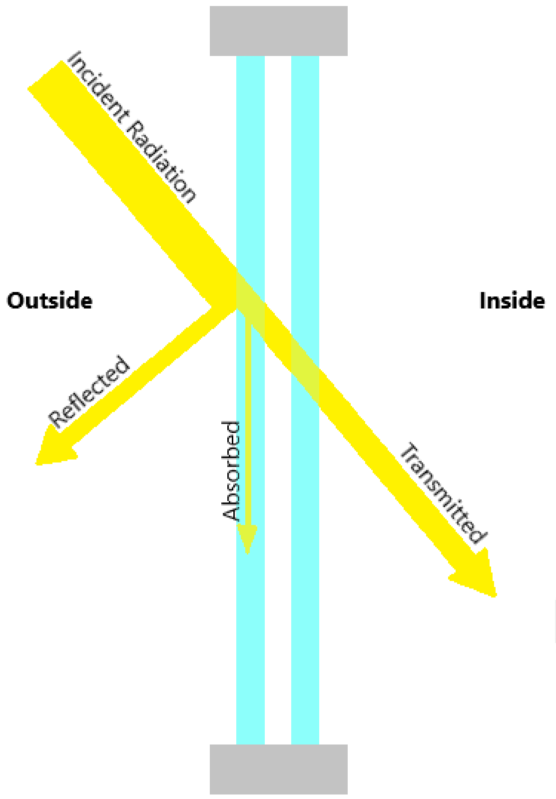

Figure 4.1: Simple sketch of reflected, absorbed and transmitted parts of incident radiation from the Sun on window.

Solar load model enables two-band spectral radiation model while being used with S2S radiation model as mentioned in Chapter 2.2.3 Radiative Heat Transfer Analysis and under Solar Load Model. Therefore, both visible and infrared absorptivity and transmissivity data is needed for the window glasses. Equation 40 derived by Chang and Rhee [70] can be used for the calculation of fraction of each band. Sum of absorptivity and transmissivity values for each band can be multiplied by the corresponding fraction will give the absorptivity and transmissivity values for the spectrum.

$$F_{0\to\lambda T} = \frac{15}{\pi^4}\sum_{m=1}^{\infty}\left[\frac{e^{-m\varsigma}}{m}\left(\varsigma^3 + \frac{3\varsigma^2}{m} + \frac{6\varsigma}{m^2} + \frac{6}{m^3}\right)\right] \tag{40}$$

where $\varsigma = C_2/\lambda T = 14387.77/\lambda T$

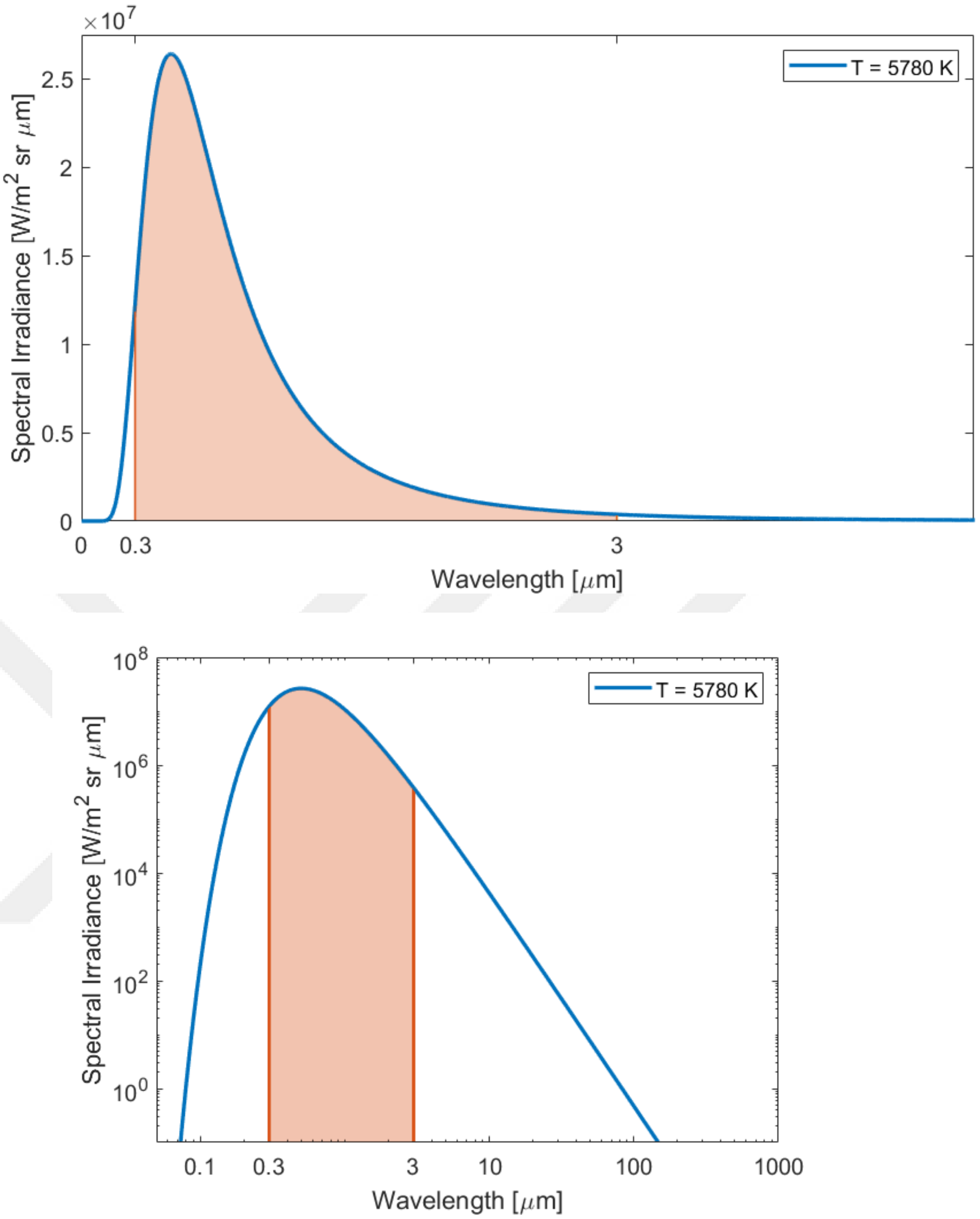

Figure 4.2: Spectral irradiance vs wavelength plot for blackbody at 5780 K (linear (upper), logarithmic (lower)).

The window glass data shown on Table 4.2 is measured for band of 0.3-3 μm and rest of the spectrum is neglected on these measurements. On Figure 4.2 measured band is marked with red and calculation of fraction of spectral irradiance on the corresponding band is done by Equation 40 with the MATLAB code on Appendix A. As seen from the results on Table 4.1 0.3-3 μm wavelength band corresponds to 94.68% of the spectral irradiance for blackbody at 5780 K. Above 3 μm wavelength the solar irradiance will not transmit through the window glass and it will be absorbed or reflected, therefore the absorbed and reflected solar irradiance on the window glass will be underestimated by 2.12%.

Table 4.1: Fraction of spectral irradiance for blackbody according to the wavelength band.

Band	Fraction of Spectral Irradiance
0 - 0.3 μm	0.0320
0.3 – 3 μm	0.9468
3 μm - infinity	0.0212

4.2. Window Glass Types

Clear and low-iron window glasses are utilized for this study. Rubin [71] did optical measurements on these types of soda lime silica glasses. Solar and visible transmissivity and absorptivity values are required by the Solar Load model coupled with S2S radiation model on ANSYS Fluent 19.2. Solar transmissivity, solar absorptivity, visible transmissivity and visible reflectivity values were given on the paper for various incident angles and glass thicknesses ranging between 2.5-25 mm. Solar reflectivity and visible absorptivity are derived from the "$\tau + \alpha + \rho = 1$" as mentioned on the previous subsection Chapter 4.1 Window Glass Optical Properties. Solar spectrum is given as 0.3-3μm on the paper and visible spectrum is 0.4-0.7 μm. Transmissivity, absorptivity and reflectivity values for infrared spectrum are derived from the using these relations.

Table 4.2: 5mm thick clear and low-iron window glasses' transmissivity (τ), absorptivity (α) and reflectivity (ρ) values for visible and infrared bands at 70° (summer) and 30° (winter) altitude angles by Rubin [71].

Altitude Angle [deg]	Window Type	$\tau_{visible}$	$\alpha_{visible}$	$\rho_{visible}$	τ_{IR}	α_{IR}	ρ_{IR}
70	Clear	0.693	0.039	0.268	0.587	0.172	0.241
70	Low-iron	0.717	0.009	0.274	0.689	0.045	0.266
70	Grey	0.325	0.479	0.196	0.346	0.456	0.198
30	Clear	0.884	0.033	0.083	0.776	0.152	0.072
30	Low-iron	0.908	0.007	0.085	0.881	0.039	0.080
30	Grey	0.480	0.464	0.056	0.505	0.439	0.056

When choosing a window glass transmissivity, absorptivity and reflectivity are the key parameters in terms of optics next to thickness of the glass itself. Absorptivity of the window glass is proportional with the amount of heat absorbed from thermal radiation and transmissivity is proportional with the amount of thermal radiation incident on the window glass that passes through. Therefore, when choosing window at hotter climates high absorptivity will help to keep the heat more on window glass rather than letting it through to interior of the building. Also, highly reflective windows will reflect most of the thermal radiation incident on them and this will help to keep the interior cooler. For colder climates low absorptivity and reflectivity should be looked for when choosing a window glass to receive most of the solar radiation by the interiors.

While calculating absorption by a single spectral line with no scattering effects there is a relationship between the spectral absorptance $\alpha_\lambda(S)$ and spectral absorption coefficient $-\kappa_\lambda$ as seen on the Equation 41 below, which is a function of the spectral absorption coefficient and distance along the path of radiation S to calculate spectral absorptance acquired from Howell et al. [7]. Distance of path can be calculated by the thickness of the glass and altitude angle of the Sun.

$$\alpha_\lambda(S) = 1 - e^{-\kappa_\lambda S} \tag{41}$$

As the glass gets thicker and the altitude angle of the Sun increases the absorptance increases and the amount of solar radiation absorbed by the window glass increases for this case. Thinner glass will absorb minimal amount of the incident radiation, which is the case for most of the window glasses. Absorption coefficients on corresponding wavelength for the glasses used on this study (can be seen on the Figure 4.3) is on a mostly increasing trend after wavelength of 0.4 µm for the rest of the spectrum. Therefore, the absorptance increases after wavelength of 0.4 µm and after 2.7 µm most of the solar radiation incident on the window glass will be absorbed and smaller percentage will be transmitted through. This will happen on the indoor side of the window glass as well for thermal radiation with wavelength above around 2.7 µm which causes the greenhouse effect for indoor environments.

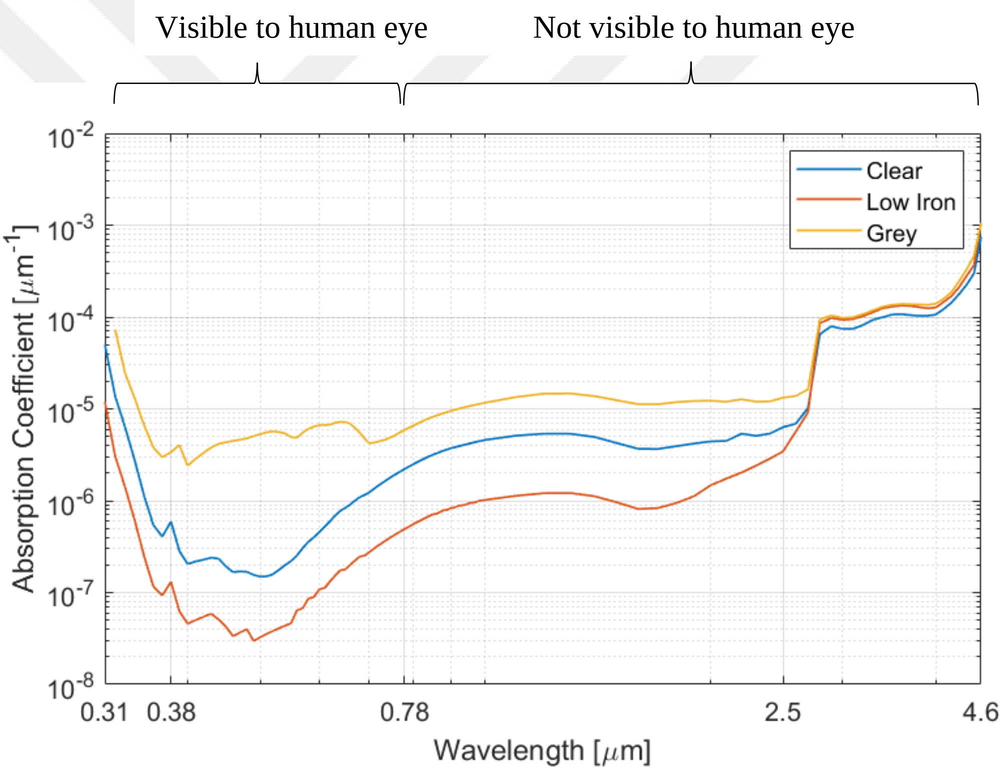

Figure 4.3: Absorption coefficients for clear, low-iron and grey soda lime silica glasses for wavelength range of 0.28-4.6 µm measured by Rubin [71].

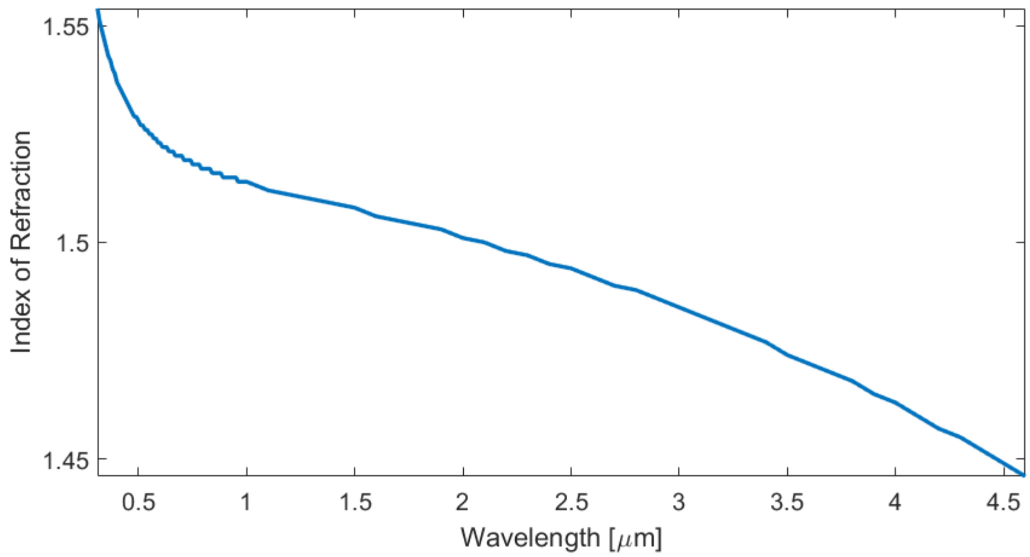

Figure 4.4: Refractive index of soda lime silica glasses for wavelength range of 0.28-4.6 μm measured by Rubin [71].

Electrochromic windows are state of the art technology and has potential to provide great solutions to thermal and visual comfort problems as shown on the work by Lee and Tavil [31], but it has a downside for now when compared to window glasses compared on this thesis, the price difference. It is a great approach for the problem and will help making some buildings more energy efficient, but that price difference cannot be justified by most of the people. Therefore, it will not have an impact on energy efficiency in the buildings soon. Eventually prices will go down as with all new technology that is when it has potential to make greater impact. Besides the price difference Lee and Tavil [31] mentioned that “Energy and peak demand reductions can be significantly greater if the reference case does not have exterior shading or state-of-the-art glass” therefore using external solar shades with regular windows can decrease the energy efficiency difference between electrochromic windows and regular windows.

CHAPTER V

PHOTOVOLTAIC PANELS FOR SOLAR SHADE INTEGRATION

5.1. *Photovoltaic Panel System*

Photovoltaic (PV) panels are used for generating electricity from solar radiation incident on them. PV panels consists of photovoltaic cells, which adds up to form the panel, work according to the photoelectric effect and the theory behind it is proposed by Albert Einstein in 1905. Photons incident on the PV panels create a flow of electrons, therefore generating electricity. Output of PV panels is in DC current and it needs to be converted to AC current to be used at our homes. Invertor makes this conversion from DC to AC current. Simple schematics of a PV panel system can be seen on Figure 5.1.

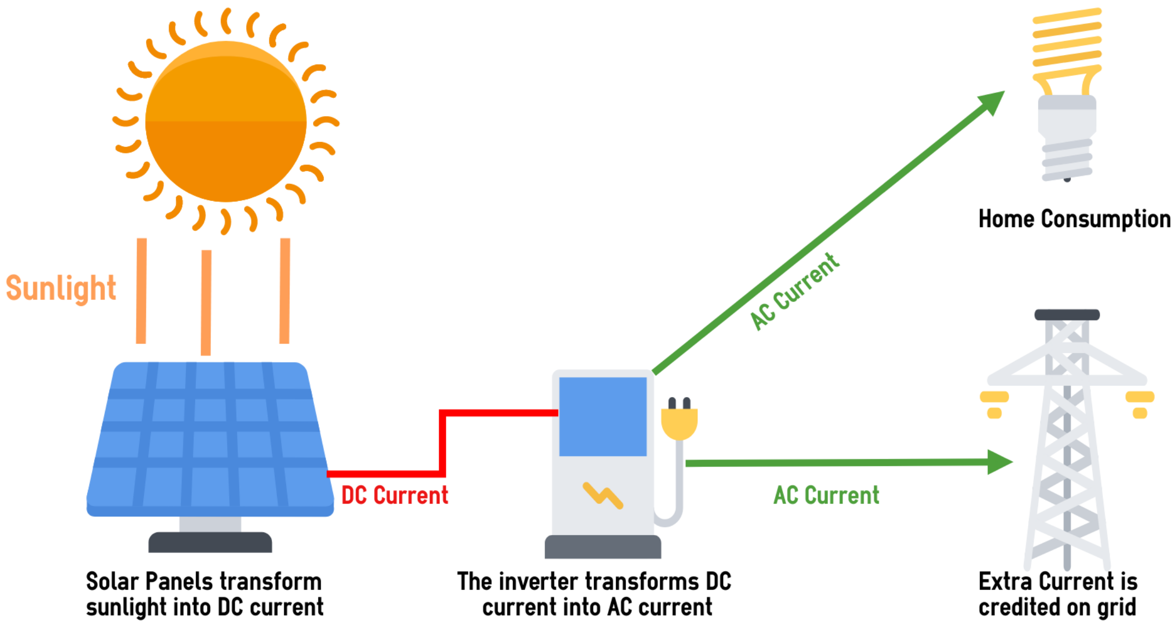

Figure 5.1: Schematics of PV Panel System [72].

Both efficiencies of PV panels and inverters effect the electricity generated. Few factors decrease the efficiency of PV panels:

- PV panels generate the maximum electricity when the light hits it perpendicularly, therefore misalignment of the PV panel can have significant power loss as the angle of misalignment increase according to D'cruz et al. [73]. (see Figure 5.2)
- Higher temperature of PV panels causes power loss according to Popovici et al. [74]. (see Figure 5.3)
- Dust on the PV panels decrease the surface area of the PV panels and decrease the electricity generation accordingly.

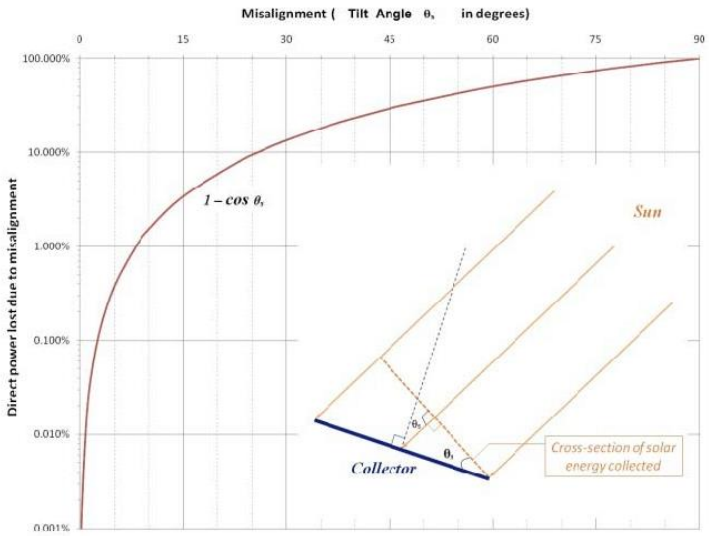

Figure 5.2: Power loss on PV panels due to angle of misalignment by D'cruz et al. [73].

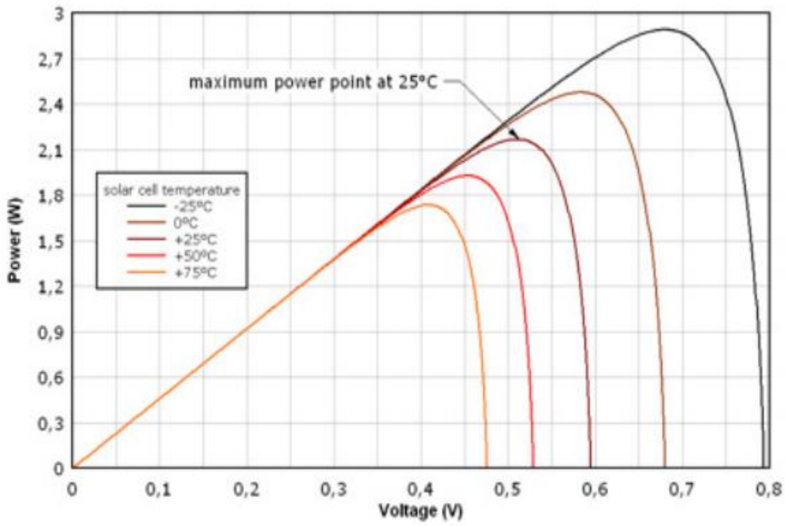

Figure 5.3: Power loss due to temperature of PV panel by Popovici et al. [74].

According to EnergySage [75] there are three major types of PV panels available on the market which are monocrystalline, polycrystalline and thin-film. Monocrystalline has the highest efficiency and thin-film has the lowest efficiency among these three types. Monocrystalline panels have efficiency higher than 20%, polycrystalline panels have efficiency around 15-17% and thin-film panels have efficiency around 11%. Monocrystalline is the most expensive type and thin-film is the least expensive type. Thin-film panels are also lightweight, flexible/semi-flexible and can be manufactured in various sizes unlike the monocrystalline and polycrystalline panels, which makes them easy to install on places that cannot withstand heavy weight of monocrystalline panels. These properties of thin-film PV panels make them ideal type of PV panel to assemble on a solar shade to generate electricity from the solar radiation that it blocks from reaching the building.

5.2. PV Panel Data and Electricity Generation Calculations

Electricity generation of a PV panel can be calculated by product of the incident solar radiation on the PV panel surface, loss factor due to misalignment from Figure 5.2, area of the PV panel that is exposed to direct solar irradiance, efficiency of the PV panel and efficiency of the inverter (usually around 98%). Then losses through the wiring and batteries can be deducted from the result.

PV panels should be chosen small and light enough to fit on solar shades without needing to design huge solar shades to provide surface area for conventional PV panels. During the past years, these small PV panels became more available in the market and Table 5.1 shows specifications of an example PV panel that can be mounted on solar shades.

Table 5.1: Specifications of an example flexible PV panel strip for electricity generation calculations sold by Shenzen Portable Electronic Technology Co. Ltd.

Type	Polycrystalline Silicon
Power	0.6 W
Voltage	6 V
Efficiency	24%
Size	151.9 x 20.8 x 2.0 mm
Weight	10 g
Price	USD$1.65
Date	March 2021

Maximum power output of 0.6 W per PV panel on Table 5.1 is supplied on optimum conditions at optimum operating temperature, when directly facing the Sun with no dust on the panel or no cloud in the sky to block the Sun and maximum amount of solar irradiance available.

According to solar irradiance calculator of Solar Electricity Handbook [76], which works with 22 years of data, comparison for stable solar shade system and monthly adjusted system has been made. For a façade facing 45° South West in Istanbul (Façade of the case study office in Ozyegin University) stable system should be kept at 49° altitude angle for maximum efficiency in terms of electricity generation from PV panels. Figure 5.4 compares the stable solar shade system to monthly adjusted system for the comparison of electricity generation. Monthly adjusting the altitude angle of solar shades to monthly optimum level provides 5.3% more solar irradiance on PV panels throughout the year and this will result in higher electricity generation.

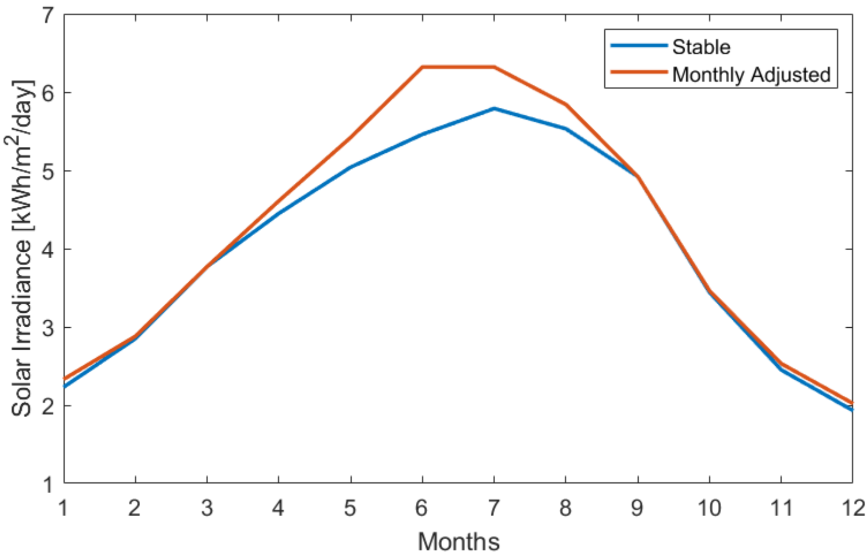

Figure 5.4: Comparison of daily average solar irradiance per meter square on PV panels for stable and monthly adjusted systems through the months.

According to International Energy Agency energy consumption per capita in Turkey was 3.3 MWh in 2019 [77]. The case study in Chapter 6 Results Based on Numerical Modeling Studies has floor area of 18.85 m^2 and window area of 3.03 m^2. Assuming a single person is living at a 50 m^2 house it would have 8.03 m^2 window area according to the window to floor area ratio of the case study. If we design a solar shade system integrated with PV panels that is shown on Table 5.1 that covers 40% of the window area, we will have 3.2 m^2 of PV panel area. The energy generation of the PV panels can be calculated according to the solar irradiance plot on Figure 5.4 for a stable system and a monthly adjusted system. Sum of solar irradiance per year is calculated by multiplying the sum of monthly average values on Figure 5.4, which will be multiplied by the PV panel area, efficiency of the PV panels and efficiency of the inverter (assumed to be 98%). The result is 13.9 MWh/year of electricity generation for monthly adjusted system and 13.2 MWh/year for a stable system. The monthly adjusted system is 5.3% is more efficient than a stable system as mentioned before. This calculation neglects the losses due to high temperature of the PV panel and blocking on the PV panel such as dirt.

5.3. *Financial Considerations of Photovoltaic Panels*

Turkey has huge potential for solar energy as mentioned in Chapter 1 Introduction with Figures 1.2 and 1.3, but we hardly make use of this readily available, free and clean energy resource. There are economical and environmental reasons to adapt solar energy into our lives. The electricity prices in Turkey are rising each year as seen on Figure 5.5 and the price has nearly tripled in the last decade. In bachelor thesis by Yelekci and Elmas [78], return on investment time of building integrated PV system and solar shade system was calculated to be 8 years for a 100 m^2 apartment. Since that study electricity became more expensive, PV panels became cheaper and more energy efficient.

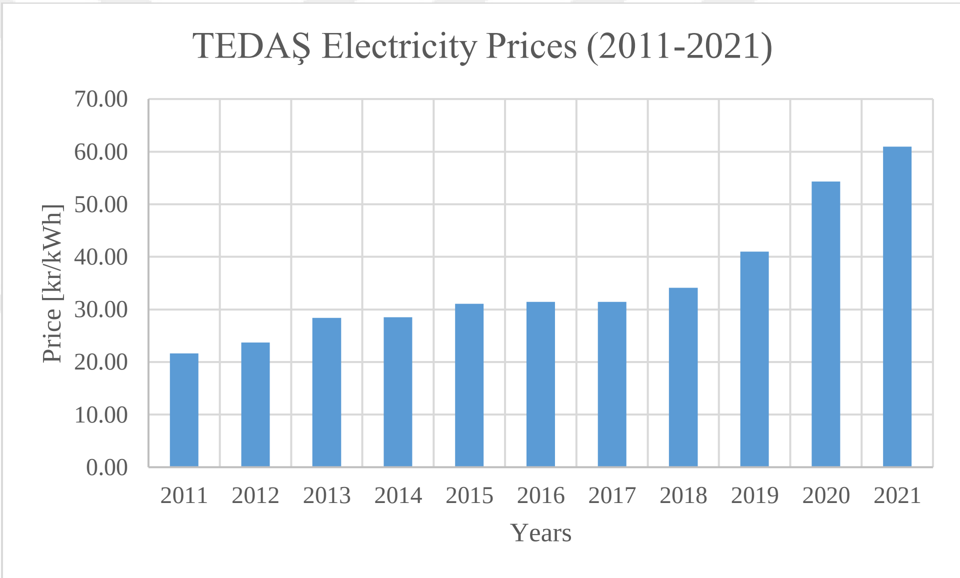

Figure 5.5: Electricity prices in Turkey between 2011-2021 [79].

On Table 5.2 first row (2017) shows the prices of semi flexible PV panels (100 W per PV panel) and a 1500 W inverter system in 2017 taken from the bachelor thesis by Yelekci and Elmas [78], second row (2021.A) is the same system with prices from 2021 and the third row (2021.B) is also same system with the prices of 2021. First two systems uses bigger PV panels (about ~1 m^2 per PV panel) but the third row uses smaller PV panels (about ~0.003 m^2 per PV panel) shown on Table 5.1. This gives better opportunities for the design of solar shade system where the PV panels. The system with bigger panels is about ~24% cheaper in 2021 compared to 2017 in terms of PV panels and an inverter. The third system is the most expensive one, but the prices of these smaller PV panels will decrease over time like the bigger PV panels as they were not readily available on the market in 2017.

Electricity prices have increased about ~94% [79] since the previous study [78] and the cost of same system has decreased about ~24%, therefore the return on investment time has decrease from 8 year to around 3.5 years. Excluding the change in prices of other components of the system.

Table 5.2: Three different PV panel system prices comparison from 2017 and 2021.

Year		Piece	Price ($)	Total Price ($)
2017	PV Panels	10	180	1800
	Inverter	1	165	165
	TOTAL			$1965
2021.A	PV Panels	10	135	1350
	Inverter	1	140	140
	TOTAL			$1490
2021.B	PV Panels	1667	1.65	2750
	Inverter	1	140	140
	TOTAL			$2890

Total solar capacity of the World is growing at an unpredictable speed. As the PV panel production increase the prices decrease. In fact "doubling production capacity reduces cost by 28%" [80]. Right now it is the cheapest power available [80]. Also with the increasing technology PV panel efficiencies inrease. Currently the record is at 40.6% efficieny, which is developed by Martin Green and his team [80]. According to Jenny Chase, head of solar analysis at BloombergNEF, "their official forecast is that solar will supply 23% of World's electricity by 2050, but she thinks that it is underestimated" [80]. It is clear from the way the PV panel industry is headed that PV panels will be dirt cheap in the near future and buildings will need to be designed to contain PV panels.

On the other hand, use of cheap solar energy is going to impact CO_2 emissions resulting from fossil-fuel use. Figure 5.6 and Figure 5.7 shows annual CO_2 emission of Turkey and World respectively according to Global Carbon Project. Significant portion of these emissions are due to heating and cooling of buildings and due to electricity production based on coal, natural gas and petroleum. It can be seen that there is a large increase in annual CO_2 emission levels over the years. Knowing that 40% of those CO_2 emissions are due to buildings according to International Energy Agency [1] we can significantly decrease annual CO_2 emissions by switching to solar energy in buildings and have an impact on global warming.

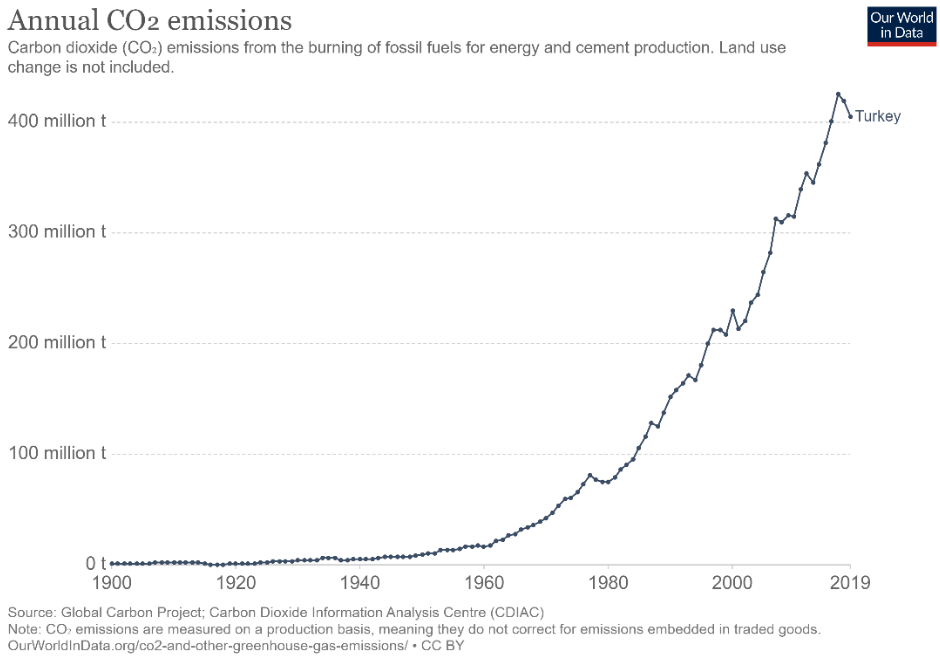

Figure 5.6: Annual CO_2 emission of Turkey between 1900-2019 in million tons [81].

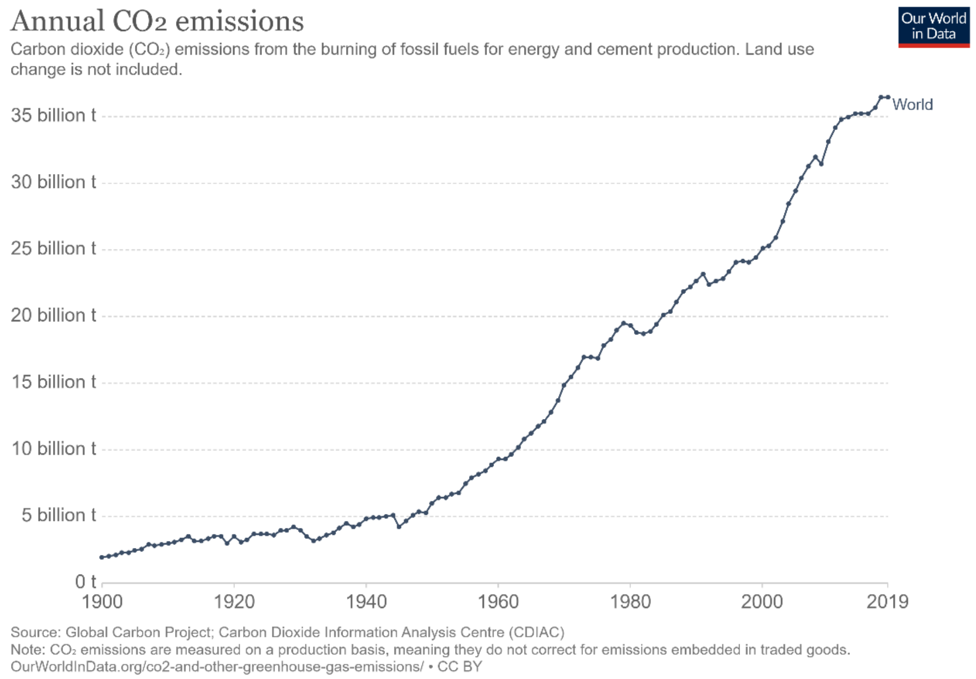

Figure 5.7: Annual CO_2 emission of the World between 1900-2019 in billion tons [81].

CHAPTER VI

RESULTS BASED ON NUMERICAL MODELING STUDIES

The effects of various parameters (window glass types, solar shade coverage factors, weather conditions, partition aspect ratio and floor material) on temperature distribution throughout the office space and thermal comfort of the occupants of the office are analyzed numerically in this section.

Cases are chosen with various combinations of the selected parameters to be analyzed. Numerical model is validated with an experimental and a numerical (CFD) study. The model contains a single window, inlet and outlet. There are two manikins located on the opposing sides of the desk divided by a partition. SpaceClaim, ANSYS Fluent 19.2 and CFD-Post 19.2 are used for this numerical analysis. Shear Stress Transport (SST) k-ω turbulence model was chosen to best model the flow near surfaces. The Surface-to-surface (S2S) radiation model is used to model the diffuse radiation along with two-band (visible and IR) solar load model. The results are shown in forms of contours, vectors, tables and plots. Finally, the results are discussed for each parameter by comparison.

All the parameters studied on this thesis interfere with the amount of sunlight incident to the office windows. This study analyzes only the thermal aspects of the solar irradiance, yet there is also visual comfort associated with the available solar light. Neglecting this aspect may cause visual discomfort and increase use of artificial lighting, which eventually decreases the energy efficiency of buildigns. ANSYS Speos can be used for the optical simulations of visual comfort in the office space and for the computation of the irradiation map for the solar load [82].

6.1. *Description of Cases Considered*

Several cases (see Table 6.1) are chosen to study combinations of three window types (clear, low-iron, and grey), three solar shade coverage fractions of the window (0.0, 0.4, and 0.8), three weather scenarios (see Table 6.2), two partition height to ceiling height aspect ratios (0.3 and 0.5), and two floor covering materials (carpet and ceramic tiles). These parameters used for these cases are chosen to analyze both the best and worst cases the test room can experience and to observe the effects of different parameters on air temperature distribution, surface temperature distribution, air velocity and mean radiant temperature of the occupants.

Table 6.1: List of cases with corresponding parameters that are analyzed on ANSYS Fluent 19.2.

Case Number	Window glass type	Solar shade coverage	Weather condition	Partition aspect ratio	Floor material
1	Clear	0	Summer	0.3	Carpet
2	Low-iron	0	Summer	0.3	Carpet
3	Grey	0	Summer	0.3	Carpet
4	Clear	0	Summer	0.3	Ceramic tile
5	Clear	0	Summer	0.5	Carpet
6	Clear	0.4	Summer	0.3	Carpet
7	Clear	0.8	Summer	0.3	Carpet
8	Clear	0.8	Summer	0.3	Ceramic tile
9	Clear	0	Summer	0.5	Ceramic tile
10	Clear	0.4	Summer	0.3	Ceramic tile
11	Clear	0	Winter	0.3	Carpet
12	Clear	0	Winter 2	0.3	Carpet
13	Low-iron	0	Winter	0.3	Carpet
14	Grey	0	Winter	0.3	Carpet
15	Clear	0.4	Winter	0.3	Carpet
16	Clear	0.8	Winter	0.3	Carpet

Cases are chosen to compare parameters at two different environments, for example cases 1, 2 and 3 compares window types at summer and cases 11,13 and 14 compares same window types at winter, while keeping the other parameters constant.

Weather data sown on Table 6.2 is acquired from Weather Spark [83]. Heat transfer coefficient (HTC) for the façade is derived from the wind speed data by the relationship used by Vincent [11] (see Figure 6.1). Summer case is average weather for 21st of June and winter case is average data for 21st of December. Winter 2 case is an extreme winter case with lower air temperature and higher wind speed. The altitude angle is highest throughout the year for summer case and lowest for the winter case.

Table 6.2: Outside air temperature, Sun's altitude angle, cloud coverage in the sky, outside heat transfer coefficient for wall and window and inlet air temperature for studied weather conditions.

Weather Condition	Temperature [°C]	Altitude angle [deg]	Cloud coverage	Heat transfer coefficient [W/m²K]	Inlet air temperature [°C]	Relative Humidity
Summer	26	70	0	23	20	65%
Winter	9	28	0.9	26.6	22	78%
Winter 2	0	28	1	45	22	78%

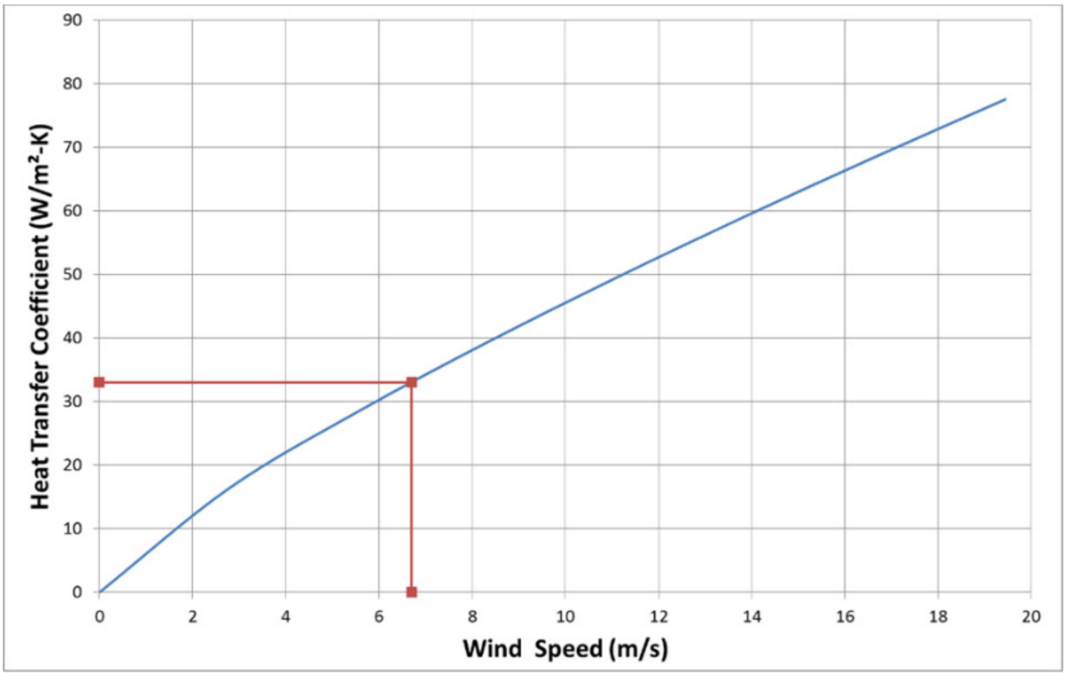

Figure 6.1: Wind speed vs HTC plot to calculate the HTC on the façade to use on CFD according to Vincent [11].

6.2. Mesh Independence and Validation of the Numerical Model

Validation study for the CFD model was done according to the experimental data obtained by Li et al. [51] and numerical validation done by Gilani et al. [52]. The experiment was done for an empty enclosure other than a cubical heat source that either had power output of 300 W or 600 W and walls were either covered with aluminum sheet or black paint according to case. There was a single inlet on the floor level and an outlet in the enclosure (can be seen on Figure 6.2).

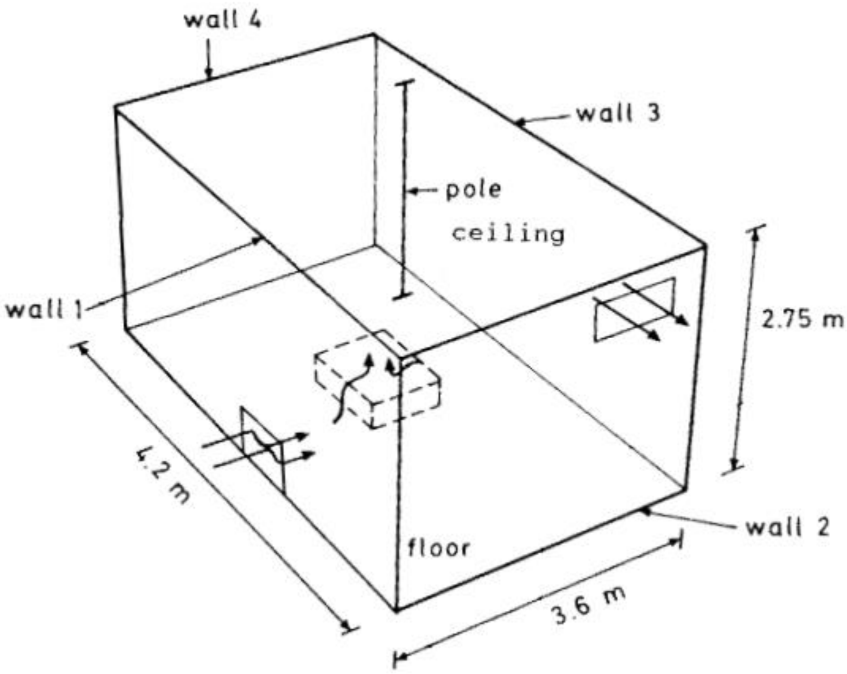

Figure 6.2: Experimental test room geometry used by Li et al. [51].

B1 case from the experiment was chosen as the validation case by Gilani et al. [52], due to most amount of result data available on the paper by Li et al. [51]. According to Gilani et al. [52] B1 case had 300 W power output at the cubical heat source, all the walls were painted black, inlet air temperature and speed were 16°C and 0.102 m/s, respectively. Measured ceiling and floor temperatures were 24.5°C and 24°C, respectively. Calculated heat transfer coefficient on the walls were 10 W/m^2-K. Pole (shown on Figure 6.2) contained 22 thermocouples on the experimental setup and validation was done by those thermocouple readings shown on Figure 6.3. Figure 6.3 indicates the aspect ratio of the point divided by the ceiling height as z/H on y-axis and temperature difference between local temperature and inlet temperature on x-axis. Validation was done for meshes with 0.3 million, 0.7 million and 1.25 million elements, as to do the mesh independence study on the same setup. As the number of elements increase results slightly converged towards the experimental data for z/H value of 0.1 to 0.4, rest remained unaffected.

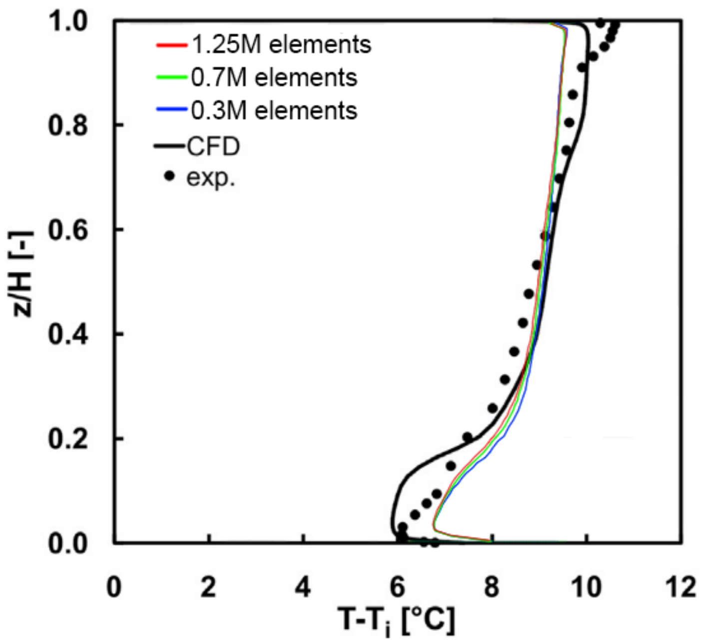

Figure 6.3: Comparison of temperature on the pole between results of experimental [51], CFD [52] and current study (blue, green, and red lines).

Validation of the CFD was conducted by ANSYS Fluent 19.2 software. Turbulence model was chosen as Shear-Stress Transport (SST) k-ω model according to Gilani et al. [52]. The Boussinesq approximation was used to simulate the buoyancy effects properly due to natural convection. Constant air density led to jet like flow from the inlet and the plume was not properly formed above the heat source, this caused divergence from the temperature contours (see Figure 6.4 below) of the validation study by Gilani et al. [52]. This issue with the validation study was solved by modelling the natural convection by the Boussinesq approximation. Air properties considered are as follows: density is 1.17 kg/m^3, specific heat is 1006.95 J/kg-K, thermal conductivity is 0.026 W/m-K, viscosity is 1.83x10^{-5} kg/m-s and thermal expansion coefficient is 0.003 K^{-1}. Operating pressure and operating density are set to 101325 Pa and 1.17 kg/m^3. Radiation model was chosen as surface-to-surface model (S2S). Pressure velocity coupling was chosen as Coupled. Pressure discretization was chosen as PRESTO! to modelling of the natural convection by buoyancy effects according to ANSYS Fluent User Guide. Momentum and energy discretization were second order upwind. Maximum y* value of 1.8 was reached as in the validation study. A chimney was modelled to the outlet to prevent the reverse flow by increasing the outlet velocity due to decreasing cross-sectional area. As can be seen by comparing

Figure 6.4.b to Figure 6.4.d this chimney model had no significant effect to the temperature distribution.

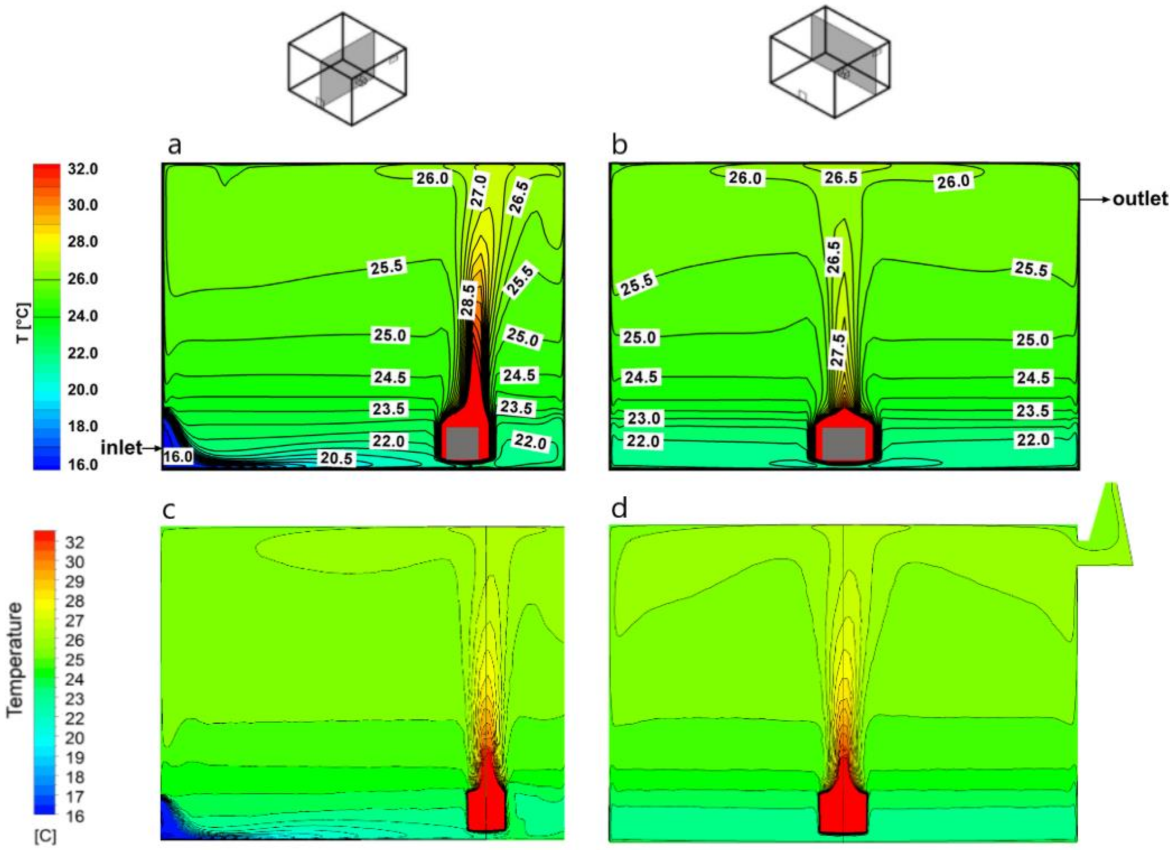

Figure 6.4: Air temperature distribution comparison of Gilani et al. [52] (a and b) to current study (c and d). Location of cross-sectional plane is indicated on top [52].

Initially the air was modelled with constant density in the numerical validation study, which lead to divergence from the results obtained by both Li et al. [51] and Gilani et al. [52]. Then changing the density of the air using the Boussinesq approximation solved this issue. The Boussinesq approximation calculates density differences when gravitational acceleration terms is present, to model the natural convection properly.

There are a few possible reasons for the temperature difference between the experimental results and this numerical validation study especially for the results near the floor and ceiling levels:

- Air rate change of 1 h^{-1} in the experimental study was converted to fixed inlet air speed of 0.102 m/s both in study by Gilani et al. [52] and this numerical validation study to conduct a steady state analysis. This was calculated from required speed of air from the inlet area in order supply air at the size of volume of the room each hour. This nonuniformity of the air supplied might have caused the difference between the experimental data and this CFD validation study near the floor.
- The inlet had diffuser on it which decreases the area to 50% in the experimental setup and instead of modeling this diffuser the inlet area was reduced both in the validation study by Gilani et al. [52] and this numerical validation study. This might have been another cause of air temperature difference between the experimental and the numerical study near the floor.
- The pole in the experimental study [51] was used to install the thermocouples in the experimental setup, but there was no detail given on the structure of the pole in the experimental study. The pole was not included in the numerical study, instead, a line was placed in the post-processing to get temperature readings in the location of the pole in experimental setup. The physical pole in the experimental study might have altered the results due to blockage on the flow on the two ends along with either the ceiling or floor.
- In their experimental study Li et al. [51] stated that “The impingement of the thermal plumes leads to radially spread flow along the ceiling. Higher temperature in the flow forms a warm gravity current along the ceiling.” According to Wang and Chen [84] the Reynolds Averaged Navier Stokes Equations (RANS) models are good for modeling simple models with plume; however, the accuracy of Large Eddy Simulation (LES) is more accurate and stable. This limitation of RANS model might be the reason for not modelling the upper portion of the plume along the ceiling accurately.
- Finally, the given temperature boundary conditions on the walls for the numerical study may be the cause of this temperature difference as also stated in the numerical validation study by Gilani et al. [52].

6.3. *Numerical Modeling of Different Cases*

6.3.1. Geometry and Mesh Selection

Geometry is based up on an office at Center for Energy, Environment and Economy (CEEE) in Academic Building 4 (AB-4) at Ozyegin University. The geometry contains a desk with partition in the middle of the desk for two occupants of the office space, a window from floor to the ceiling, single inlet, and outlet for ventilation, and two occupants (see Figure 6.5). There are two different geometries used on this study first one has a partition with partition height to ceiling height aspect ratio of 0.30 and the second geometry has partition height to ceiling height aspect ratio of 0.50.

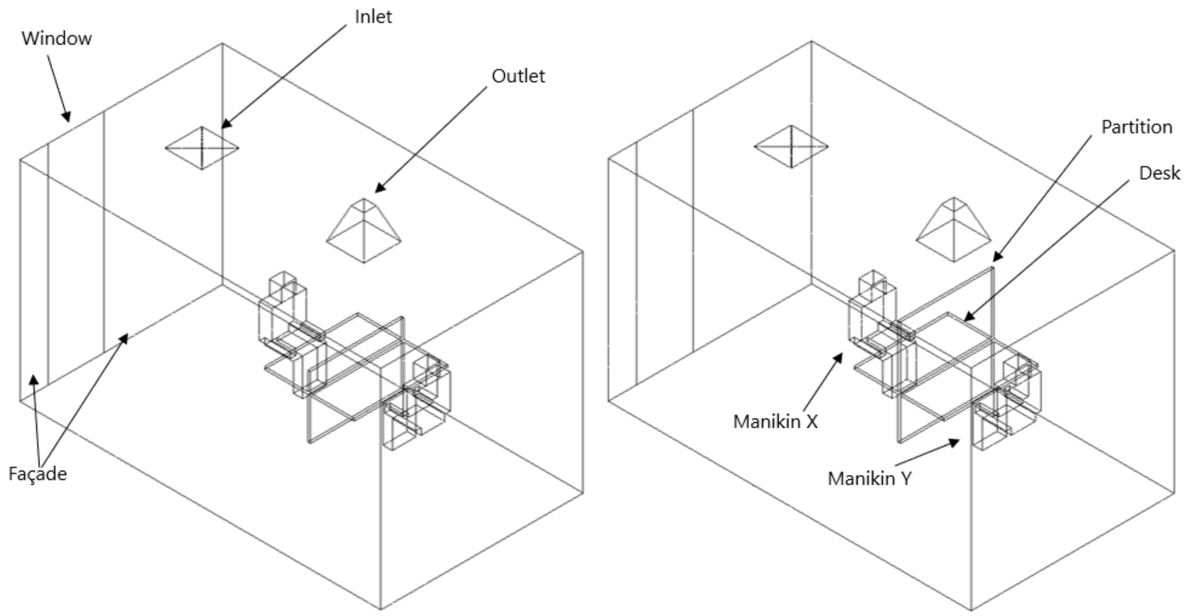

Figure 6.5: Two geometries of the office for CFD analysis with two manikins with 0.30 partition aspect ratio (left) and 0.50 partition aspect ratio (right).

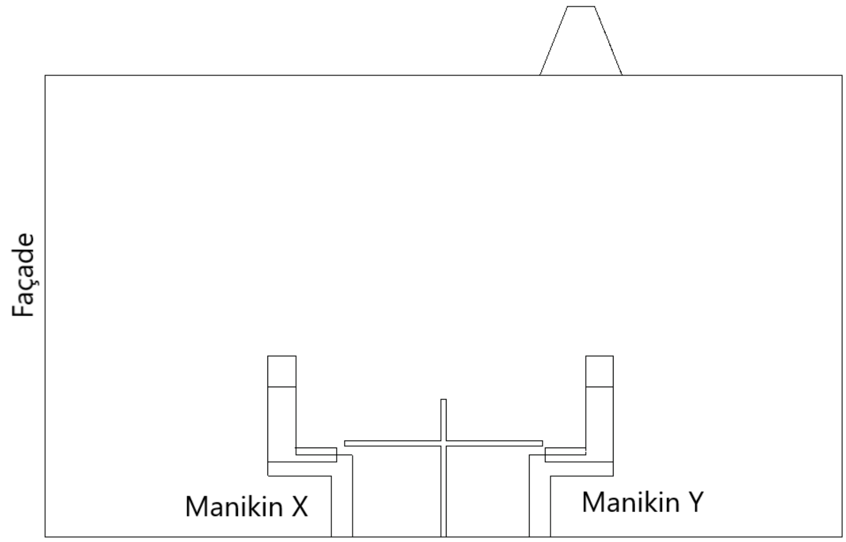

Figure 6.6: Side view of the CFD geometry (window is located to the left) with 0.3 partition aspect ratio.

Both inlet and outlet are 0.6 x 0.6 m. The inlet is divided into four parts by two diagonal lines (see Figure 6.9) each quadrant of the inlet blows air with 1 m/s speed and direction from center to the outer corner of the quadrant with a 20° angle from the ceiling. This approach is used on the paper by Sun and Smith [85] to keep the mesh element sizes minimum by not modelling a diffuser, which increases the mesh count and required computational power significantly. Outlet area is decreasing to 10% of the initial area with rising height like a chimney as mentioned on the validation CFD analysis. This is modelled to prevent reverse flow which might occur in the CFD analysis and has no significant effect on the results as shown on the Chapter 6.2 Mesh Independence and Validation of the Numerical Model. Desk is adjacent to the wall, and it is 2.88 m away from the façade. It has height of 0.7 m, width of 1.5 m, length of 1.4 m and thickness of 0.04 m. Only the façade and window are exposed to outside. All other walls, ceiling and floor are internal walls. Two simple manikins are sitting on the opposing sides of the desk with no chair modelled under them. Each one is divided into three regions: head, upper body, and lower body.

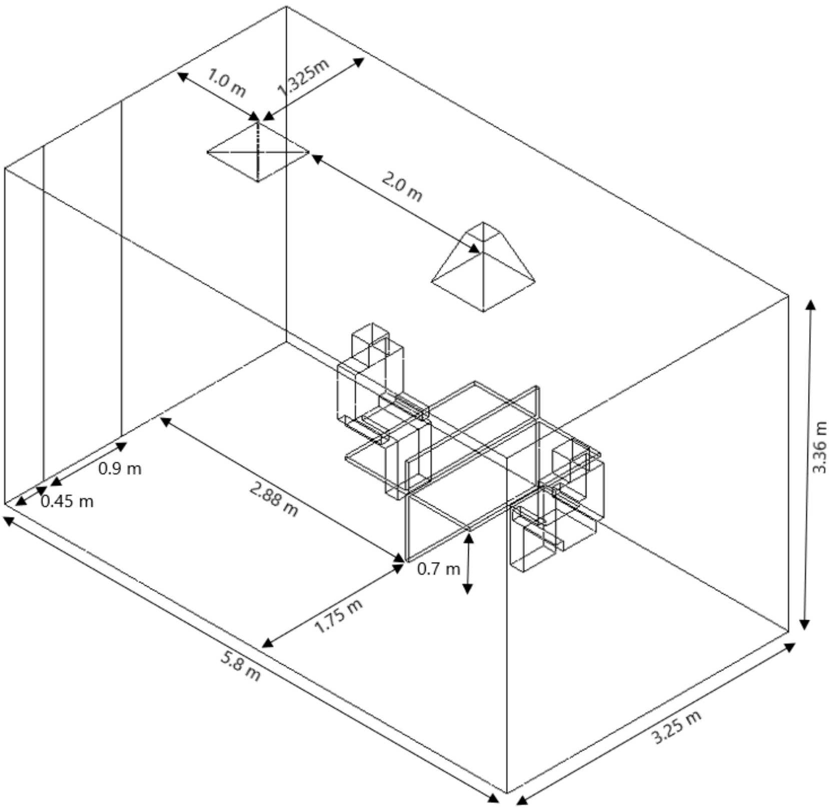

Figure 6.7: Geometry with dimensions.

Materials assigned to desk and partition are oak wood, window is glass (0.010 m thick in total), interior walls and ceiling are concrete (0.15 m thickness), floor is either carpet (0.005 m thickness) or ceramic tiles (0.020 m thickness) depending on the case, façade is concrete (0.15 m thickness) and urethane (0.075 m thickness) for insulation. All the properties required for the Fluent are given on Table 6.3. Only the desk and partition are modelled as solid in the analysis, all other surfaces are modelled as shell conduction by inputting the thickness and materials. Manikins are modelled hollow, and emissivity of the manikins are taken as 0.95 according to de Dear et al. [86].

Table 6.3: Material properties for glass, concrete, wood (oak), urethane, carpet, and ceramic tiles. ([a]Çengel and Ghajar[56], [b] McNeil [87], [c] King [88]).

Materials	Density [kg/m3]	Specific heat [J/kg-K]	Thermal conductivity [W/m-K]	Emissivity
Glass	2800[a]	750[a]	0.7[a]	0.9[a]
Concrete	2300[a]	880[a]	1.4[a]	0.93[a]
Wood (Oak)	545[a]	2385[a]	0.17[a]	0.9[a]
Urethane	70[a]	0.026[a]	1045[a]	-
Carpet	345[b]	1420[a]	0.193[b]	0.75[a]
Ceramic tiles	2350[c]	1260[a]	1.484[c]	0.85[a]

The mesh is a polyhedral mesh generated in ANSYS Fluent Meshing 19.2. Watertight mesh workflow is used. First the surface mesh is generated with maximum element size of 75 mm, minimum element size of 10 mm and growth rate of 1.2. Then volume mesh is generated with maximum cell length of 100 mm and growth rate of 1.2. The inflation method is uniform first layer height is 1 mm with 15 layers and growth rate is 1.3. Inflation dimensions are chosen to provide smooth transition to the volume mesh. Inlet and outlet were chosen as walls during the meshing process to prevent stair stepping or contraction (see Figure 6.10, inflation is uninterrupted on the ceiling), which would decrease the quality of the mesh. They are converted back into velocity inlet and pressure outlet boundary conditions from the solver. Mesh for both geometries have decent minimum orthogonal quality as seen on Table 6.4, which at least needs to be 0.15. Maximum y+ value for both meshes is under 5, which makes them usable for Shear Stress Transport (SST) k-ω turbulence model.

Table 6.4: Cell counts and minimum orthogonal qualities of both meshes.

Geometry	Cell Count	Minimum Orthogonal Quality	Maximum y+
0.30 Partition aspect ratio	739,069	0.24	4.3
0.50 Partition aspect ratio	750,830	0.21	4.7

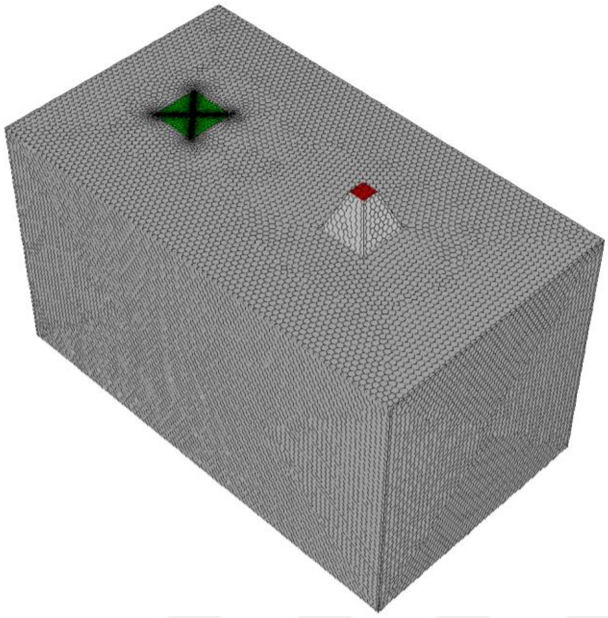

Figure 6.8: Polyhedral mesh of the geometry from outside iso view.

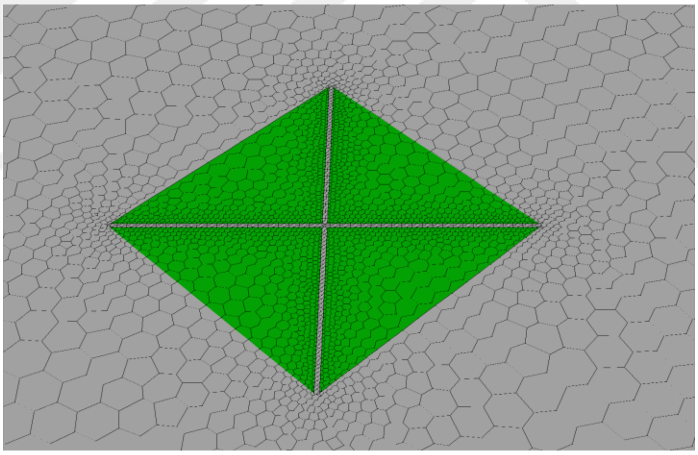

Figure 6.9: Close-up mesh of the inlet (0.6 x 0.6 m).

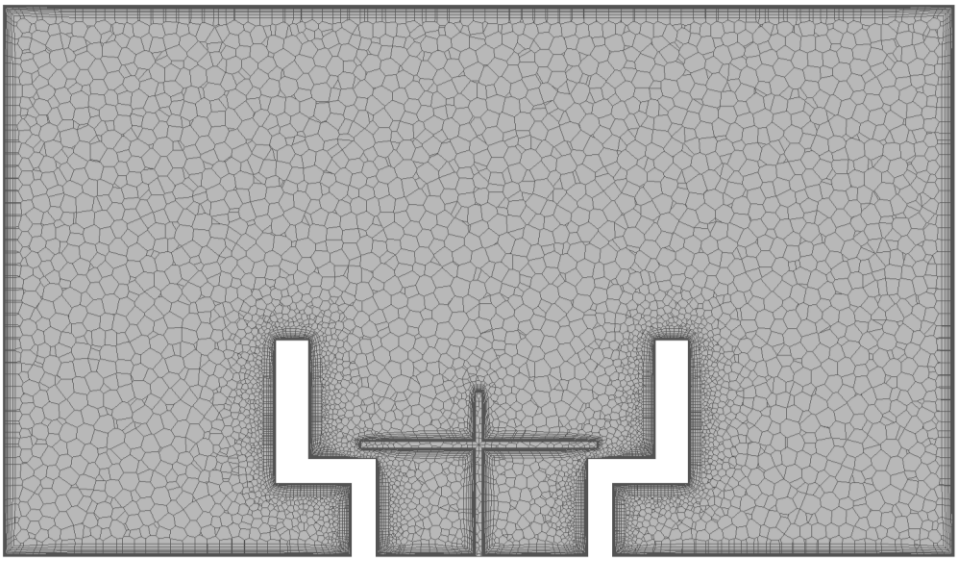

Figure 6.10: Slice of the mesh through the desk, partition and manikins showing the inflation layers.

6.3.2. Solver Settings and Parameters

- *Physical Models*

These analyses were run on steady state pressure based solver. Operating conditions are set to 101325 Pa operating pressure, 24.5°C operating temperature for Boussinesq approximation parameters and operating density of 1.17 kg/m^3.

Shear Stress Transport (SST) k-ω turbulence model was chosen. There are various studies in literature for SST k-ω and k-ε turbulence models. Generally, k-ω models the near wall regions and k-ε models the volume better. The reason behind choosing SST k-ω for this study is because near wall regions are the concern of this study and the CFD validation study by Gilani et al. [52] of the experimental study Li et al. [51] is done by the SST k-ω turbulence model.

The Surface-to-surface (S2S) radiation model is used because the case is diffuse and there is no participating media in the case studied. One radiation iteration was run per ten energy iterations not to increase the required computational power. Radiation residual convergence criteria is set to 1e-06. For view factor calculations clustering is set to manual and one face is assigned per surface cluster for flow boundary zones. View factor method was chosen as Ray Tracing and resolution is set to 100. Resolution can be increased to increase the quality of the view factors, but this increases the computational time significantly, like increasing the quality of mesh file. View factor file with these settings and hardware mentioned on Chapter 6.3.3 Hardware and Software Information took around 3 hours. Solar load model uses ray tracing algorithm, and both the Sun direction vector and illumination parameters were set manually according to the case. Direction of the Sun direction vector needs to be set from the observer to the Sun. Direct solar irradiation is set 1366 W/m^2 and diffuse solar irradiation is set to 10% of the direct solar irradiation, which is 136.6 W/m^2. If the solar shade is present in the case amount of blockage is deducted from both the direct and diffuse components. Amount of cloud coverage in the sky is deducted only from the direct component. This way effect of solar shade is modelled without modelling the solar shade itself. This decreases the mesh, view factor calculations and solution time significantly. Spectral fraction is set to 0.4 as mentioned in Chapter 2.2.3 Radiative Heat Transfer Analysis and under Solar Load Model.

- *Air Properties*

Boussinesq approximation is used to model the natural convection heat transfer best according to ANSYS Fluent User Guide 19.2. Boussinesq approximation requires density and thermal expansion coefficient input for the air and operating temperature under operating conditions. Properties of air are set to; density of 1.17 kg/m^3 with Boussinesq approximation, specific heat of 1006.95 J/kg-K, thermal conductivity of 0.026 W/m-K, viscosity of $1.83x10^{-5}$ kg/m-s and thermal expansion coefficient of 0.003 K^{-1}. According to weather data collected by CustomWeather [89] between 1985-2015 from Istanbul, lowest monthly average relative humidity is in July at 65% and highest is in January at 78%. When checking psychrometric chart for the expected room temperature of 22°C, there is 1 g/m^3 difference in density and 2 J/kg-K difference in specific heat between 65% and 78% relative humidity values. Therefore, it is neglected in the CFD analysis but later the effect of relative humidity will be discussed in the thermal comfort calculations.

- *Cell Zones*

There are two cell zone regions in the CFD model, which are desk and partition solid and volume as fluid. Rest of the walls are modelled with shell conduction, which can calculate the conduction inside the solid without having the solid on the geometry to keep the mesh minimal.

- *Boundary Conditions*

All the interior walls, ceiling and floor are set to temperature boundary condition of 22°C under thermal boundary conditions and shell conduction is set with corresponding material of the wall. In radiation boundary conditions both direct visible and direct IR absorptivity values are set same due to lack of data. They are participating both in solar ray tracing and view factor calculations.

Inlets are set to velocity inlet with magnitude of 1 m/s and direction components are entered to blow the air with 20° angle from the ceiling. Inlet air temperature is set under thermal boundary condition. Outlet is set to pressure outlet. Internal emissivity under radiation boundary conditions is set to 1 for both inlet and outlet not to alter the radiation calculations inside the office. Both participates in solar ray tracing and view factor calculations and solar transmissivity factor is set to 0 not to let solar irradiance in through the ceiling.

All the surfaces of the desk and partition is set to coupled under thermal boundary conditions due to presence of solid model underneath. Only the absorptivity values are set under radiation boundary conditions. Both participates in solar ray tracing and view factor calculations.

Both façade and window are set to mixed thermal boundary condition. Heat transfer coefficient for the outer surface is supplied from the Figure 6.1 according to wind speeds. Free stream temperature is set to outside temperature and external radiation temperature is also set to outside temperature. Temperature of the Sun is taken into calculations by the solar load model. External emissivity is set for outer surface. Under radiation boundary conditions façade is modelled as opaque and absorptivity values are entered the same for direct visible and direct IR. Radiation boundary condition for window is set to semi-transparent and direct visible and IR components of both absorptivity and transmissivity is supplied from Table 4.2 in Chapter 4.2 Window Glass Types. Diffuse hemispherical absorptivity and transmissivity values are set to 0.1 and 0.5, respectively, according to study by Adhikari et al. [90]. The view factors needs to be calculated after setting the radiation boundary conditions, because changing the surface type between opaque and semi-transparent changes the view factors.

- *Methods*

Pressure-velocity coupling is done by Coupled Algorithm. First the SIMPLE algorithm was chosen but results did not converge as they did with the Coupled Algorithm. First model was run with following spatial discretization: gradient is set to least squares cell based, pressure is set to standard, momentum is set to first order upwind, turbulent kinetic energy is set to first order upwind, specific dissipation rate is set to first order upwind, energy is set to first order upwind. After converging with these models' pressure is changed to PRESTO! to provide better modelling of natural convection due to buoyancy according to ANSYS Fluent 19.2 User Guide [60], momentum and energy are changed to second order upwind. Converging the CFD analysis with first order models and then switching up to second order models gives better convergence.

- *Initialization*

Hybrid initialization is provided for 20 iterations. Residuals converged below 1e-07 during the initialization, which yield no problem in terms of convergence of the analysis.

- *Convergence criterion*

Convergence criterion for the residuals under ANSYS Fluent 19.2 are set to; 1e-03 for continuity, x-velocity, y-velocity, z-velocity, k, omega and 1e-06 for energy equation. Control points are set on the critical regions such as desk and partition to read out both average and maximum temperatures to observe the convergence along side the residuals which may not always show the true convergence of the results. Finally, the difference between the inlet mass flow rate and outlet mass flow rate was used (shown on Table 6.5) as a convergence criterion.

- *Controls*

Controls are used to converge the CFD analysis by changing the Flow Courant Number, momentum under explicit relaxation factors, turbulent kinetic energy, specific dissipation rate, turbulent viscosity, and energy under under-relaxation factors. Decreasing these values decreases the change in results in each iteration and this can prevent the possible divergence of the analysis, but also slows down the analysis which will increase the required computational power. For the first order upwind solution of the CFD analysis Flow Courant Number is started at 100 and decreased to 50 when the residuals start to diverge. After the convergence and changing models to second order Flow Courant Number is decreased from 50 to 1 gradually by observing the residuals. Also, momentum under explicit relaxation factors is decrease from 0.5 to 0.35 and under under-relaxation factors; turbulent kinetic energy is decreased from 0.8 to 0.7, specific dissipation rate is decreased from 0.8 to 0.7, turbulent viscosity is decreased from 1 to 0.9, energy is decreased from 1 to 0.95. These explicit relaxation factors and under-relaxation factors decrease the fluctuation of the residuals as well.

The requirements of increased accuracy from computational simulations leads to longer duration simulations causes computational bottlenecks in the industry. This can be solved either by better performing computers or more efficient simulation codes, which delivers faster convergence for complex problems.

6.3.3. Hardware and Software Information

The geometries were prepared on ANSYS SpaceClaim [91] software. All the meshing and CFD analysis were done using the ANSYS Fluent 19.2 software and post-processing is done both on ANSYS Fluent 19.2 and ANSYS CFD-Post 19.2 running on HP® Z420 Workstation with hyperthreaded 12-core Intel® Xeon CPU E5-1650 v2 @ 3.50GHz processors and 32 GB RAM on 64-bit Windows® 7 Professional operating system.

6.4. *Discussion of Results*

The simulations for different cases have been carried out. These numerical simulations took about 1000 to 3000 iterations for the solution to converge depending on the case (summer cases converged faster than winter cases at around 1000 vs 3000 iterations). Figure 6.11 shows the plot for residuals corresponding to case 1.

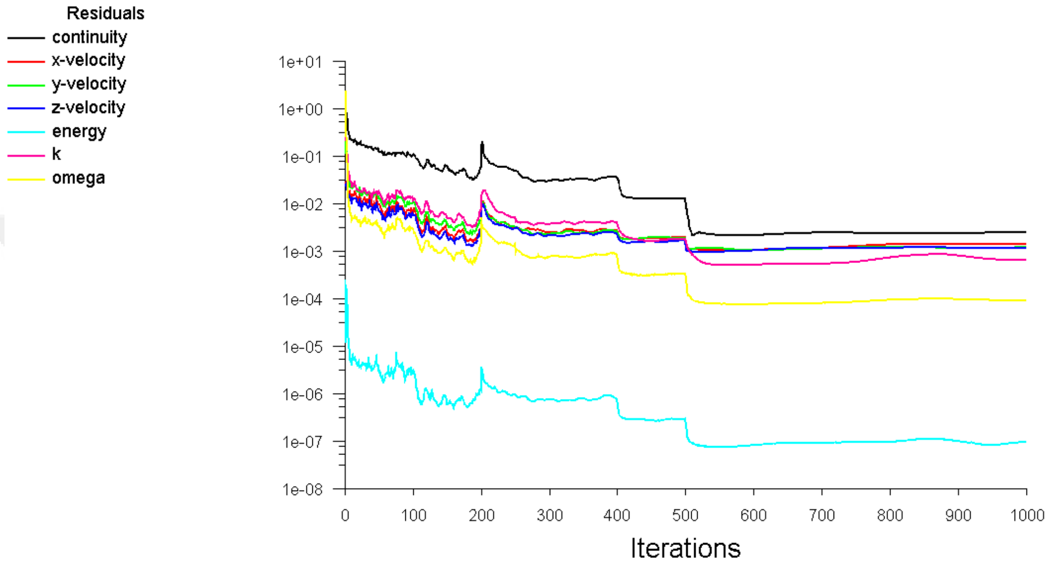

Figure 6.11: Residuals plot of case 1.

Table 6.5: Pressure difference between inlets and outlet and mass flow difference between the inlets and the outlet.

Case #	ΔP [P]	Δm_{dot} [kg/s]	Case #	ΔP [P]	Δm_{dot} [kg/s]
1	35.2	2.98E-04	**9**	35.7	-1.70E-05
2	35.1	1.34E-04	**10**	35.2	-4.50E-05
3	35.2	-2.90E-05	**11**	35.1	-5.70E-05
4	35.2	1.88E-04	**12**	34.8	5.92E-04
5	35.8	-1.60E-05	**13**	35.1	-1.80E-05
6	35.2	-2.01E-04	**14**	35.2	-1.60E-05
7	35.1	-1.08E-04	**15**	35.1	-2.30E-05
8	35.2	-2.40E-05	**16**	35.1	-1.00E-06

Note: While referring to manikins and parts of the manikins X represent the manikin closer to the façade and Y represents the manikin away from the façade on the opposing side of the desk (as shown on Figure 6.5 and 6.6).

Table 6.6: Average surface temperatures for ceiling, desk and partition facing the façade, desk and partition facing interior, floor, façade and window and average volume temperatures of desk and partition (solid) and air for each case.

Case #	Average Surface Temperature [°C]						Average Volume Temperature [°C]	
	Ceiling	Desk and partition facing façade	Desk and partition facing interior	Floor	Façade	Window	Desk and Partition	Air
1	22.2	22.7	22.6	22.4	24.0	28.7	22.9	21.7
2	22.2	22.7	22.7	22.4	23.9	27.0	22.9	21.7
3	22.2	22.5	22.5	22.2	23.9	33.4	22.7	21.7
4	22.1	22.5	22.5	22.2	23.8	28.8	22.7	21.6
5	22.2	22.7	22.7	22.3	23.9	28.8	22.9	21.7
6	22.1	22.3	22.3	22.2	23.8	27.4	22.5	21.6
7	22.0	22.0	22.0	22.1	23.7	26.1	22.0	21.5
8	21.9	22.1	22.0	22.0	23.6	26.0	22.0	21.5
9	22.1	22.6	22.5	22.2	23.8	28.8	22.7	21.6
10	22.0	22.3	22.2	22.1	23.7	27.4	22.4	21.6
11	21.8	21.8	22.0	22.0	16.1	11.8	22.1	21.0
12	21.5	20.8	21.3	21.7	11.4	2.8	21.2	20.1
13	21.8	21.8	22.1	22.0	16.1	11.5	22.1	21.0
14	21.8	21.7	21.0	21.9	16.1	13.2	22.0	21.1
15	21.7	21.5	21.8	21.9	16.0	11.4	21.7	21.0
16	21.7	21.3	21.5	21.8	15.9	11.0	21.4	20.9

Table 6.7: PMV and PPD values calculated from CBE Thermal Comfort Tool [92] for each part of both manikins for each case.

Case #	Head X		Head Y		Upper Body X		Upper Body Y		Lower Body X		Lower Body Y	
	PMV	PPD	PMV	PPD	PMV	PPD	PMV	PPD	PMV	PPD	PMV	PPD
1	-1.17	34	-1.23	37	-1.16	33	-1.22	36	-1.19	35	-1.22	36
2	-1.18	34	-1.23	37	-1.17	34	-1.23	37	-1.19	35	-1.21	36
3	-1.14	32	-1.22	36	-1.14	32	-1.23	37	-1.20	35	-1.24	37
4	-1.20	35	-1.25	38	-1.20	35	-1.26	38	-1.23	37	-1.26	38
5	-1.17	34	-1.25	38	-1.16	33	-1.24	37	-1.20	35	-1.22	36
6	-1.23	37	-1.28	39	-1.22	36	-1.28	39	-1.26	38	-1.28	39
7	-1.28	39	-1.33	42	-1.28	39	-1.34	42	-1.32	41	-1.34	42
8	-1.28	39	-1.33	42	-1.28	39	-1.34	42	-1.32	41	-1.34	43
9	-1.19	35	-1.27	39	-1.19	35	-1.27	39	-1.23	37	-1.25	38
10	-1.24	37	-1.29	40	-1.24	37	-1.30	40	-1.27	39	-1.30	40
11	-0.58	12	-0.39	8	-0.49	10	-0.36	8	-0.39	8	-0.34	7
12	-0.88	21	-0.61	13	-0.80	19	-0.58	12	-0.64	14	-0.54	11
13	-0.58	12	-0.39	8	-0.49	10	-0.36	8	-0.39	8	-0.33	7
14	-0.57	12	-0.38	8	-0.48	10	-0.36	8	-0.39	8	-0.34	7
15	-0.61	13	-0.41	9	-0.52	11	-0.39	8	-0.42	9	-0.37	8
16	-0.63	13	-0.44	9	-0.54	11	-0.42	9	-0.45	9	-0.40	8

Table 6.8: Vertical temperature difference between ankle and head of both manikins for each case (negative values represent thermal discomfort).

Case #	**Vertical Temperature Difference [°C]**	
	Manikin X	**Manikin Y**
1	-0.7	-0.5
2	-0.6	-0.6
3	-0.5	-0.4
4	-0.4	-0.4
5	-0.6	-0.5
6	-0.4	-0.2
7	-0.1	0.0
8	-0.1	0.0
9	-0.6	-0.4
10	-0.3	-0.2
11	0.5	0.1
12	1.4	0.7
13	0.5	0.1
14	0.6	0.1
15	0.8	0.3
16	0.9	0.5

All the vertical temperatures are under the limit of 3°C set by ASHRAE Standard 55 [6] for a seated occupant. PPD value is less than 2 for all the cases as seen on Figure 2.7 in Chapter 2.3 Thermal Comfort. Therefore, thermal comfort is provided in terms of vertical temperature differences, except for the negative vertical temperature difference, where they had cooler air around their ankle comparing to their head. These manikins refers to the occupants of the office shown on Figure 1.1.

Calculation of PMV and PPD values are done by the CBE Thermal Comfort Tool [92] is used as mentioned at Chapter 2.3 Thermal Comfort. Operative temperature is calculated as the arithmetic average of air temperature and mean radiant temperatures. Air speed is the average air speed near the region of occupant, which is 0.15 m/s. Relative humidity is 65% for summer and 78% for winter. Activity level is set to 1.0 met for reading or writing, seated. Clothing level for summer cases is chosen as 0.57 clo (trousers, short-sleeve shirt, socks, shoes, underwear) and for winter cases it is chosen as 1.0 clo (typical winter indoor clothing). PMV values until -0.5 represents neutral and until -1.5 represents slightly cool thermal comfort level.

Table 6.9: Mean radiant temperature (MRT) of head, upper body, and lower body for both manikins.

Case #	Mean Radiant Temperature [°C]					
	Head X	**Head Y**	**Upper Body X**	**Upper Body Y**	**Lower Body X**	**Lower Body Y**
1	22.7	22.4	22.7	22.4	22.6	22.4
2	22.6	22.4	22.7	22.4	22.6	22.4
3	22.8	22.4	22.8	22.3	22.5	22.3
4	22.6	22.3	22.6	22.3	22.4	22.3
5	22.7	22.3	22.7	22.3	22.6	22.4
6	22.5	22.2	22.5	22.2	22.3	22.2
7	22.3	22.1	22.3	22.0	22.1	22.0
8	22.3	22.1	22.3	22.0	22.1	22.0
9	22.6	22.2	22.6	22.2	22.4	22.3
10	22.4	22.2	22.5	22.2	22.3	22.1
11	20.7	21.6	20.8	21.7	21.5	21.9
12	19.5	20.9	19.5	21.1	20.7	21.4
13	20.7	21.6	20.8	21.7	21.5	21.9
14	20.8	21.6	20.8	21.7	21.5	21.9
15	20.6	21.5	20.7	21.6	21.4	21.8
16	20.5	21.4	20.5	21.5	21.2	21.6

Table 6.10: Average floor surface temperatures under manikin X and manikin Y and maximum floor temperature in front of window.

Case #	**Average Floor Temperature under Manikin X [°C]**	**Average Floor Temperature under Manikin Y [°C]**	**Maximum Floor Temperature [°C]**
1	22.1	22.1	27.1
2	22.1	22.1	27.9
3	22.1	22.1	24.6
4	22.0	22.0	25.3
5	22.1	22.1	27.0
6	22.1	22.0	25.1
7	22.0	22.0	23.1
8	22.0	22.0	22.8
9	22.1	22.0	25.3
10	22.0	22.0	24.1
11	21.9	22.0	22.6
12	21.6	21.9	22.0
13	21.9	22.0	22.7
14	21.9	22.0	22.4
15	21.9	21.9	22.3
16	21.8	21.9	22.1

All the floor temperatures are around 22°C, which is near the optimum floor temperature of 23°C as seen on Figure 2.8 in Chapter 2.3 Thermal Comfort. PPD value is less than 7 for all the cases. Therefore, thermal comfort is provided in terms of floor temperatures at all cases.

The corresponding values of the Grashof number (see Equation 11), the Rayleigh number (see Equation 13) and the Gr/Re^2 ratio are shown on Table 6.11 below for various locations. Partition X represent the upper portion of the partition, which is on top of the desk, that faces the façade and partition Y represents the upper portion of the partition facing to the other side. Wall is the opposing wall to the façade inside the office space. These surfaces are chosen because they are all critical regions in the numerical model with variations in temperatures and near wall air velocities. Cases 1 and 5 are same cases with different partition aspect ratios of 0.3 and 0.5, respectively. Case 11 is same as case 1 other than the weather condition is winter on case 11 and summer on case 1.

Table 6.11: Grashof, Rayleigh and Gr/Re^2 values for cases 1, 5, and 11 on various locations.

Case #	**Location**	**Gr**	**Ra**	**Gr/Re$^2_{min}$**	**Gr/Re$^2_{max}$**
1	Partition X	2.06E+06	1.46E+06	2.36E-01	5.30E+03
	Partition Y	1.88E+06	1.33E+06	4.84E-01	4.84E+01
	Façade	5.87E+09	4.16E+09	4.89E-01	1.27E+03
	Window	1.78E+10	1.26E+10	1.48E+00	3.86E+03
	Wall	1.16E+09	8.22E+08	1.12E+00	2.51E+02
5	Partition X	6.76E+07	4.79E+07	7.75E+00	1.74E+03
	Partition Y	6.24E+07	4.42E+07	1.61E+01	1.61E+03
	Façade	5.67E+09	4.02E+09	4.37E-01	1.23E+03
	Window	1.81E+10	1.29E+10	1.40E+00	3.93E+03
	Wall	1.14E+09	8.10E+08	1.26E+00	2.48E+02
11	Partition X	1.13E+06	7.99E+05	4.55E-01	2.91E+01
	Partition Y	1.73E+06	1.23E+06	1.24E+00	4.47E+01
	Façade	1.28E+10	9.10E+09	1.11E+00	2.78E+03
	Window	2.43E+10	1.72E+10	2.11E+00	5.27E+03
	Wall	2.31E+09	1.64E+09	3.48E+00	5.01E+02

The Grashof numbers values are calculated from the average surface temperatures, since there is minimal temperature change through the surfaces. The Rayleigh numbers are calculated by multiplying with the Prandtl number (Equation 12 above) of 0.7087, which was constant throughout all cases. The Gr/Re^2 ratios are calculated from maximum and minimum near wall air velocities to observe whether the entire surface has natural or forced convection or have mixed natural and forced convection.

$Ra<10^8$ states that the flow is laminar and $10^8<Ra<10^{10}$ states that the flow is turbulent. All three cases shown on Table 6.11 have turbulent flow near façade and window due to the Rayleigh numbers are being greater than 10^8. The opposing wall to the façade has Rayleigh number in the transition between laminar and turbulent flow for summer weather cases of 1 and 5, but it is turbulent in the winter weather case of 11. There is laminar flow on both sides of the partition above the desk for the same three cases. Increasing the height of the partition from case 1 to 5 increased Rayleigh numbers, so turbulent flow around the partition can be expected for a larger partition height to ceiling height aspect ratio in this geometry. Colder weather conditions provided colder surface temperature for the side of the partition facing to the façade and window. This decrease in surface temperature resulted in decreasing of the Rayleigh number on case 11 from case 1. These results shows that the utilization of SST k-ω turbulence model was required to accurately model the turbulent flow regions present in the numerical domain.

The convective heat transfer is determined according to the ratio of Gr/Re^2 if $Gr/Re^2>>1$ natural convection takes place and if $Gr/Re^2<<1$ forced convection takes place. As seen from the maximum and minimum Gr/Re^2 results on Table 6.11 all the surfaces on all cases have combination of natural and forced convection. This shows that the use of the Boussinesq approximation and PRESTO! pressure discretization made the numerical model more accurate by modelling the natural convection occurring on some parts of the surfaces.

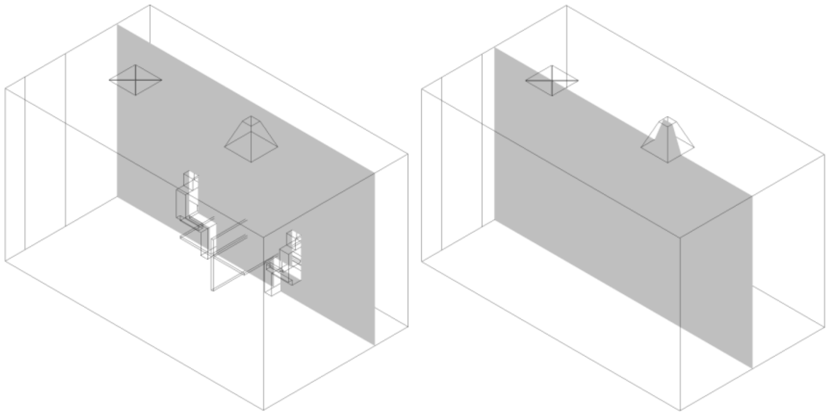

Figure 6.12: Locations for contour planes that cuts through occupants and desk (left) and cut through inlet and outlet (right).

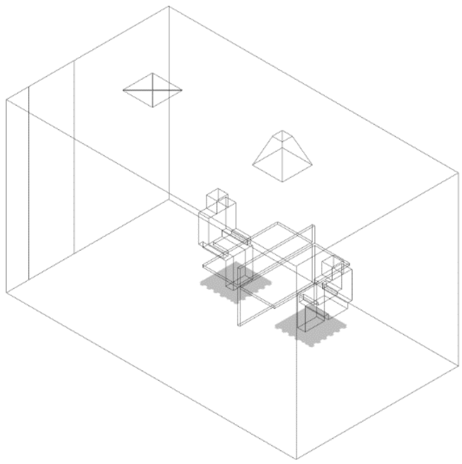

Figure 6.13: Floor locations under manikin X and manikin Y for average local floor temperatures.

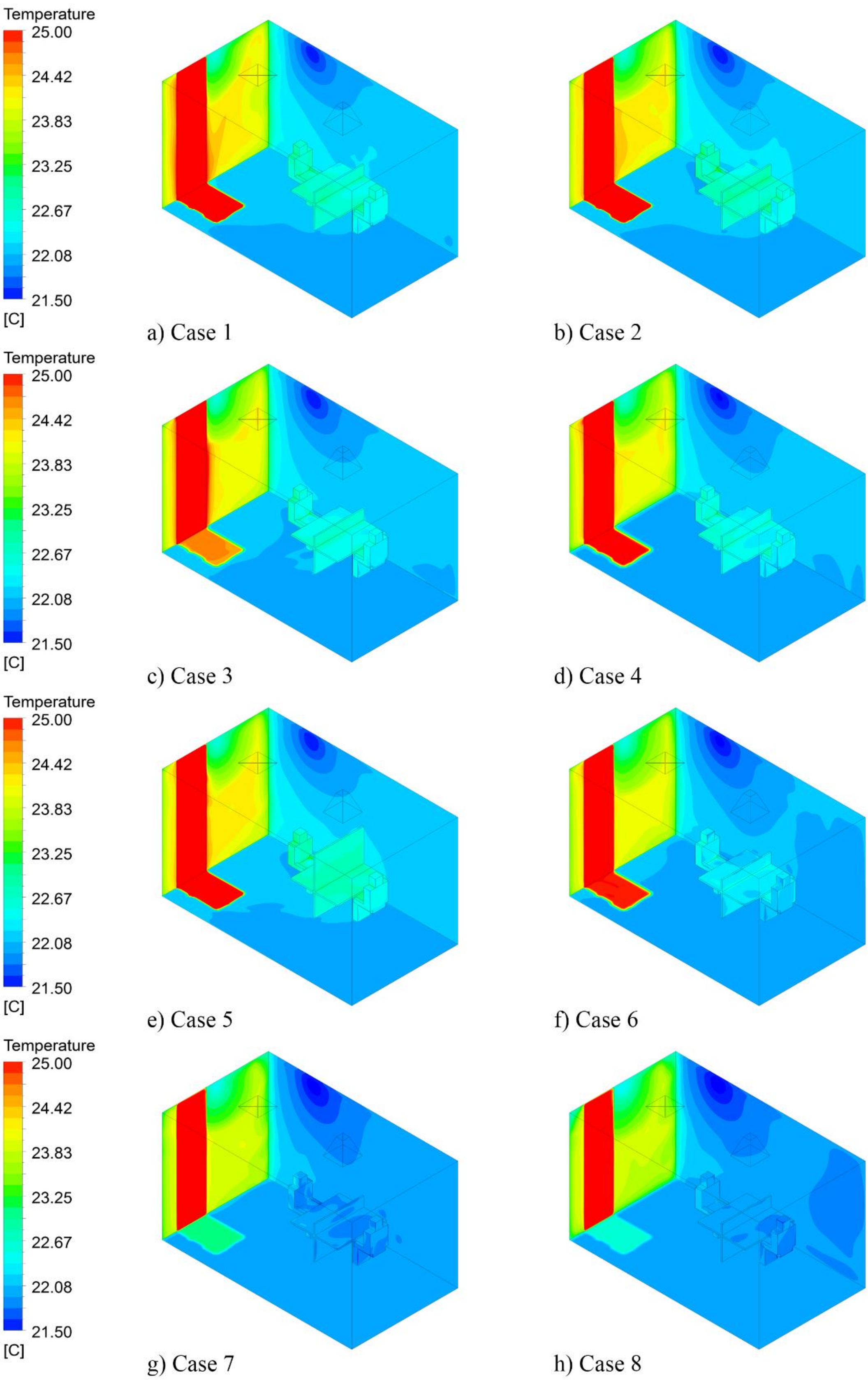

Figure 6.14: Surface temperatures contours from isometric view of all the cases with legends on the left for each row.

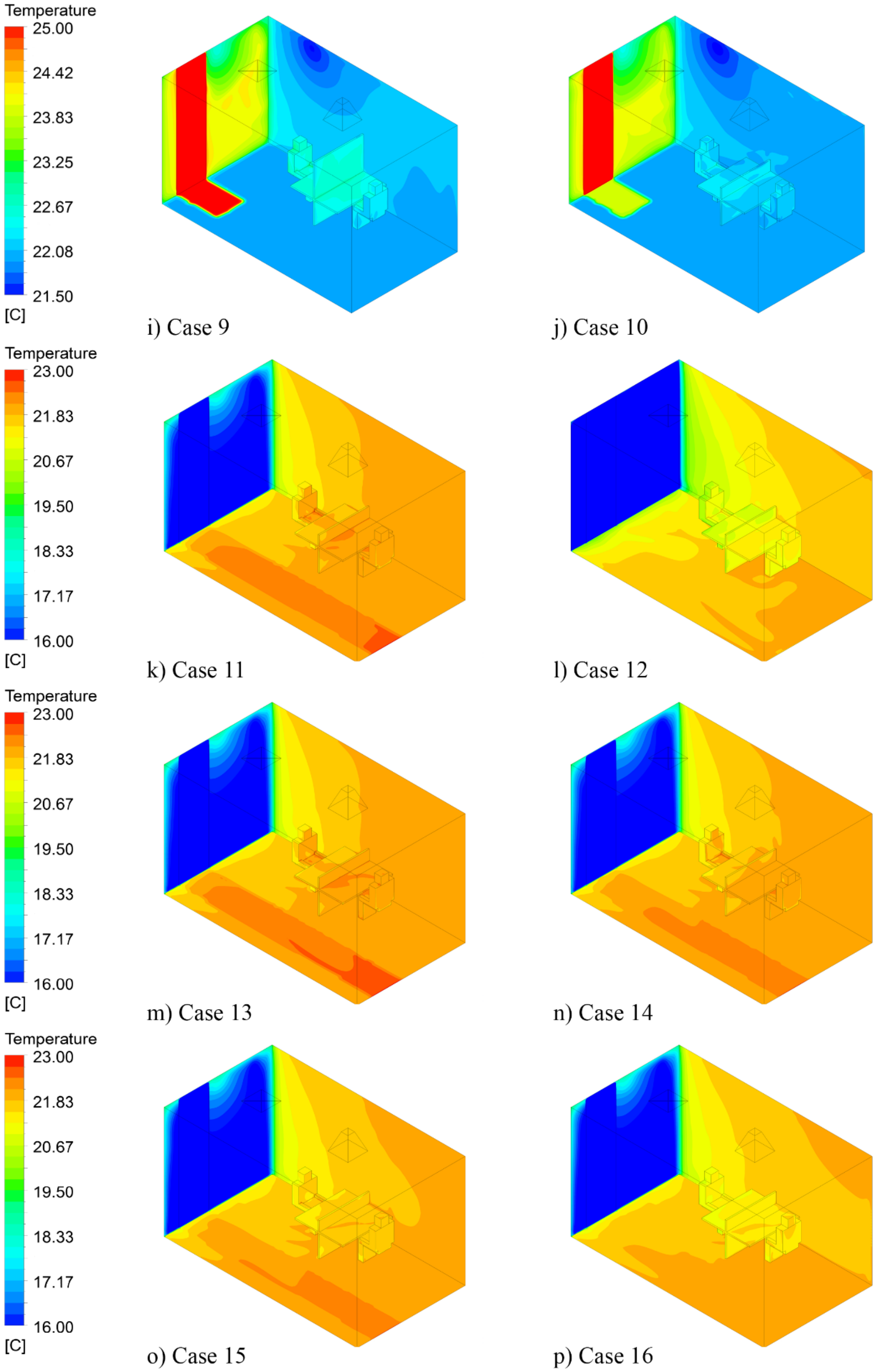

Figure 6.14 (cont.): Surface temperatures contours from isometric view with legends on the left for each row.

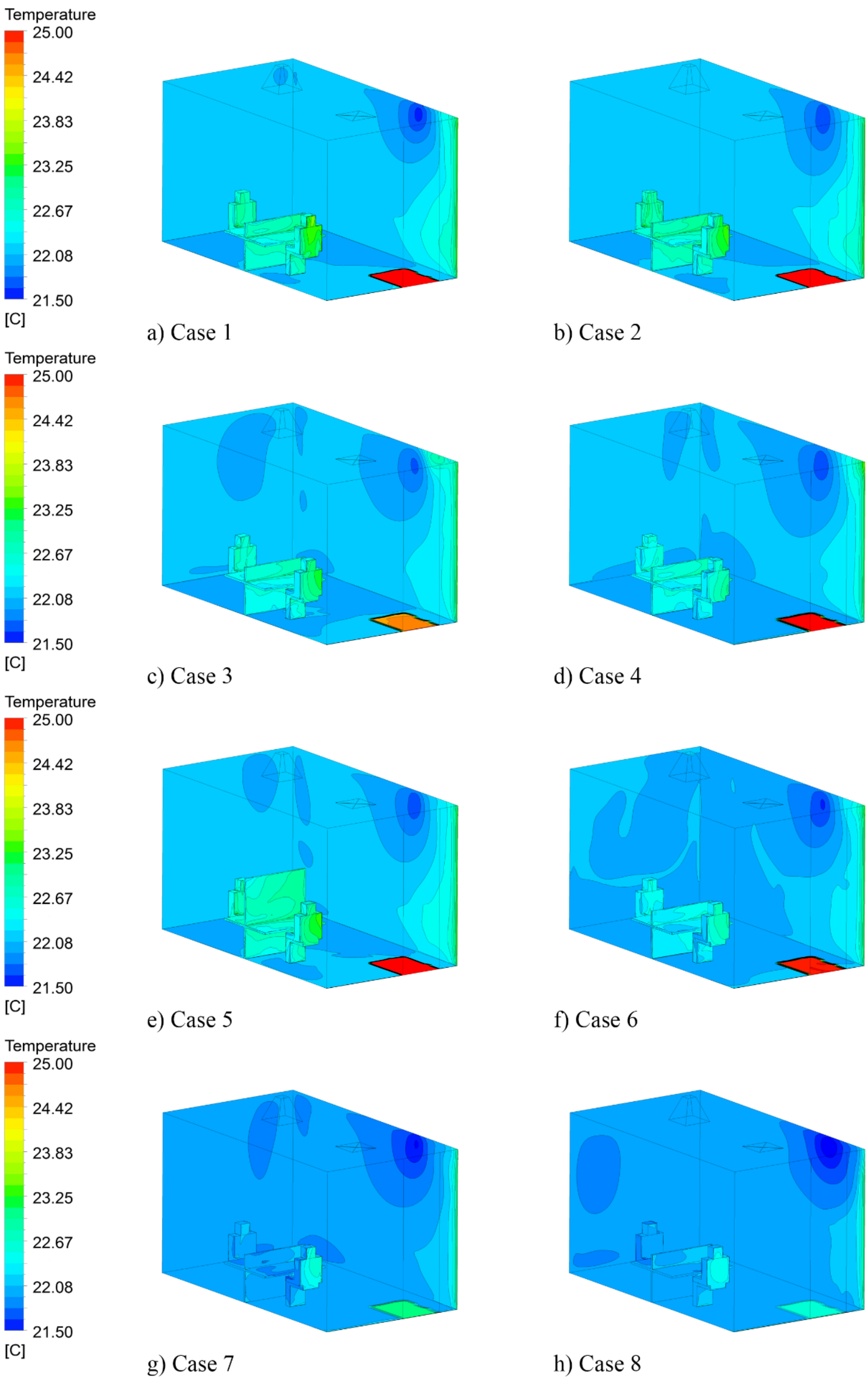

Figure 6.15: Surface temperatures contours from isometric view with legends on the left for each row.

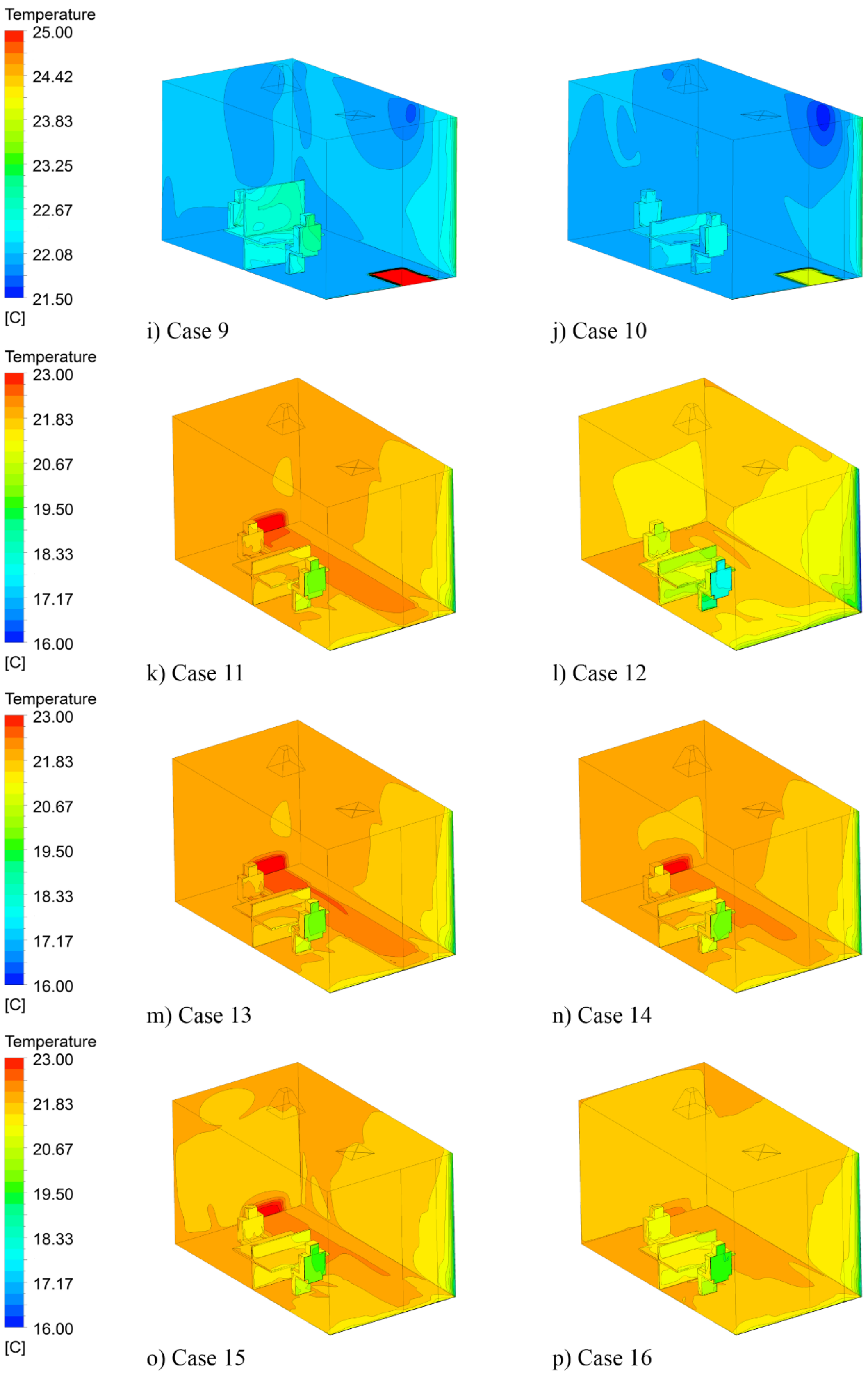

Figure 6.15 (cont.): Surface temperatures contours from isometric view with legends on the left for each row.

Below results are discussed for each parameter (window glass types, external solar shade coverage fractions on window, floor covering materials, partition heights and weather conditions) under their own subsection. First surface and air temperatures are compared using plots and then thermal comfort parameters are compared according to the manikins that represents average humans in terms of thermal comfort.

Window glass types:

Three types of window glasses are used for this comparison. Cases 1, 2 and 3 (clear, low-iron and grey, respectively) are compared for the summertime performance and cases 11, 13 and 14 (clear, low-iron and grey, respectively) are compared for wintertime performances of the same glass types, all other parameters are kept same for all six cases.

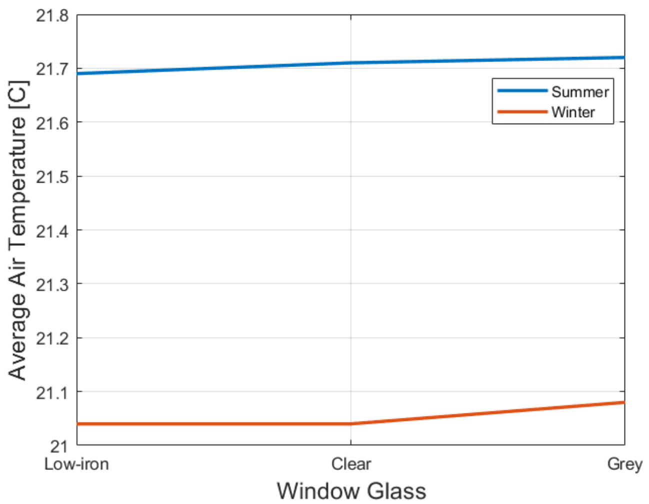

Figure 6.16: Average air temperatures for different window glasses and weather conditions.

There was no change in the air temperature both in summer and winter cases except the case 14, which is grey window glass at winter weather condition. Average air temperature increased slightly with the increasing absorptivity of the window glass.

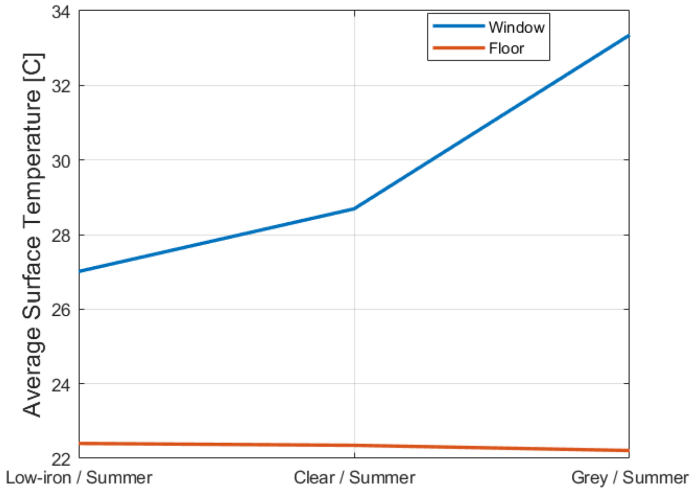

Figure 6.17: Comparison of average window and floor surface temperatures for summer cases with low-iron (case 2), clear (case 1) and grey (case 3) glasses.

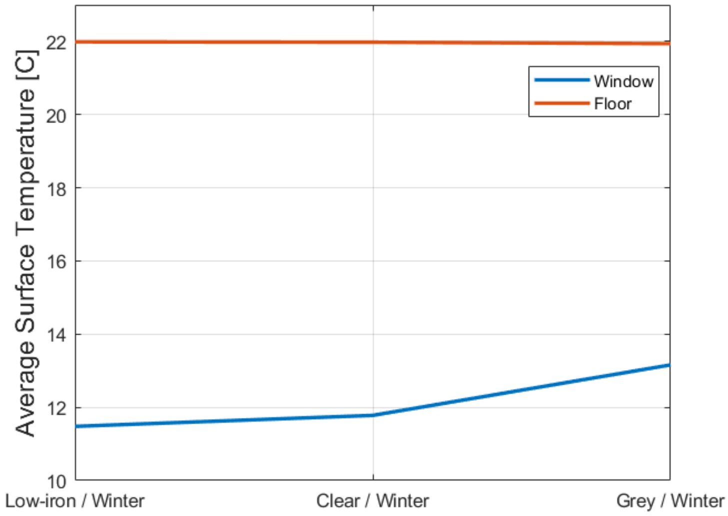

Figure 6.18: Comparison of average window and floor surface temperatures for winter cases with low-iron (case 13), clear (case 11) and grey (case 14) glasses.

There is an increase in the average surface temperature of the window from low-iron to clear to grey glasses, due to increase in absorptivity of the glass both in visible and IR spectrum. This increase is higher in the summer cases due to higher solar irradiance. There is a slight decrease in the average floor surface temperatures in the same order, this is due to decreasing transmissivity of the glasses. Slight increase in the average air temperature in the same window glass order is due to convective heat transfer from window to the air inside the room that can be observed on Figure 6.31.

Floor temperatures show the average floor temperature of the entire floor of the office. Floor X and floor Y are local average floor temperatures under manikin X and manikin Y.

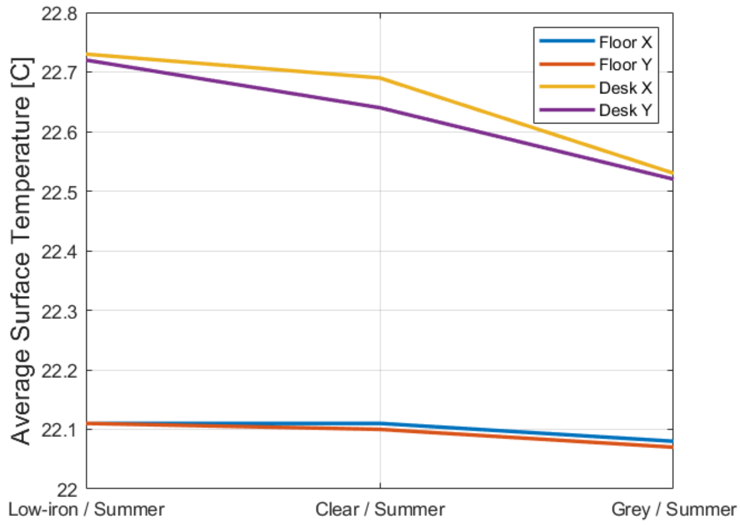

Figure 6.19: Comparison of average floor, desk and partition (combined as desk on plot) surface temperatures at opposing sides of the desk for manikin X and manikin Y for summer cases with low-iron (case 2), clear (case 1) and grey (case 3) glasses.

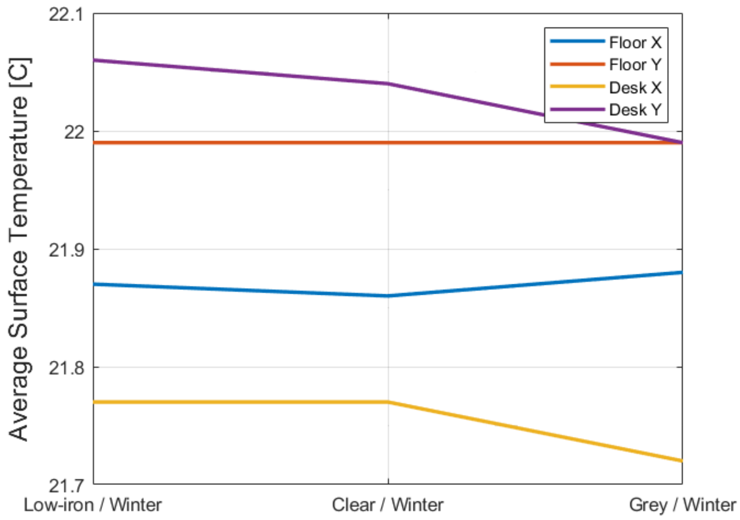

Figure 6.20: Comparison of average floor, desk and partition (combined as desk on plot) surface temperatures at opposing sides of the desk for manikin X and manikin Y for winter cases with low-iron (case 13), clear (case 11) and grey (case 14) glasses.

Floor, desk and partition average surface temperatures decreased with the increasing absorptivity of the window glass on summer weather condition cases, but the change in desk and partition average surface temperatures are greater when compared to the average floor surface temperatures. Desk and partition having higher view factor compared to the floor caused them to be affected more from the emitted radiation from the window back into the office. There is a small difference in average surface temperatures between both sides of the desk, because the temperatures of the window and façade are not much higher than rest of the surfaces inside the office. In winter cases window and façade are significantly colder than rest of the surfaces inside the office and this is caused by the surfaces facing the façade and window to lose heat to them by thermal radiative heat transfer. The temperature difference on both sides of the desk increased with the increasing temperature difference between the façade and window with the rest of the surfaces.

In terms of PMV and PPD results on Table 6.7 there is a small difference in thermal comfort for summer weather cases, both manikins are at slightly cool thermal condition. For winter weather cases both manikins are at neutral thermal condition, but there is higher difference between the manikins where manikin Y has higher thermal comfort on all body parts compared to manikin X due to same reason of façade and window being much cooler than rest of the office.

In terms of vertical temperature differences on Table 6.10 manikin Y has higher thermal comfort than manikin X in all types of window glasses for both summer and winter weather condition cases. The region near the façade and window has higher temperature contrast. Therefore, there are higher temperature gradients that cause the slight thermal discomfort. At all summer weather cases both manikins have slight thermal discomfort because cooler temperature around their ankle level than their head levels, both manikins are thermally comfortable with vertical temperature differences below 3°C for all winter weather cases.

External solar shade coverage fractions on window:

Solar shade area coverage fractions on the window are chosen as 0.0, 0.4 and 0.8. They are compared on cases 1, 6 and 7 for summer weather conditions and cases 11, 15 and 16 for winter weather conditions, while keeping other parameters unchanged.

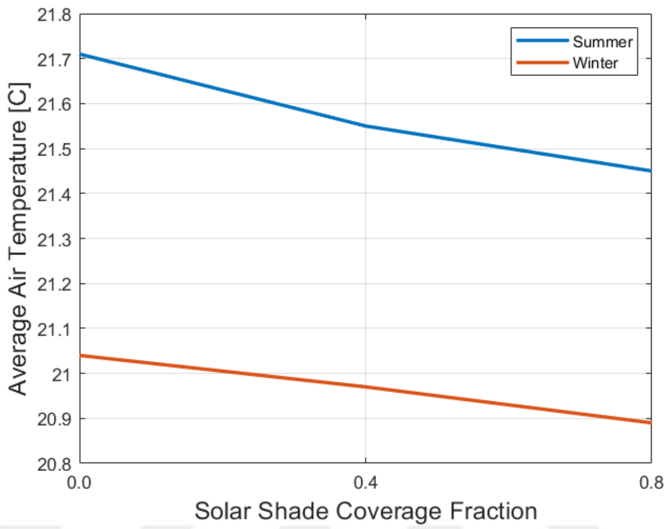

Figure 6.21: Average air temperatures for different solar shade window coverage fractions and weather conditions.

The average air temperature decreased with the increasing solar shade coverage on window as the solar irradiance incident on the office decreased. Solar shade effected the summer weather more due to significantly higher direct component of the solar irradiance.

This blocked solar irradiance was used for electricity generation via photovoltaic panels located on top of the external solar shades, which increases the overall efficiency of the office space. In the summer weather cases these external solar shades help decrease the indoor temperatures as well as generate electricity from blocked solar irradiance.

PV panels are becoming dirt cheap [80]. Therefore, soon we will start to implement them to building design as much as possible, but for most buildings roof area is not sufficient. This is where the solar shade integrated photovoltaic designs will come in to make the buildings more energy efficient.

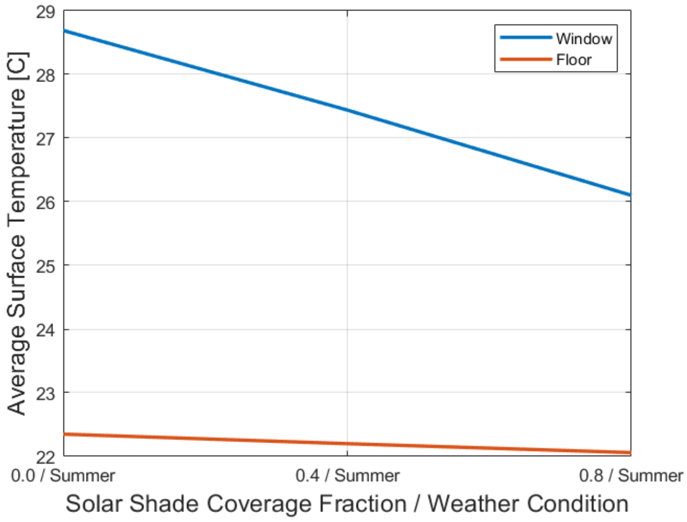

Figure 6.22: Comparison of average window and floor surface temperatures for summer cases with solar shade coverage fraction on window of 0.0 (case 1), 0.4 (case 6) and 0.8 (case 7).

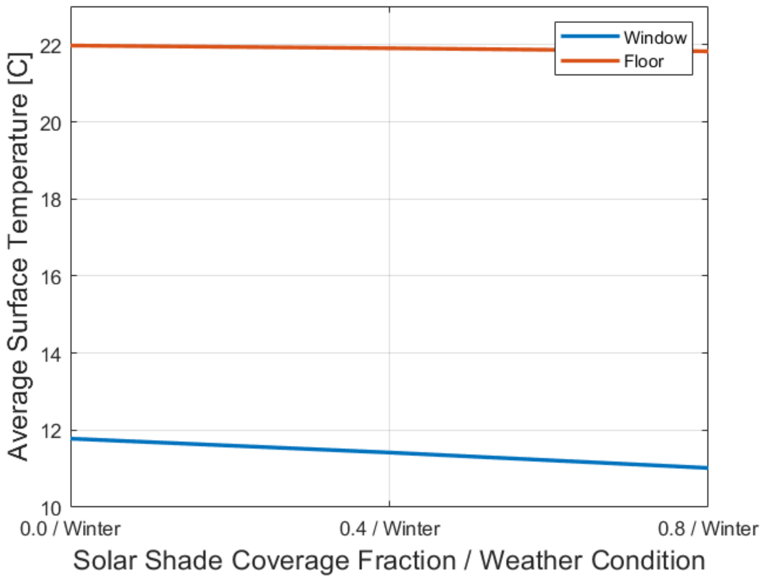

Figure 6.23: Comparison of average window and floor surface temperatures for winter cases with solar shade coverage fraction on window of 0.0 (case 11), 0.4 (case 15) and 0.8 (case 16).

The average surface temperatures of both window and floor decreased with the increasing solar shade coverage, due to decreasing solar irradiance. This decrease is more noticeable on the window than on the floor, because window encounters the solar irradiance first before transmitting it on the floor and only 5.8% of the floor area is exposed to direct solar irradiance when the solar altitude angle is at 70° during summer (can be seen on Figure 6.26.a – Figure 6.26.j as red spot in front of the window). During the winter weather cases, the altitude angle is decreased to 28° which exposes much more area of the floor (30.2%) to direct solar irradiance (can be seen on Figure 6.26.k – Figure 6.26.p), but the direct solar irradiance in winter is modelled as 10% of the summer solar irradiance due to 90% cloudiness of the sky. This shows that direct solar irradiance has smaller effect on the average temperature of the entire office floor than it does on the window. The direct solar irradiance controls the local temperature of the floor in front of the window (see Figure 6.26), rather than the entire floor.

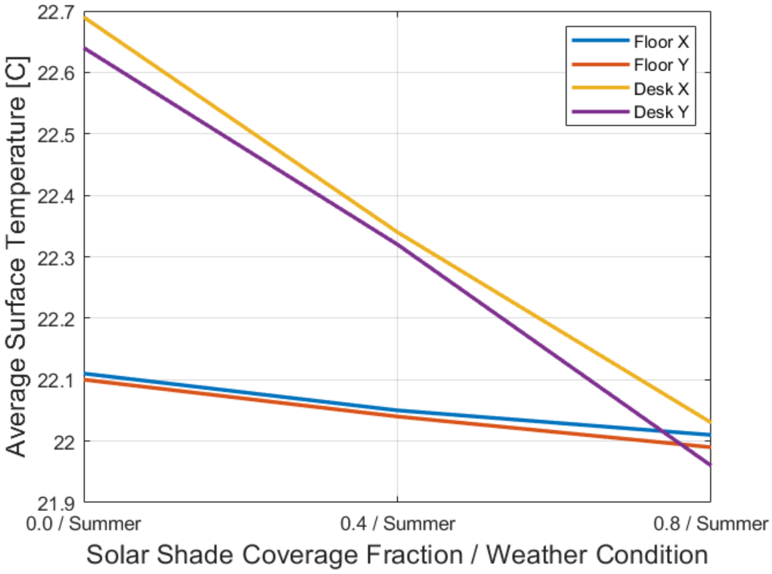

Figure 6.24: Comparison of average floor, desk and partition (combined as desk on plot) surface temperatures at opposing sides of the desk for manikin X and manikin Y for summer cases with solar shade coverage fraction on window of 0.0 (case 1), 0.4 (case 6) and 0.8 (case 7).

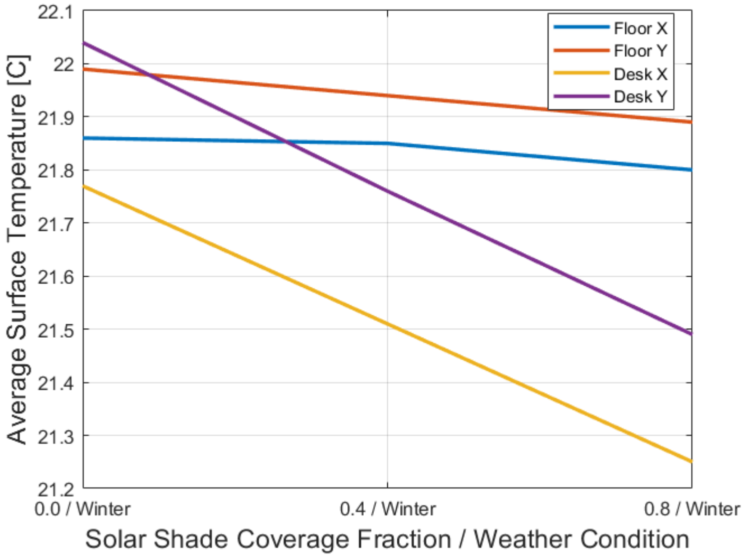

Figure 6.25: Comparison of average floor, desk and partition (combined as desk on plot) surface temperatures at opposing sides of the desk for manikin X and manikin Y for winter cases with solar shade coverage fraction on window of 0.0 (case 11), 0.4 (case 15) and 0.8 (case 16).

Local floor, desk and partition surface average temperatures have decreased for sides of both manikins with the increasing solar shade coverage on the window. Decrease at desk and partition temperatures were higher compared to floor due to higher view factor from window and façade, which is the main surface that controls their temperature. Average surface temperatures for both sides are closer to each other on the summer weather compared to winter weather, because at winter weather cases temperature difference between the window and façade and rest of the office is greater than in summer cases. This causes the side that is facing the façade to lose heat to them with radiation heat transfer as discussed in while discussing effects of window glass types previously.

In terms of PMV and PPD results on Table 6.7 both manikins are at similar thermal comfort state for summer weather with minimal differences, manikin X has slightly higher thermal comfort than manikin Y. This similarity in thermal comfort can also be seen from the results on Figure 6.24. On winter weather cases manikin Y has higher thermal comfort than manikin X due to manikin X being near the cold façade and window and losing heat to them via thermal radiation heat transfer.

In terms of vertical temperature differences on Table 6.10 air around the head of both manikins are hotter than air around their ankles for summer weather cases, where manikin Y is thermally more comfortable than manikin X. On winter weather cases both manikins are at thermal comfort according to ASHRAE Standard 55-2017 [6] in terms of vertical temperature difference, where manikin Y is thermally more comfortable than manikin X like in the summer weather cases. This is because near the façade and window there is higher temperature contrast when compared to the opposite side of the desk, where there is smaller temperature gradients.

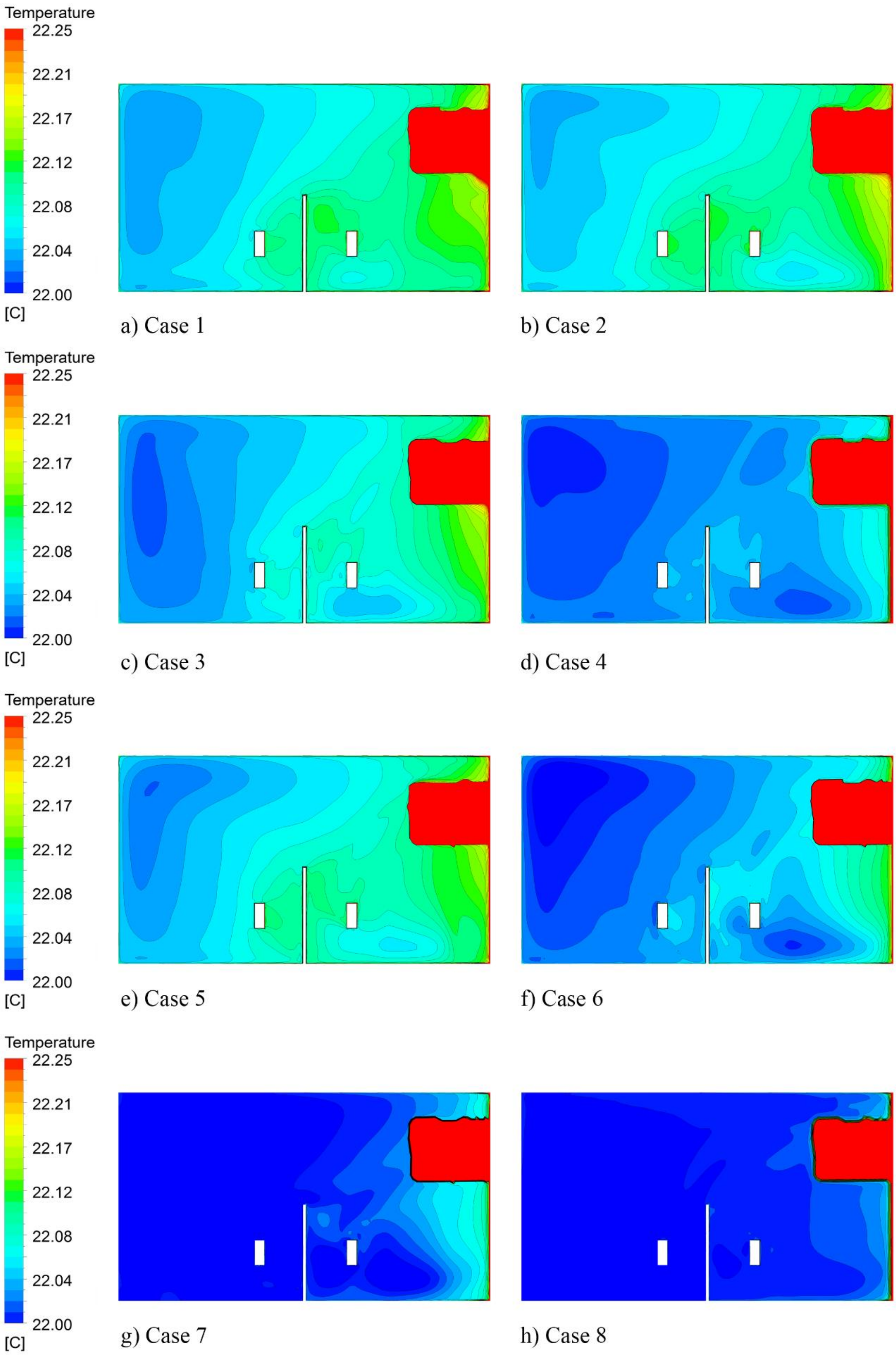

Figure 6.26: Floor surface temperatures contours from top view (façade is to the right) with legends on the left for each row.

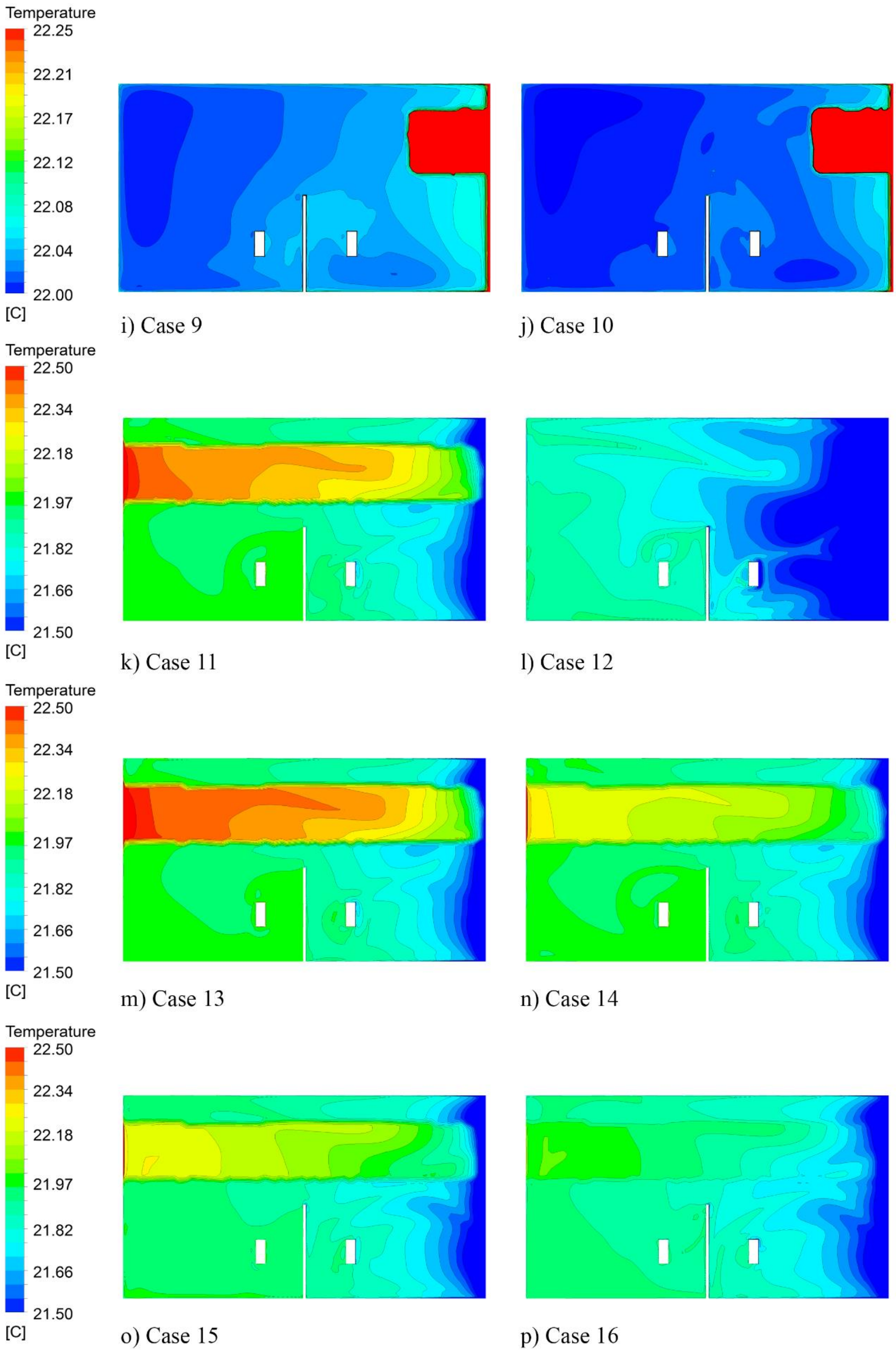

Figure 6.26 (cont.): Floor surface temperatures contours from top view (façade is to the right) with legends on the left for each row.

Floor covering materials:

Floor temperature distribution is more uniform at summer weather cases (see Figure 6.26.a -Figure 6.26.j) then winter weather cases (see Figure 6.26.k - Figure 6.26.p) when comparing floor temperature contours. Maximum floor temperatures due to direct solar irradiance are not shown on contours to show detailed temperature distribution the floor but can be seen on Table 6.10 for each case. The effect of partition on the floor temperature distribution can be clearly seen on winter weather cases due to façade and window being significantly cooler than the rest of the office and causing the surfaces to lose heat to them via thermal radiative heat transfer. Surfaces closer and more aligned to the window and façade lose more heat due to having higher view factors.

There are two types of floor covering materials compared which are carpet and ceramic tiles. They are compared in two different solar shade coverage fractions on the window (0.0 and 0.4), while keeping other parameters same. Cases 1 and 4 compares two floor materials with solar shade area coverage of 0.0 and case 6 and 10 compares two floor materials with solar shade area coverage of 0.4.

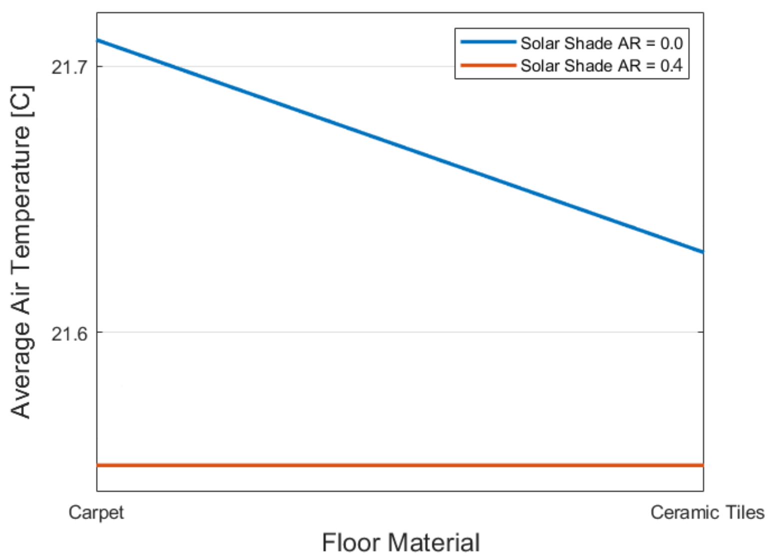

Figure 6.27: Average air temperatures for different floor materials and solar shade covering to window area aspect ratios (AR).

The air temperature is 0.1°C cooler when using ceramic tiles rather than carpet when there is more solar irradiance present with solar shade covering fraction of 0.0, but the air temperature remained unchanged for solar shade covering fraction of 0.4. Higher thermal conductivity of the ceramic tiles comparing to carpet helped dissipating the heat while carpet retains the heat. Higher the heat flux into the office space higher the difference will be in air temperature as well as other surface temperatures.

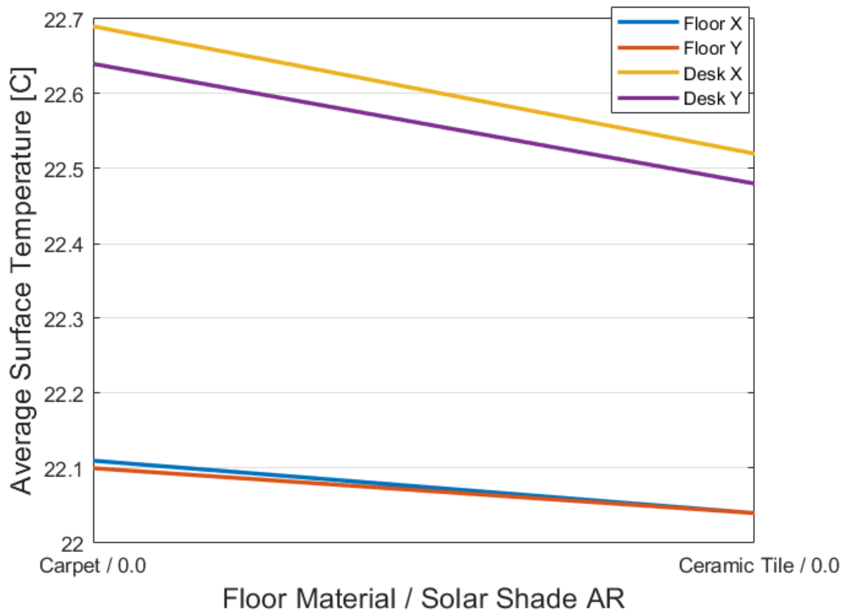

Figure 6.28: Comparison of average floor, desk and partition (combined as desk on plot) surface temperatures at opposing sides of the desk for manikin X and manikin Y for solar shade coverage fraction on window of 0.0 cases with floor material as carpet (case 1) and ceramic tile (case 4).

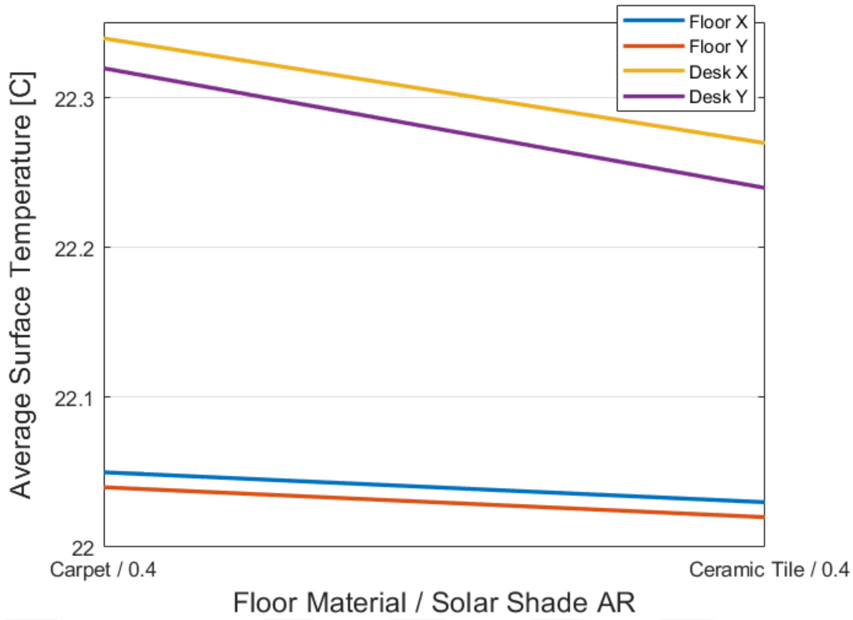

Figure 6.29: Comparison of average floor, desk and partition (combined as desk on plot) surface temperatures at opposing sides of the desk for manikin X and manikin Y for solar shade coverage fraction on window of 0.4 cases with floor material as carpet (case 1) and ceramic tile (case 6).

Local floor, desk and partition average surface temperatures were lower for both sides of the partition when ceramic tiles were chosen as floor covering material over carpet at both solar shade coverage fractions on the window. Side of the manikin Y is cooler than manikin X at all cases because manikin X is located near the façade and window which is hotter than rest of the office. Except the local floor temperatures are equal when there is no solar shade blockage on the window and ceramic tiles were used as floor materials. This is due to higher thermal conductivity of the ceramic tiles over the carpet and can be seen on Figure 6.26.a and Figure 6.26.d.

In terms of PMV and PPD results shown on Table 6.7 both manikins are slightly cool side of the thermal comfort state for both floor materials. The corresponding PMV and PPD results are very close at corresponding body parts, where manikin X is slightly more comfortable due to being at the hotter side of the partition and the carpet provided more thermal comfort since it kept the environment warmer as shown on Figure 6.27. This thermal comfort difference between both manikins and thermal comfort of each manikin decreases with increase in solar shade coverage fraction on the window since the heat input is decreased accordingly.

In terms of vertical temperature differences shown on Table 6.10 all cases have higher air temperature around the manikin's head than at their ankles. The lowest difference is when using ceramic tiles with solar shade coverage fraction of 0.4 due to ceramic tiles having higher emissivity than carpet and radiating more heat and helping more uniform temperature distributions. Also, lower heat input due to solar shade blockage causes lower temperature contrasts.

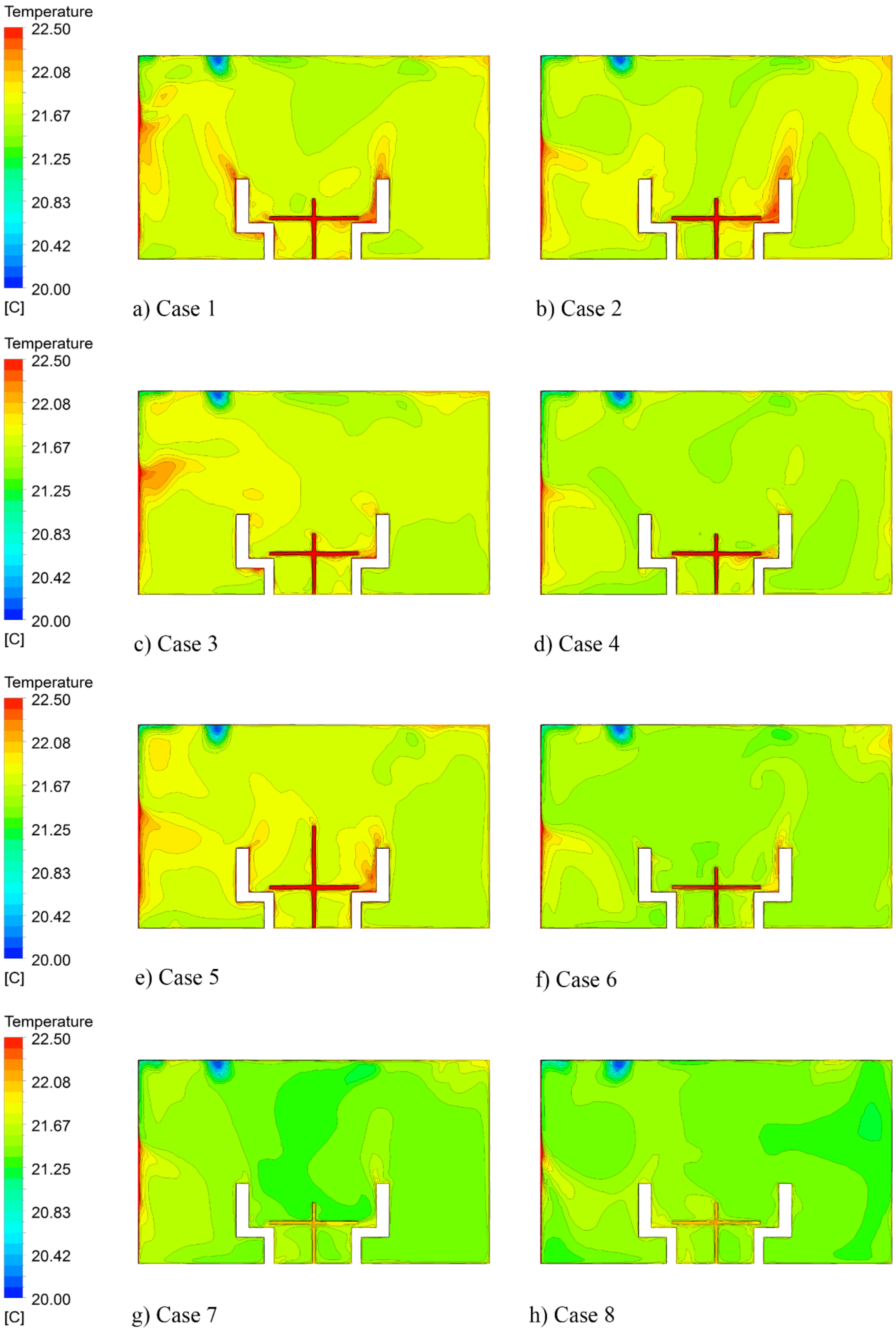

Figure 6.30: Air temperature contours from side view (façade is to the left) on a plane through manikins and the desk (see left figure on Figure 6.12) legends on the left for each row.

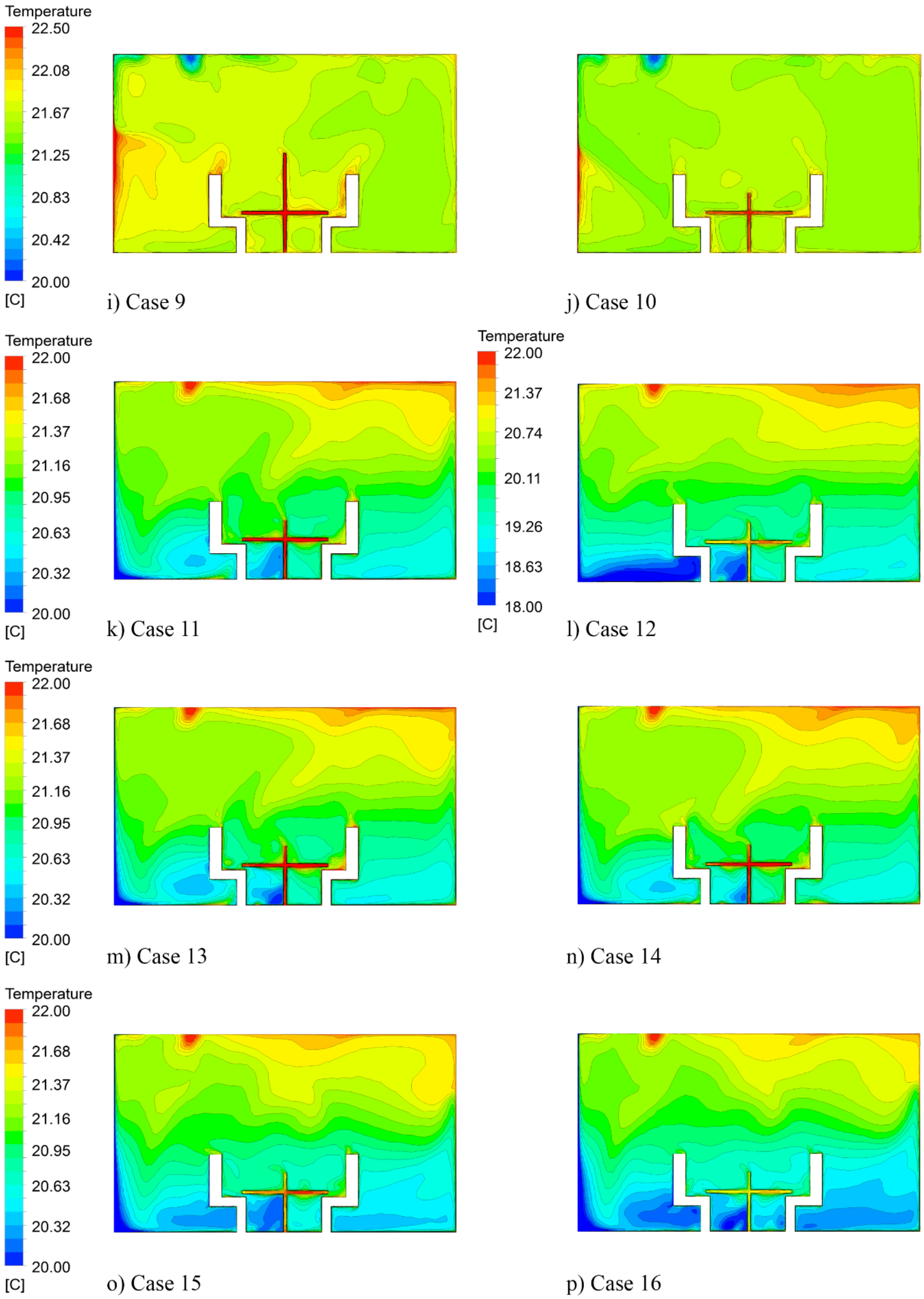

Figure 6.30 (cont.): Air temperature contours from side view (façade is to the left) on a plane through manikins and the desk (see left figure on Figure 6.12) legends on the left for each row.

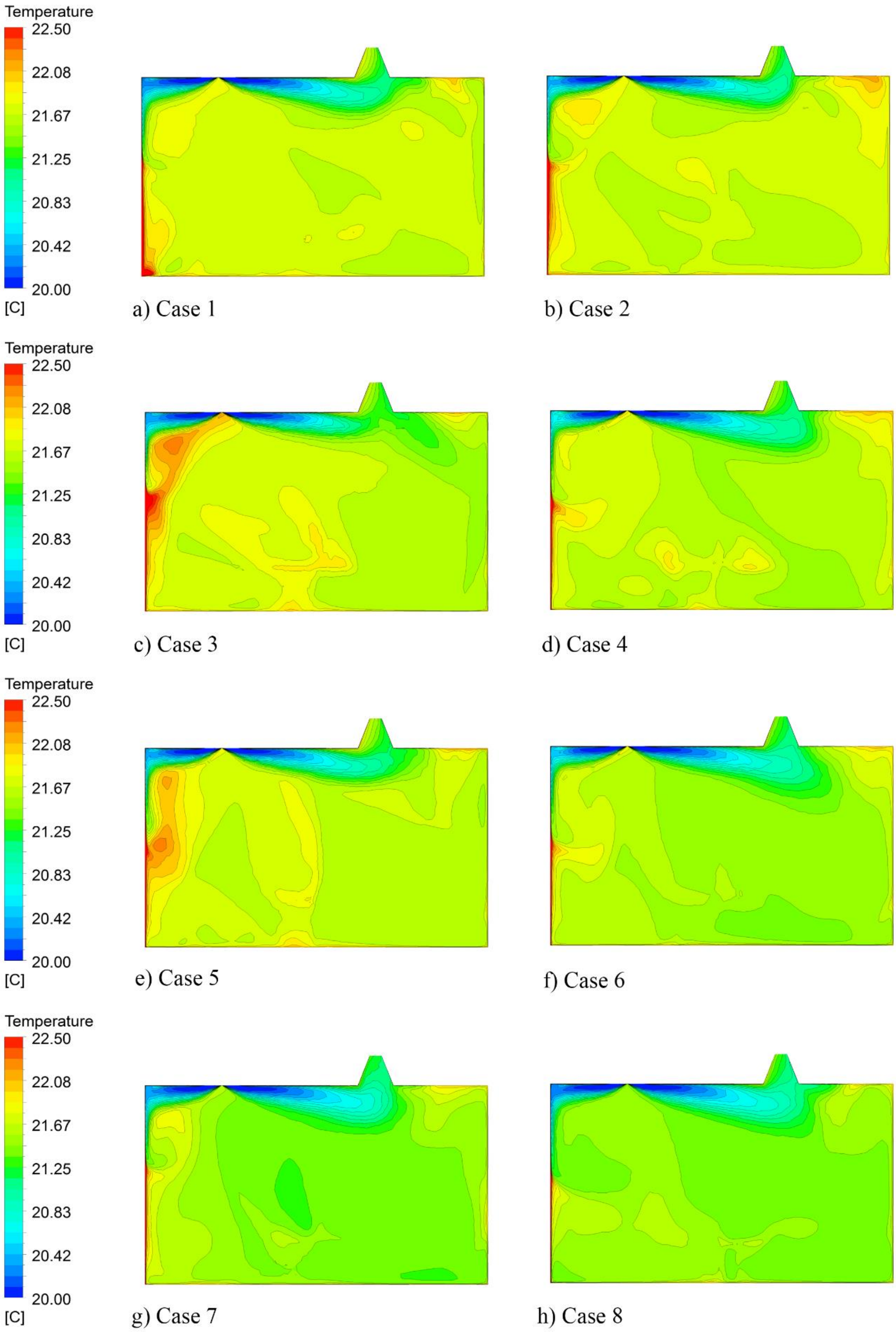

Figure 6.31: Air temperature contours from side view (façade is to the left) on a plane through inlets and outlet (see right figure on Figure 6.12) legends on the left for each row.

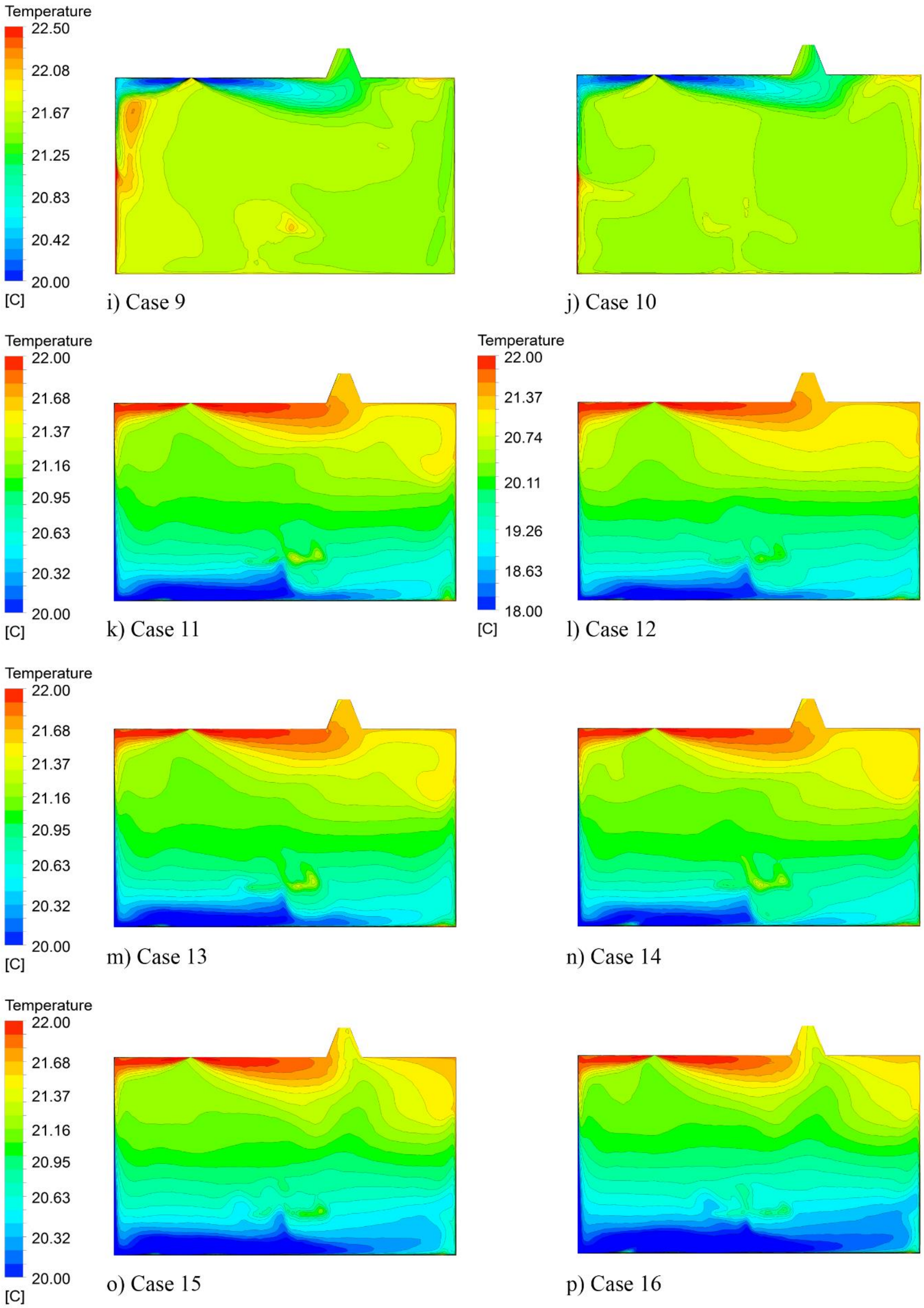

Figure 6.31 (cont.): Air temperature contours from side view (façade is to the left) on a plane through inlets and outlet (see right figure on Figure 6.12) legends on the left for each row.

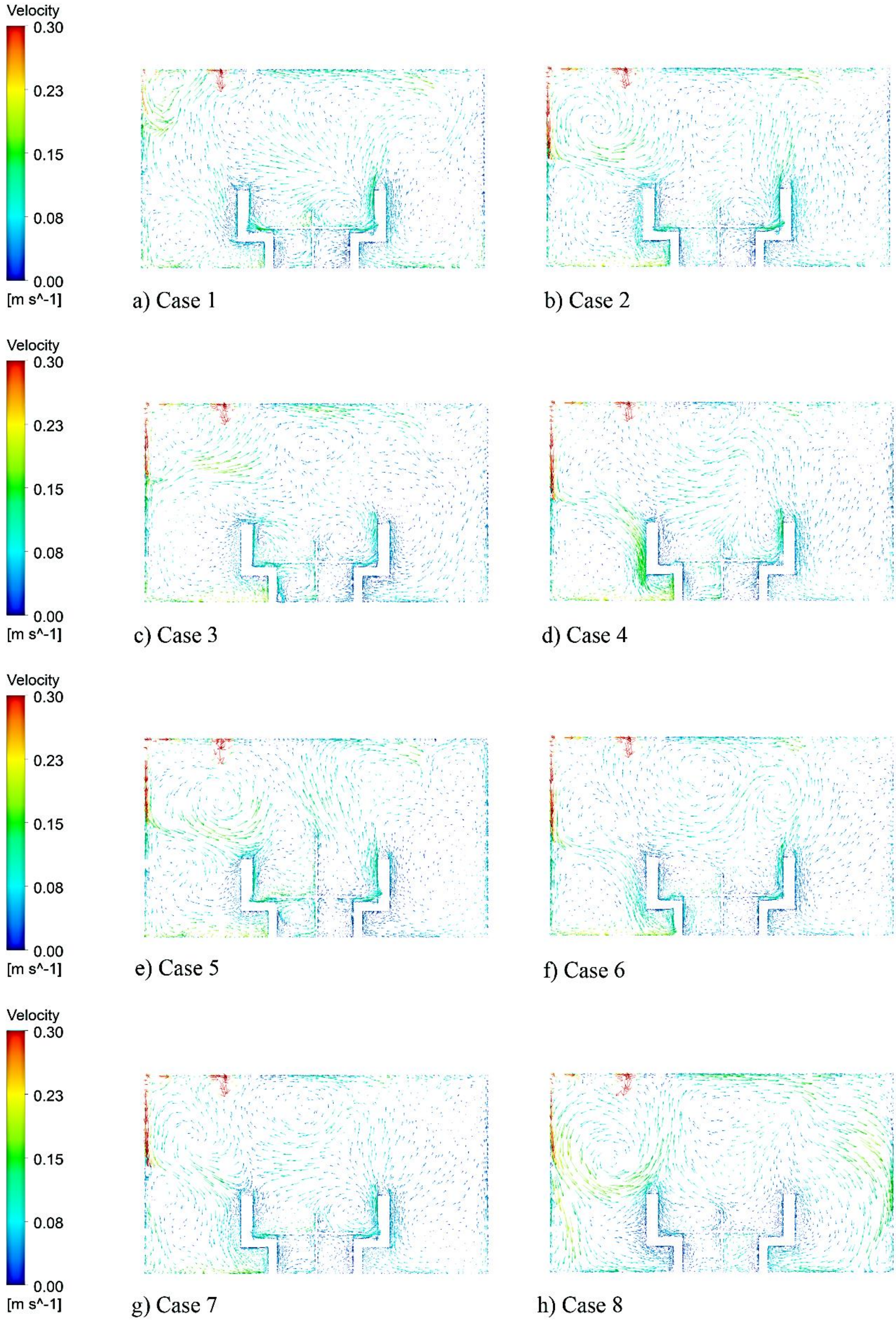

Figure 6.32: Air velocity vectors from side view (façade is to the left) on a plane through manikins and the desk (see left figure on Figure 6.12) legends on the left for each row.

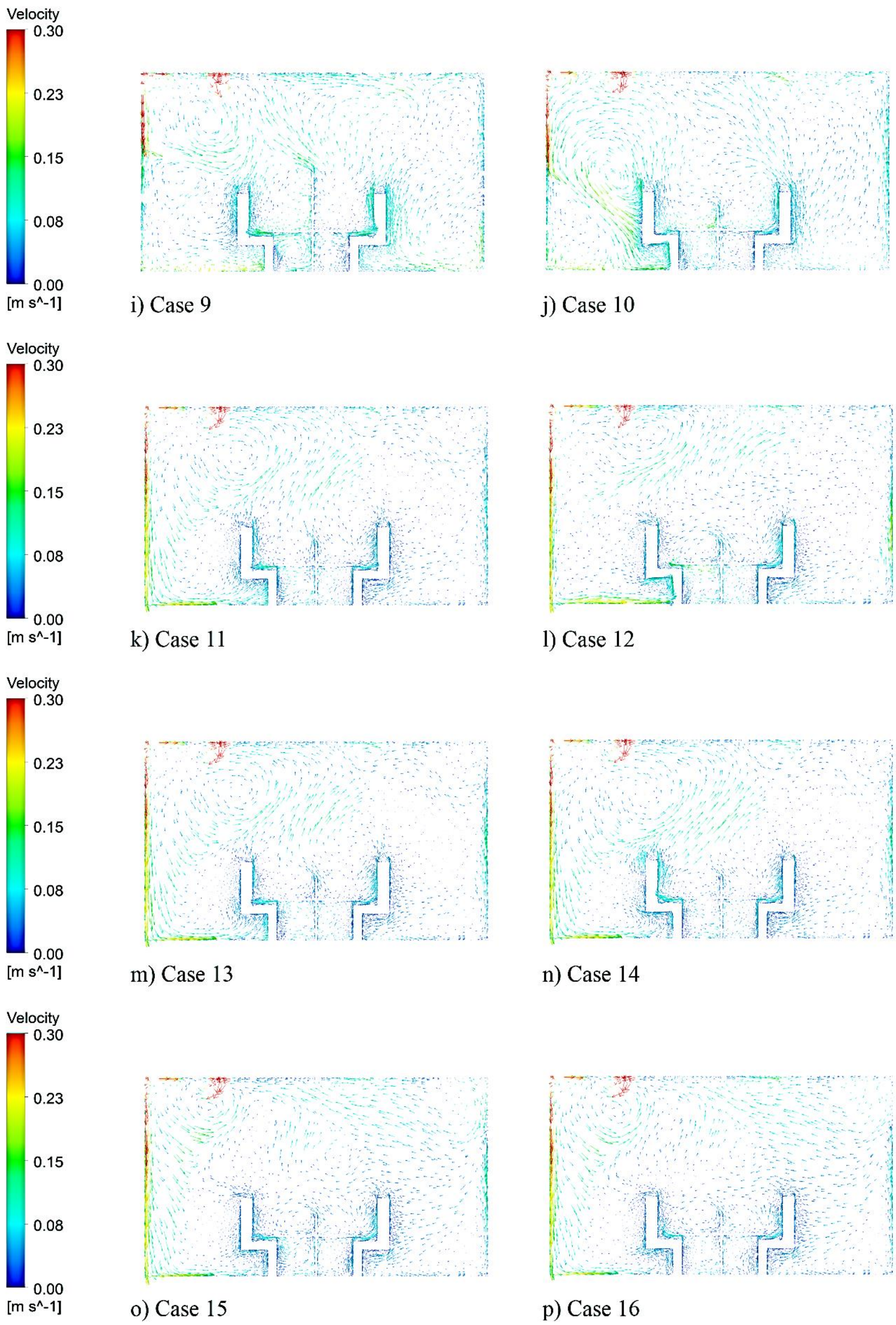

Figure 6.32 (cont.): Air velocity vectors from side view (façade is to the left) on a plane through manikins and the desk (see left figure on Figure 6.12) legends on the left for each row.

Partition height to ceiling height aspect ratios:

Colder air near floor on winter cases is blocked by the partition that can be seen on the Figure 6.30 and this blockage still effects the air temperature near the partition that can be seen on Figure 6.31. Air velocity does not exceed 0.2 m/s near both manikins at all cases (see Figure 6.32) as suggested by ASHRAE Standard 55-2017 [6]. Also, blockage of air circulation inside the office can be seen on air velocity vectors. The increase of partition height to ceiling height aspect ratio blocks more air flow inside the office and creates additional vortices. These vortices might cause thermal discomfort if the air velocity around the occupants exceeds 0.2 m/s.

There are two different partition height to ceiling height aspect ratios compared in this study, which are 0.3 and 0.5. They are compared when floor covering material is both carpet (cases 1 and 5) and ceramic tiles (cases 4 and 9), while keeping rest of the parameters same.

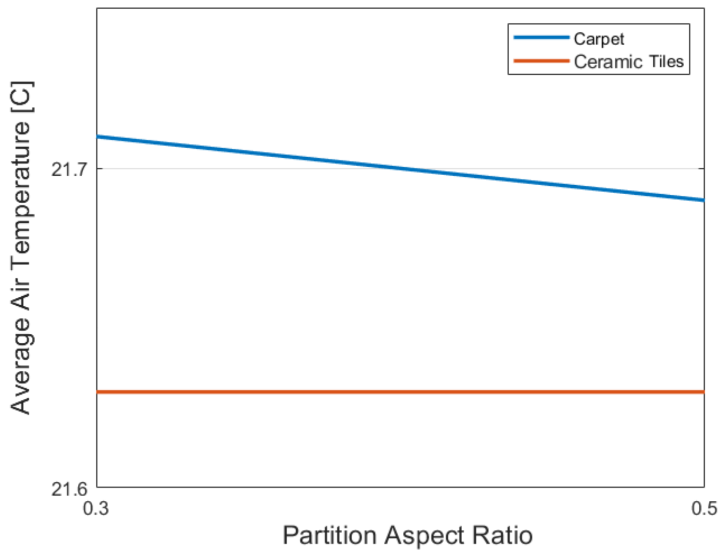

Figure 6.33: Average air temperatures for different floor materials and partition height to ceiling aspect ratios.

The indoor average air temperature slightly decreased as the partition height to ceiling height aspect ratio increased from 0.3 to 0.5 when carpet is used as floor material but remained unchanged when ceramic tiles were used. Thermal conductivity of the carpet is lower than ceramic tiles and increasing the partition aspect ratio blocks the solar irradiance as well as blocking the air circulation inside the office. This blockage lowers the average air temperature of the air, but high thermal conductivity of ceramic tiles conducts the heat to rest of the office and decreases the effect of blockage. However, ceramic tiles provided cooler air temperature than carpet for both partition aspect ratios as discussed under floor materials.

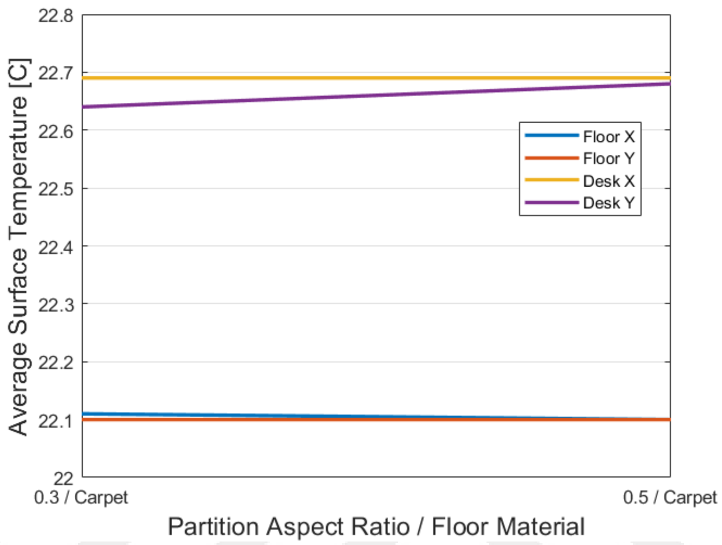

Figure 6.34: Comparisons of average floor, desk and partition (combined as desk on plot) surface temperatures at opposing sides of the desk for manikin X and manikin Y for floor material as carpet and partition aspect ratio of 0.3 (case 1) and 0.5 (case 5).

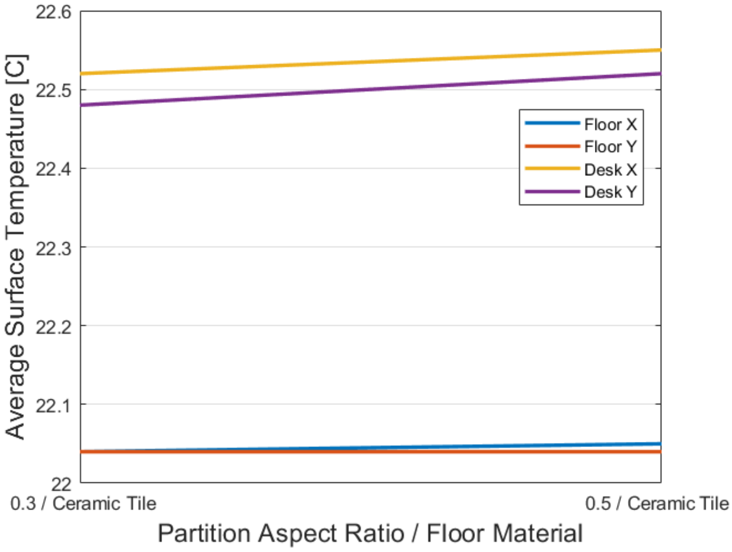

Figure 6.35: Comparisons of average floor, desk and partition (combined as desk on plot) surface temperatures at opposing sides of the desk for manikin X and manikin Y for floor material as ceramic tile and partition aspect ratio of 0.3 (case 4) and 0.5 (case 9).

The average local floor temperatures under both manikins had minimal to no change with increasing partition aspect ratios. For the cases with carpet, desk and partition average surface temperature for the manikin X kept unchanged but they slightly increased for the manikin Y. When ceramic tiles were used as floor covering material, average surface temperature of both sides of the desk increased simultaneously where the manikin Y's side kept slightly cooler. Increasing the partition aspect ratio increases the surface area and therefore the view factors from façade and window to the partition and causing higher heat gain via thermal radiation heat transfer from them.

In terms of PMV and PPD results shown on Table 6.7, all body parts of both manikins are at similar thermal condition (slightly cool), where for partition aspect ratio of 0.5 thermal comfort of both occupants are slightly less (still slightly cool).

In terms of vertical temperature differences shown on Table 6.10, all cases have higher air temperature around the manikin's head than at their ankles. Increasing partition aspect ratio from 0.3 to 0.5 decreased the vertical temperature difference for both manikins, therefore increased the thermal comfort, when the carpet is used as floor material. When comparing the Figure 6.32.a and Figure 6.32.e the increase in air velocity towards the ceiling near head can be observed, which helps increase the convective heat transfer causes the head of manikin X to cool down.

Weather conditions:

There are three different weather conditions chosen for this study, which are summer, winter and winter 2. Summer and winter weathers are average weather conditions for June 21st and December 21st, respectively. Winter 2 is chosen as extreme winter case, by increasing the parameters used for winter weather condition with no reference. Cases 1, 11 and 12 are used to compare these three weather conditions.

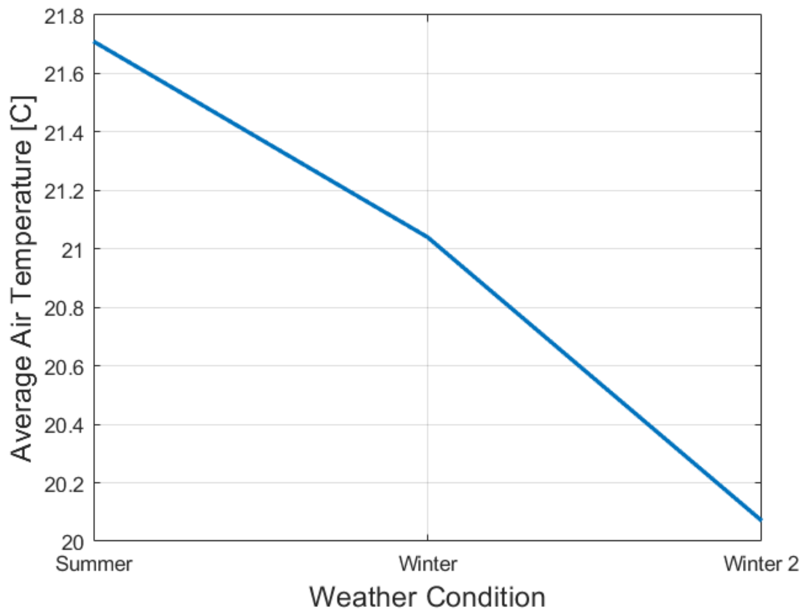

Figure 6.36: Average air temperatures for different weather conditions.

Average air temperatures inside the office decreased with the weather getting colder and heat transfer coefficient of the outer side of both façade and window increased, as expected.

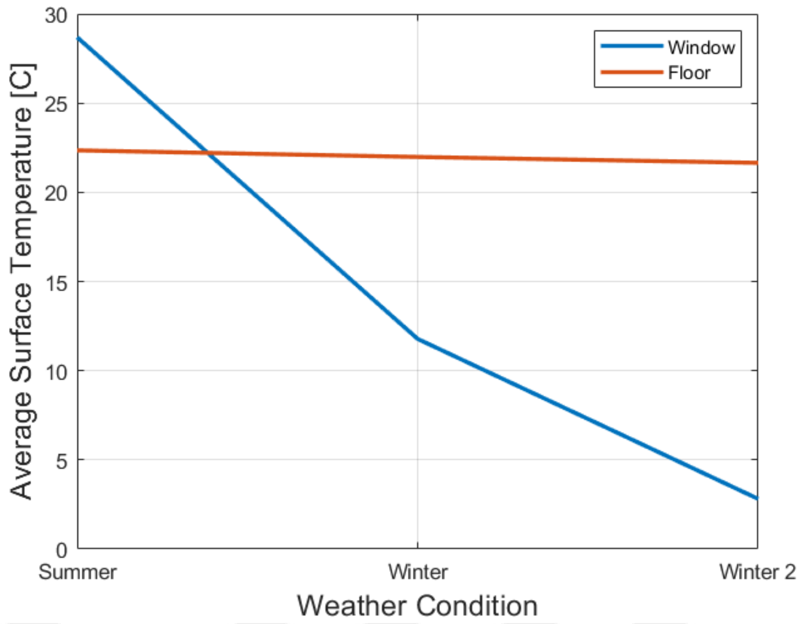

Figure 6.37: Comparison of average window and floor surface temperatures different weather conditions of summer (case 1), winter (case 11), and winter 2 (case 12).

The average surface temperature of the window changed drastically compared to the floor average surface temperature. This is due to the window being in contact with the outside weather condition and getting effected by it directly, while the floor average surface temperature is affected from interior of the façade and the window via conduction, convection and radiation heat transfer, as well as the solar irradiance transmitted through the window incident on the floor.

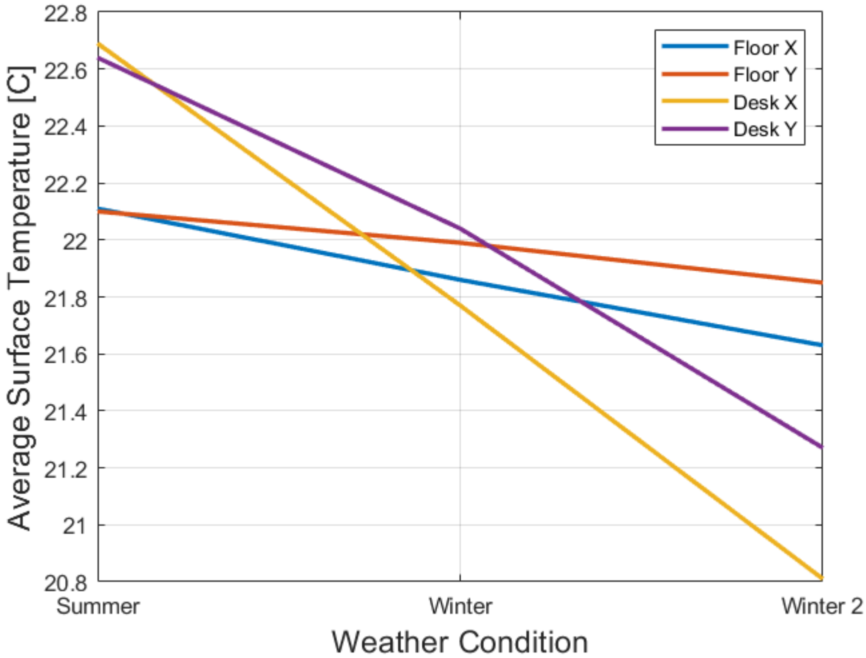

Figure 6.38: Comparison of average floor, desk and partition (combined as desk on plot) surface temperatures at opposing sides of the desk for manikin X and manikin Y for different weather conditions of summer (case 1), winter (case 11), and winter 2 (case 12).

During the summer weather cases, side of manikin X is slightly hotter when compared to the side of manikin Y, but as the outside weather temperature gets lower and convective heat transfer to the outside increases due to winds, the side of manikin X gets colder than manikin Y. Temperature of the façade and the window are the only outside walls of the office and therefore standing closer to them makes the occupants experience the outside weather more. Manikin Y is not affected from the outside weather condition as much as manikin X, because of the partition located in between them and manikin Y is further away from the façade and window.

Plume is a flow that is driven by buoyancy effects from a hot spot. Case 2 has the highest maximum floor temperature of 27.9 ℃ (seen on Table 6.10 above) in front of the window due to direct solar irradiance. That is the reason that Case 2 has been chosen the observe the plume from the hot spot on the floor. Figure 6.39 shows the plane that temperature contour on Figure 6.40 and velocity vectors on Figure 6.41 are taken.

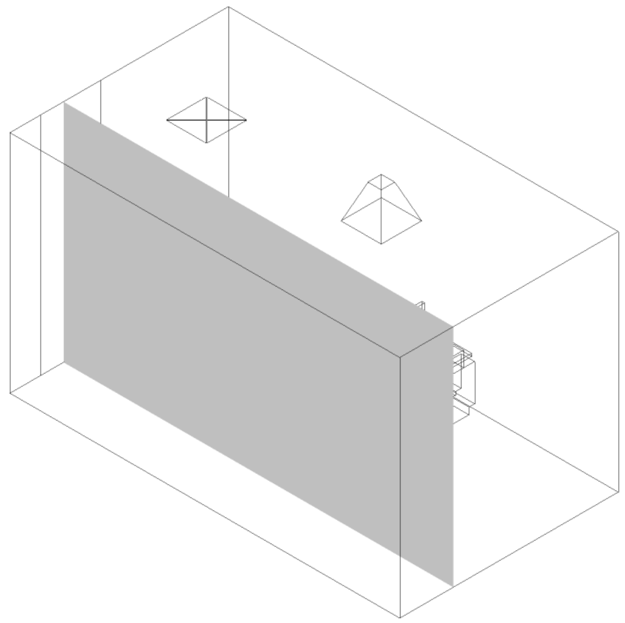

Figure 6.39: Location of the plane that cuts through the middle of the window.

On the temperature contour below (Figure 6.40) the window is to the left and the hot spot from the direct solar irradiance on the floor is to the bottom left. Since the air inside the office space is modelled as non-participating media hot flow rising from the floor is purely convective heat transfer forming a plume. This RANS model has modelled plume in average values with the SST k-ω turbulence model. LES could be used for better modelling the plume inside the office space.

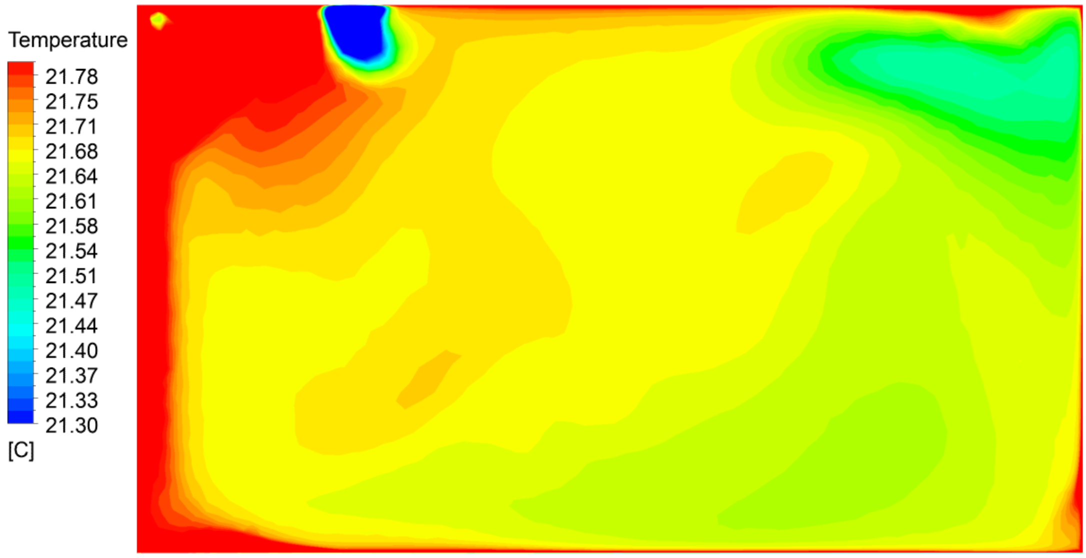

Figure 6.40: Temperature contour of case 2 on the plane that cuts through the window.

The flow driving the plume on Figure 6.40 can be seen below on the Figure 6.41 with the velocity vectors that represent the flow from floor to the ceiling near the window. This upward motion due to buoyancy effects (left side of the Figure 6.40) are balanced with the downward flow from ceiling to the floor on the opposite side of the office space (right side of the Figure 6.40). Both of these motions create a big vortex in the office space.

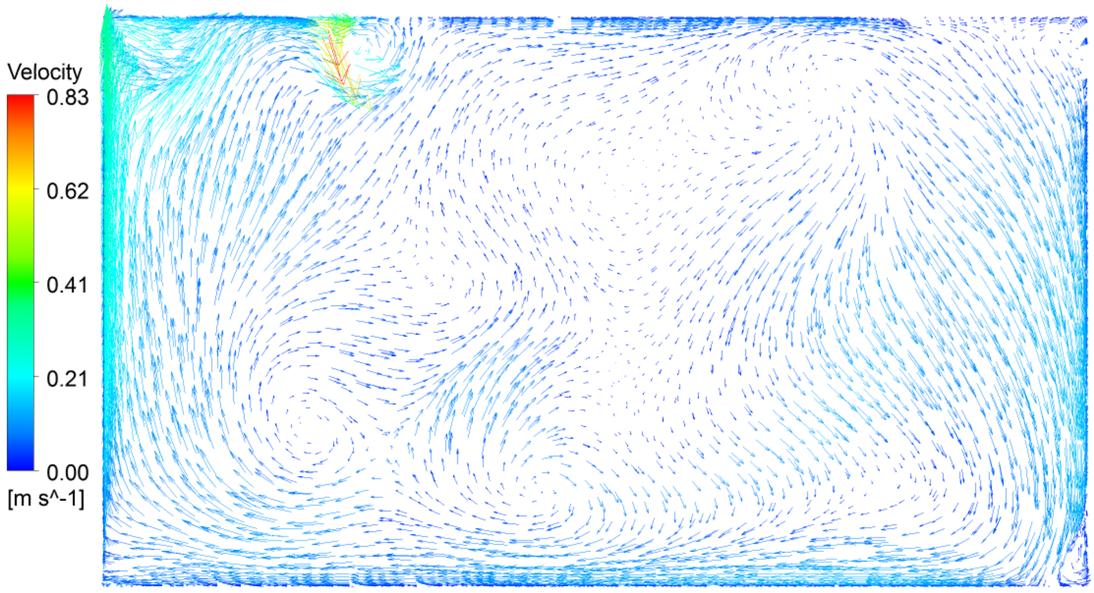

Figure 6.41: Velocity vectors of case 2 on the plane that cuts through the window.

CHAPTER VII

CONCLUDING REMARKS

7.1. Conclusion

This thesis has provided a framework for the design considerations of more energy efficient and comfortable buildings. Specifically, the focus was on the combined effects on thermal comfort of the external solar shades, various window glasses, partitions located between desks and floor materials in an office due to solar radiation. The framework was tested for several different cases. The change in geometry will require the analyses to be repeated according to their boundary conditions and geometry. These analyses can be conducted for another office space based on the details outlined.

Numerical studies have been conducted for an office at Center for Energy, Environment and Economy (CEEE) in the Academic Building 4 (AB-4) at Ozyegin University. Combined effects of components in an office space that interferes with thermal comfort of the occupants due to solar radiation are analyzed such as partitions, solar shades, window types and floor materials. Ventilation took place from a single inlet and single outlet. There was heat transfer with the surroundings just from the façade and all interior walls are assumed adiabatic. There was a single window in the office that acted as a radiation heat source by letting solar radiation in. These components are analyzed at three different weather conditions (summer, winter and extreme winter). Variations in surface temperature distribution, air temperature, air velocity and thermal comfort of average human according to the two manikins inside the office due to change of parameters are analyzed according to the Predicted Mean Vote (PMV) and Percentage of Dissatisfied (PPD) methods by Fanger [37].

Different cases and various types of external solar shades have been discussed based on the previous studies reported in the literature. Design parameters have been discussed on the chosen horizontal slat type solar shade such as thickness, width, length, gap in between slats, angle of solar shade, and zenith angle. The design was determined to be mostly affected from length of the solar shade, gap in between slats and angle of the solar shade parameters. Therefore, the design process should consider these three parameters according to the zenith angle for the desired performance from a solar shade. The design process considered the maximum possible electricity generation by blocking most of the incident solar radiation from the integrated photovoltaic panels on the solar shade slats, but the design parameters can be altered to let more sunlight in. Decreasing the length or increasing the gap in between slats in the design stage will let more sunlight in through the solar shade. Designing the system as dynamic rather than stable lets occupants to adjust the angle of the solar shade so that desired amount of sunlight can be let in. This design decision of using a dynamic system will cost more in the initial investment and will require higher maintenance, because more parts makes the system more complex, and the moving parts will require more maintenance than stable parts. However, with the freedom of controlling the amount of sunlight let in by an adjustable external solar shade system can help occupants alter their thermal and visual comfort on their desire rather than adhering to ASHRAE Standard 55 [6] or ISO Standard 7730 [63].

Window optical properties are discussed for modelling transmission of solar and ambient radiative energy to the office. The wavelength band within the 0.3-3 μm range band was used for the numerical analysis. It was shown that this range includes 94.68% of the spectral solar irradiance. Above 3 μm wavelength most of the radiation will be absorbed by the window glass as seen on the measurements by Rubin [71], therefore it is safe to say that the modeled window glass absorbs 2% less solar irradiance than it should be. The window glass types considered in the analyses are chosen to compare effects of different transmissivity, absorptivity and reflectivity fractions on numerical analysis.

Photovoltaic panels were assumed to be installed on the external solar shades to generate electricity from the solar irradiance that was blocked by the shades. The entire system of PV panels have been discussed to generate electricity and types of PV panels have been compared with their advantages and disadvantages from one another and thin-film PV panels have been decided as the best type to be mounted on an external solar shade due to lighter weight and smaller size. Electricity generation was calculated for a test case of 50 m^2 space with around 8 m^2 window area facing 45° South West in Istanbul. If the PV panels cover 40% of the window it was shown to have the potential to generate 13.9 MWh/year for a monthly adjusted system and 13.2 MWh/year for a stable system, based on the PV panels considered. This shows that monthly adjusted system provides 5.3% more electricity generation and therefore 5.3% less solar irradiance transmitting through the window into the office. Along with the freedom to operate the solar shade to desired angle to have optimum thermal and visual comfort for the occupant, being able to generate more electricity was the reason to choose the adjustable over the stable solar shade system despite using a more complex system, which will require more maintenance and potentially be less reliable.

Finally, the reason to use solar have been discussed both from the environmental and economical impact point of view. Never ending rise of CO2 emissions both in the World and in Turkey have been shown due to use of fossil fuels. In the economic side, prices of electricity and PV panels in 2021 have been compared to 2017 and found out that electricity has became about ~94% [79] more expensive in Turkey. Yet, similar PV panels and inverters became about ~24% cheaper during the same 4 years. This should have been an expected outcome since the electricity generation from solar energy is booming right now with an unpredictable speed and “every time production capacity doubles production costs are decreased by 28%” [80]. It is clear from the way the PV panel industry is headed that PV panels will be dirt cheap soon and buildings will need to be designed to contain PV panels. This will bring the problem of having small roof areas to mount PV panels and solar shade integrated designs will come up.

The summary of the numerical study is given below:

- Based on studied manikin, average human is at slightly cool thermal comfort for most of the summer cases and neutral at winter cases according to

ASHRAE Standard 55, due to slightly over ventilation. Higher inlet temperature or lower inlet velocity would change the average human’s thermal comfort level from slightly cool to neutral.

- Thermal comfort was achieved for local floor temperatures for average human according to the studied manikins at all cases. At mostly summer cases average human experienced thermal discomfort due to negative vertical temperature differences, which means higher air temperatures around their head comparing to their ankles.
- Absorptivity and emissivity of the window glass effects the air temperature slightly. Therefore, for the window types considered, they do not have direct effect air temperature since the air inside the office is a nonparticipating media.
- When there is more solar irradiance present (in summer weather) the absorptivity of the window glass plays greater role in determination of its temperature.
- Façades and window being the only walls that are in contact with the outside environment makes them effected from the weather conditions much easier than any other walls in the office. This causes them to control the temperature distribution throughout the office. Surfaces having higher view factor with the window and façade will be affected mostly via emitted radiative heat transfer and closer surfaces will also be affected via conductive and convective heat transfer. Partition has higher view factor with those surfaces than floor due to being aligned with them where floor is perpendicular to those surfaces. This causes the partition temperature to be affected more. In terms of thermal comfort especially in extreme winter case back of occupant closer to the façade is significantly colder than rest of the body due to higher view factor with the façade and the window.
- Direct solar irradiance affects the window and local floor temperatures. Only the emitted radiation from these surfaces’ effects the occupants and their thermal comfort levels. If the direct solar irradiance was incident on either of the occupants, the thermal comfort difference between the occupants would have been greater.
- Façade and window interfere with the air movement inside the office that is

initially started by the ventilation, due to natural convection between these surfaces and the air.

- Increasing solar shade coverage on the window decreased the overall temperature of the office, but it had bigger effects for the summer weather due to significantly higher direct component of the solar irradiance being blocked by the solar shade.
- Temperature distribution on the floor is more even for summer weather cases than winter weather cases. The effect of partition on the floor temperature distribution can be clearly seen on winter cases due to façade and window being significantly cooler than the rest of the office, where in summer cases temperature difference between the façade and rest of the office is smaller. This causes the surfaces to lose heat to them through thermal radiation heat transfer during winter weather.
- Ceramic tiles kept the office air and surface temperatures lower due to higher thermal conductivity of the ceramic tiles compared to carpet. This helped dissipating the heat for ceramic tiles while the carpet retaining the heat. Higher the heat flux into the office higher the difference will be in air and surface temperatures.
- Partition creates two zones with different temperature distributions, air velocities and thermal comfort levels by literally dividing the office space. These two zones can be used for the advantage, since all humans do not prefer the same thermal conditions, occupants can be seated according to their thermal comfort preferences.
- The increase of partition height to ceiling height aspect ratio influences the air flow inside the office and creates additional vortices. In other office layouts or designs these vortices might cause thermal discomfort for the air velocities above 0.2 m/s near occupants.
- The partition can also be used to create healthier office environment during the COVID-19 pandemic or another pandemic future holds, as it helps create two different zones by preventing the air around each occupant to mix.
- According to Rayleigh numbers and Gr/Re^2 ratios of critical surfaces inside the

office space there are both turbulent and laminar flow regions as well as natural and forced convection regions. This evaluation shows that utilization of SST k-w turbulence model for better modelling the turbulent flow and utilization of Boussinesq approximation and PRESTO! pressure discretization for better modelling the natural convection was necessary.

- When the parameters are compared to each other, external solar shades had the most effect on the overall temperature distributions, contrasts and thermal comfort of the occupants because it controls the amount of solar radiation in the office space, which is the main heat source in these cases. Followed by floor covering materials and window glass materials. Finally, partition had local effects rather than effecting the thermal state of the entire office space and altering the air flow inside the office space.

7.1. Future Work

This study can be carried out further with following studies:

- Visual comfort can be studied numerically for the same cases to analyze combined thermal and visual comfort effects of the same parameters.
- Effect of various wall colors on thermal and visual comfort can be studied.
- Semi-transparent partitions can be studied as they are currently being used in indoor spaces due to the COVID-19 pandemic.

BIBLIOGRAPHY

[1] Buildings, International Energy Agency. [Online]. Available: https://www.iea.org/topics/buildings. [Accessed: 2020].

[2] A. Baïri, A. Martín-garín, K. Adeyeye, K. She, and J. A. Millán-garcía, “Enhancement of natural convection for improvement of Trombe wall performance. An experimental study,” Energy Build., vol. 211, no. 109788, 2020, doi: 10.1016/j.enbuild.2020.109788.

[3] “T.C. Enerji ve Tabii Kaynaklar Bakanlığı - Elektrik,” 2019. [Online]. Available: https://www.enerji.gov.tr/tr-TR/Sayfalar/Elektrik. [Accessed: 2020].

[4] SOLARGIS Global Horizontal Irradiance Map. [Online]. Available: https://solargis.com/maps-and-gis-data/download/world. [Accessed: 2019].

[5] SOLARGIS Turkey Horizontal Irradiance Map. [Online]. Available: https://solargis.com/maps-and-gis-data/download/turkey. [Accessed: 2019].

[6] Thermal Environmental Conditions for Human Occupancy, ASHRAE Standard 55, 2017.

[7] J. R. Howell, M. P. Mengüç, K. Daun and R. Siegel, Thermal Radiation Heat Transfer. 7th edition, CRC Press, 2021.

[8] F. A. Dominguez Espinosa and L. R. Glicksman, “Effect of furniture and partitions on the surface temperatures in an office under forced flow,” Energy Build., vol. 147, pp. 155–165, 2017, doi: 10.1016/j.enbuild.2017.04.067.

[9] M. Cavazzuti and M. A. Corticelli, “An algorithm for solving steady-state heat conduction in arbitrarily complex composite planar walls with temperature-dependent thermal conductivities,” Appl. Therm. Eng., vol. 115, pp. 825–831, 2017, doi: 10.1016/j.applthermaleng.2017.01.030.

[10] E. Sartori, “Convection coefficient equations for forced air flow over flat surfaces,” Sol. Energy, vol. 80, no. 9, pp. 1063–1071, 2006, doi: 10.1016/j.solener.2005.11.001.

[11] P. B. Vincent, “CFD Modeling for Thermal Comfort in an Open Workspace,” in eSim 2018, 2018, pp. 276–285.

[12] B. Moreno and J. A. Hernández, “Analytical solutions to evaluate solar radiation overheating in simplified glazed rooms,” Build. Environ., vol. 140, pp. 162–172, 2018, doi: 10.1016/j.buildenv.2018.05.037.

[13] S. J. Rees and P. Haves, “An experimental study of air flow and temperature distribution in a room with displacement ventilation and a chilled ceiling,” Build. Environ., vol. 59, pp. 358–368, 2013, doi: 10.1016/j.buildenv.2012.09.001.

[14] V. Vitale and G. Salerno, “A numerical prediction of the passive cooling effects on thermal comfort for a historical building in Rome,” Energy Build., vol. 157, pp. 1–10, 2017, doi: 10.1016/j.enbuild.2017.06.049.

[15] T. Karimipanah, H. B. Awbi, M. Sandberg, and C. Blomqvist, “Investigation of air quality, comfort parameters and effectiveness for two floor-level air supply systems in classrooms,” Build. Environ., vol. 42, no. 2, pp. 647–655, 2005, doi: 10.1016/j.buildenv.2005.10.016.

[16] S. G. Martyushev and M. A. Sheremet, “Conjugate natural convection combined with surface thermal radiation in a three-dimensional enclosure with a heat source,” Int. J. Heat Mass Transf., vol. 73, pp. 340–353, 2014, doi: 10.1016/j.ijheatmasstransfer.2014.02.009.

[17] M. F. Modest, “A general model for the calculation of daylighting in interior spaces,” Energy Build., vol. 5, no. 1, pp. 69–79, 1982, doi: 10.1016/0378-7788(82)90030-5.

[18] M. Parmananda, A. Dalal, and G. Natarajan, “The influence of partitions on predicting heat transfer due to the combined effects of convection and thermal

radiation in cubical enclosures," Int. J. Heat Mass Transf., vol. 121, pp. 1179–1200, 2018, doi: 10.1016/j.ijheatmasstransfer.2018.01.031.

[19] M. W. Nansteel and R. Greif, "Natural Confection in Undivided and Partially Divided Rectangular Enclosures," J. Heat Transfer, vol. 103, no. November 1981, pp. 623–629, 1981.

[20] D. A. Olson, L. R. Glicksman, and H. M. Ferm, "Steady-state natural convection in empty and partitioned enclosures at high rayleigh numbers," J. Heat Transfer, vol. 112, no. 3, pp. 640–647, 1990, doi: 10.1115/1.2910435.

[21] L. Bellia, C. Marino, F. Minichiello, and A. Pedace, "An overview on solar shading systems for buildings," Energy Procedia, vol. 62, pp. 309–317, 2014, doi: 10.1016/j.egypro.2014.12.392.

[22] M. David, M. Donn, F. Garde, and A. Lenoir, "Assessment of the thermal and visual ef fi ciency of solar shades," Build. Environ., vol. 46, no. 7, pp. 1489–1496, 2011, doi: 10.1016/j.buildenv.2011.01.022.

[23] N. Khamporn and S. Chaiyapinunt, "Effect of installing a venetian blind to a glass window on human thermal comfort," Build. Environ., vol. 82, pp. 713–725, 2014, doi: 10.1016/j.buildenv.2014.10.022.

[24] G. Kim, H. Soo, T. Sub, L. Schaefer, and J. Tai, "Comparative advantage of an exterior shading device in thermal performance for residential buildings," Energy Build., vol. 46, pp. 105–111, 2012, doi: 10.1016/j.enbuild.2011.10.040.

[25] L. Sun, L. Lu, and H. Yang, "Optimum design of shading-type building-integrated photovoltaic claddings with different surface azimuth angles," Appl. Energy, vol. 90, no. 1, pp. 233–240, 2012, doi: 10.1016/j.apenergy.2011.01.062.

[26] M. Arici and H. Karabay, "Determination of optimum thickness of double-glazed windows for the climatic regions of Turkey," Energy Build., vol. 42, no. 10, pp. 1773–1778, Oct. 2010, doi: 10.1016/j.enbuild.2010.05.013.

[27] Á. Moreno, D. Chemisana, R. Vaillon, A. Riverola, and A. Solans, “Energy and luminous performance investigation of an OPV/ETFE glazing element for building integration,” Energies, vol. 12, no. 10, 2019, doi: 10.3390/en12101870.

[28] J. Xamán, J. Arce, G. Álvarez, and Y. Chávez, “Laminar and turbulent natural convection combined with surface thermal radiation in a square cavity with a glass wall,” Int. J. Therm. Sci., vol. 47, pp. 1630–1638, 2008, doi: 10.1016/j.ijthermalsci.2008.01.012.

[29] Y. Olazo-Gómez, J. Xamán, M. Gijón-Rivera, F. Noh-Pat, E. Simá, and Y. Chávez, “Mathematical modelling of conjugate laminar and turbulent heat transfer in a cavity: Effect of a vertical glazed wall,” Int. J. Therm. Sci., vol. 152, no. August 2019, 2020, doi: 10.1016/j.ijthermalsci.2020.106310.

[30] A. Heltzel, T. Mann, and J. R. Howell, “Metamaterial window glass,” J. Therm. Sci. Eng. Appl., vol. 10, no. 5, pp. 1–6, 2018, doi: 10.1115/1.4039921.

[31] E. S. Lee and A. Tavil, “Energy and visual comfort performance of electrochromic windows with overhangs,” *Build. Environ.*, vol. 42, no. 6, pp. 2439–2449, 2007, doi: 10.1016/j.buildenv.2006.04.016.

[32] E. Roumpakias, O. Zogou, and A. Stamatelos, “Correlation of actual efficiency of photovoltaic panels with air mass,” Renew. Energy, vol. 74, pp. 70–77, 2015, doi: 10.1016/j.renene.2014.07.051.

[33] G. Gan and S. B. Riffat, “CFD modelling of air flow and thermal performance of an atrium integrated with photovoltaics,” Build. Environ., vol. 39, no. 7, pp. 735–748, 2004, doi: 10.1016/j.buildenv.2004.01.027.

[35] E. Halawa, J. Van Hoof, and V. Soebarto, “The impacts of the thermal radiation field on thermal comfort, energy consumption and control - A critical overview,” Renew. Sustain. Energy Rev., vol. 37, pp. 907–918, 2014, doi: 10.1016/j.rser.2014.05.040.

[34] C. Peng, Y. Huang, and Z. Wu, “Building-integrated photovoltaics (BIPV) in architectural design in China,” *Energy Build.*, vol. 43, no. 12, pp. 3592–3598, 2011, doi: 10.1016/j.enbuild.2011.09.032.

[36] H. Zhang, R. Yang, S. You, W. Zheng, X. Zheng, and T. Ye, “The CPMV index for evaluating indoor thermal comfort in buildings with solar radiation,” Build. Environ., vol. 134, no. February, pp. 1–9, 2018, doi: 10.1016/j.buildenv.2018.02.037.

[37] P. O. Fanger, Thermal comfort: analysis and applications in environmental engineering. Malabar, FL: Krieger, 1970.

[38] M. Bessoudo, A. Tzempelikos, A. K. Athienitis, and R. Zmeureanu, “Indoor thermal environmental conditions near glazed facades with shading devices - Part I: Experiments and building thermal model,” Build. Environ., vol. 45, no. 11, pp. 2506–2516, 2010, doi: 10.1016/j.buildenv.2010.05.013.

[39] C. Buratti, D. Palladino, and E. Moretti, “Prediction of Indoor Conditions and Thermal Comfort Using CFD Simulations: A Case Study Based on Experimental Data,” Energy Procedia, vol. 126, pp. 115–122, 2017, doi: 10.1016/j.egypro.2017.08.130.

[40] M. Hajdukiewicz, M. Geron, and M. M. Keane, “Calibrated CFD simulation to evaluate thermal comfort in a highly-glazed naturally ventilated room,” Build. Environ., vol. 70, pp. 73–89, 2013, doi: 10.1016/j.buildenv.2013.08.020.

[41] C. Marino, A. Nucara, and M. Pietrafesa, “Mapping of the indoor comfort conditions considering the effect of solar radiation,” Sol. Energy, vol. 113, pp. 63–77, 2015, doi: 10.1016/j.solener.2014.12.020.

[42] G. Cannistraro, M. Cannistraro, and R. Restivo, “Some observations on the radiative exchanges influence on thermal comfort in rectangular open-space environments,” Int. J. Heat Technol., vol. 33, no. 2, pp. 79–84, 2015, doi: 10.18280/ijht.330213.

[43] A. Tzempelikos, M. Bessoudo, A. K. Athienitis, and R. Zmeureanu, “Indoor thermal environmental conditions near glazed facades with shading devices - Part II: Thermal comfort simulation and impact of glazing and shading properties,” Build. Environ., vol. 45, no. 11, pp. 2517–2525, 2010, doi: 10.1016/j.buildenv.2010.05.014.

[44] M. S. Alwetaishi, “Impact of Building Function on Thermal Comfort: A Review Paper,” American Journal of Engineering and Applied Sciences, vol. 9 (4), pp. 928-945, 2016, doi: 10.3844/ajeassp.2016.928.945.

[45] C. Keskin, “Augmenting Occupant Thermal Experience with Cyber-Physical-Social Systems: A Case-Study on Adaptive Vents,” PhD Thesis, Department of Mechanical Engineering, Özyeğin University, Istanbul, Turkey, 2020.

[46] C. Keskin, M. P. Mengüç, “On Occupant Behavior and Innovation Studies Towards High Performance Buildings: A Transdisciplinary Approach,” *Sustainability*, Vol. 10(10), p. 3567, 2018.

[47] C. Keskin and M. P. Mengüç, ‘An Adaptive Vent System for Localized and Customized Thermal Management in Buildings,’ *ASME Journal of Heat Transfer*, DOI: 10.1115/1.4045664, 2020.

[48] S. Carlucci, F. Causone, F. De Rosa, and L. Pagliano, “A review of indices for assessing visual comfort with a view to their use in optimization processes to support building integrated design,” Renew. Sustain. Energy Rev., vol. 47, no. 7491, pp. 1016–1033, 2015, doi: 10.1016/j.rser.2015.03.062.

[49] A. Nabil and J. Mardaljevic, “Useful daylight illuminances: A replacement for daylight factors,” Energy Build., vol. 38, no. 7, pp. 905–913, 2006, doi: 10.1016/j.enbuild.2006.03.013.

[50] P. Bakmohammadi and E. Noorzai, “Optimization of the design of the primary school classrooms in terms of energy and daylight performance considering occupants’ thermal and visual comfort,” Energy Reports, vol. 6, pp. 1590–1607, 2020, doi: 10.1016/j.egyr.2020.06.008.

[51] Y. Li, M. Sandberg, and L. Fuchs, "Vertical Temperature Profiles in Rooms Ventilated by Displacement: Full-Scale Measurement and Nodal Modelling," Indoor Air, vol. 2, no. 4, pp. 225–243, 1992, doi: 10.1111/j.1600-0668.1992.00005.x.

[52] S. Gilani, H. Montazeri, and B. Blocken, "CFD simulation of stratified indoor environment in displacement ventilation: Validation and sensitivity analysis," Build. Environ., vol. 95, pp. 299–313, 2016, doi: 10.1016/j.buildenv.2015.09.010.

[53] J. Khalesi, N. Goudarzi, "Thermal comfort investigation of stratified indoor environment in displacement ventilation: Climate-adaptive building with smart windows," Sustain. Cities Soc., vol. 46, no. September 2018, 2019, doi: 10.1016/j.scs.2018.11.029.

[54] N. Martinho, A. Lopes, and M. Gameiro da Silva, "Evaluation of errors on the CFD computation of air flow and heat transfer around the human body," Build. Environ., vol. 58, pp. 58–69, 2012, doi: 10.1016/j.buildenv.2012.06.018.

[55] D. N. Sørensen and L. K. Voigt, "Modelling flow and heat transfer around a seated human body by computational fluid dynamics," Build. Environ., vol. 38, no. 6, pp. 753–762, 2003, doi: 10.1016/S0360-1323(03)00027-1.

[56] A. Y. Çengel and A. J. Ghajar, Heat and Mass Transfer: Fundamentals and Applications, Fifth Edit. New York: McGraw-Hill Education, 2003.

[57] Fluent Theory Guide, 19.2, ANSYS Inc., Canonsburg, Pennsylvania, 2019.

[58] Azimuth & Altitude: The Horizontal Coordinate System. [Online]. Available: https://www.timeanddate.com/astronomy/horizontal-coordinate-system.html. [Accessed: 2020].

[59] Bjarne Siewertsen, 2006, Danish Meteorological Institute [Online]. Available: https://campingoutinamerica.com/2011/06/22/a-different-kind-of-day/. [Accessed: 2020].

[60] Fluent User Guide, 19.2, ANSYS Inc., Canonsburg, Pennsylvania, 2019.

[61] R. B. Farrington, J. P. Rugh, and G. D. Barber, "SAE TECHNICAL Effect of Solar-Reflective Glazing on Fuel Economy , Tailpipe Emissions , and Thermal Comfort," SAE Tech. Pap., vol. 2000-01–26, 2000.

[62] P. Wolkoff and S. K. Kjærgaard, "The dichotomy of relative humidity on indoor air quality," Environ. Int., vol. 33, no. 6, pp. 850–857, 2007, doi: 10.1016/j.envint.2007.04.004.

[63] Ergonomics of the thermal environment – Analytical determination and interpretation of thermal comfort using calculation of the PMV and PPD indices and local thermal comfort criteria, ISO Standard 7730, 2005.

[64] J. P. Varughese and M. M. John, "Effect of emissivity of shading device and air flow inside cavity of Double Skin Facade for energy saving and Thermal Comfort in buildings: A CFD modeling," 2016 Int. Conf. Energy Effic. Technol. Sustain. ICEETS 2016, pp. 815–820, 2016, doi: 10.1109/ICEETS.2016.7583859.

[65] Kepenk. [Online]. Available: https://www.teverahsap.com/wp-content/uploads/2016/08/kepenk01.jpg. [Accessed: 2020].

[66] Aerobrise Sun Louvres External Aluminum Louvers for Building Façade. [Online]. Available: : https://image.made-in-china.com/2f0j00iNhQAGIWqEut/Aerobrise-Sun-Louvres-External-Aluminum-Louvers-for-Building-Facade.jpg. [Accessed: 2020].

[67] [Online]. Available: https://img.archiexpo.com/images_ae/photo-g/50763-14497927.jpg. [Accessed: 2020].

[68] A new type of overhangs. [Online]. Available: https://www.researchgate.net/profile/Chin_Haw_Lim/publication/277307488/figure/fig4/AS:667643178659844@1536189946437/A-new-types-of-overhangs-4-4-Fixed-louvers-Fixed-louvers-are-useful-for-any-exposure-of_Q320.jpg. [Accessed: 2020].

[69] [Online].
Available: https://i.pinimg.com/originals/8c/48/7c/8c487c1cbeb4aa795a43d83ea7183cd6.jpg. [Accessed: 2020].

[70] S. L. Chang and K. T. Rhee, "Blackbody Radiation Functions," Int. Commun. Heat Mass Transf., vol. 11, pp. 451–455, 1984.

[71] M. Rubin, "Optical properties of soda lime silica glasses," Sol. Energy Mater., vol. 12, no. 4, pp. 275–288, 1985, doi: 10.1016/0165-1633(85)90052-8.

[72] The best flexible solar panels in 2019 – The ultimate guide. [Online]. Available: https://www.reliablecounter.com/blog/the-best-flexible-solar-panels-in-2019-the-ultimate-guide/. [Accessed: 2020].

[73] H. J. D'cruz, K. Baskaran, and V. Geetha, "Implementation of Incremental Conductance Algorithm in Dual Axis Solar Tracker for Maximum Solar Panel Output," J. Basic Appl. Eng. Res., vol. 1, no. 11, pp. 39–44, 2014.

[74] C. G. Popovici, S. V. Hudişteanu, T. D. Mateescu, and N. C. Cherecheş, "Efficiency Improvement of Photovoltaic Panels by Using Air Cooled Heat Sinks," Energy Procedia, vol. 85, no. November 2015, pp. 425–432, 2016, doi: 10.1016/j.egypro.2015.12.223.

[75] Types of solar panels, 2020, EnergySage. [Online]. Available: https://www.energysage.com/solar/101/types-solar-panels/#:~:text=There%20are%20three%20major%20types,property%20and%20desired%20system%20characteristics. [Accessed: 2020].

[76] Solar Electricity Handbook, 2019, Greenstream Publishing. [Online]. Available: http://www.solarelectricityhandbook.com/solar-irradiance.html. [Accessed: 2020].

[77] Electricity consumption per capita, Turkey 1990-2019, International Energy Agency. [Online]. Available: https://www.iea.org/data-and-

statistics?country=TURKEY&fuel=Energy%20consumption&indicator=ElecConsPerCapita. [Accessed: 2021].

[78] A. C. Yelekci, İ. Elmas, and P. M. Mengüç, "Project Title : Design of a Building Integrated PV System and Solar Shade System," Ozyegin University, 2017.

[79] Elektrik Tarifeleri, 2021, TEDAŞ. [Online]. Available: https://www.tedas.gov.tr/#!tedas_tarifeler. [Accessed: 2021].

[80] E R. Kurmelovs, "'Insanely cheap energy': how solar power continues to shock the world", *The Guardian*, April 24, 2021. [Online]. Available: https://www.theguardian.com/australia-news/2021/apr/25/insanely-cheap-energy-how-solar-power-continues-to-shock-the-world?utm_term=52bcff799a6c687e50d1d445a01d9883&utm_campaign=GreenLight&utm_source=esp&utm_medium=Email&CMP=greenlight_email. [Accessed May 2, 2021].

[81] Annual CO2 emissions, Global Carbon Project: Carbon Dioxide Information Analysis Centre (CDIAC). [Online]. Available: https://www.ourworldindata.org/co2-and-other-greenhouse-gas-emissions/. [Accessed: 2021].

[82] Ansys SPEOS Design and Validation of Optical Systems, ANSYS [Online]. Available: https://www.ansys.com/products/optics-vr/ansys-speos. [Accessed: 2021].

[83] Average Weather in Istanbul, Weather Spark. [Online]. Available: https://weatherspark.com/y/95434/Average-Weather-in-%C4%B0stanbul-Turkey-Year-Round. [Accessed: 2020].

[84] M. Wang and Q. Chen, "Assessment of various turbulence models for transitional flows in an enclosed environment" HVAC&R Research, vol. 15, pp. 1099-1119, 2009.

[85] Y. Sun and T. F. Smith, “Air flow characteristics of a room with square cone diffusers,” Build. Environ., vol. 40, no. 5, pp. 589–600, 2005, doi: 10.1016/j.buildenv.2004.07.018.

[86] R. J. de Dear, E. Arens, Z. Hui, M. Oguro, “Convective and radiative heat transfer coeffcients for individual human body segments,” International Journal of Biometeorology, vol. 40, pp. 141-156, 1997.

[87] S. Mcneil, T. Bulletin, and N. Zealand, “The Thermal Properties of Wool Carpets,” 2016.

[88] W.A. King, (2010). U.S. Patent No. WO2010132452A2. Washington, DC: U.S. Patent and Trademark Office.

[89] Annual Weather Averages Near Istanbul. [Online]. Available: https://www.timeanddate.com/weather/turkey/istanbul/climate. [Accessed: 2020].

[90] V. P. Adhikari, A. Nassar, and Q. H. Nagpurwala, “Numerical Studies on the Effect of Cooling Vent Setting and Solar Radiation on Air Flow and Temperature Distribution in a Passenger Car,” SAE Tech. Pap., vol. 2009-December, 2009, doi: 10.4271/2009-28-0048.

[91] Ansys SpaceClaim, ANSYS [Online]. Available: https://www.ansys.com/products/3d-design/ansys-spaceclaim. [Accessed: 2021].

[92] CBE Thermal Comfort Tool, Berkeley, University of California, 2020. [Online]. Available: https://comfort.cbe.berkeley.edu/. [Accessed: 2020].

APPENDIX A

MATLAB SCRIPTS

MATLAB Script for Figure 4.2:

Spectral irradiance vs wavelength plot for blackbody at 5780 K was plotted with the MATLAB script below using the Equation 40 by Chang and Rhee [70].

```
C1 = 0.595522e08;
C2 = 14388;
n = 1;

lambda = linspace(0,100,100000);
T = 5780;
x = [0.3 3];

I =
(2*pi.*C1)./((n.^2).*(lambda.^5).*(exp((C2)./(n.*T.*lambd
a))-1))/pi;
plot(lambda,I,'LineWidth',2)
hold on;

for i = 1:2
    plot([x(i) x(i)],[1e-01
(2*pi.*C1)./((n.^2).*(x(i).^5).*(exp((C2)./(n.*T.*x(i)))-
1))/pi],'LineWidth',1)
end

hold off
xlim([0 5])
ylim([0 2.75e07])
xticks([0 0.3 3])
xlabel('Wavelength [\mum]','FontSize',14)
ylabel('Spectral Irradiance [W/m^2 sr
\mum]','FontSize',14)
legend('T = 5780 K')
set(gca,'FontSize',12)
```

MATLAB Script for Table 4.1:

MATLAB script below calculates the fraction of spectral irradiance using the Equation 40 by Chang and Rhee [70].

```
syms m

% Variables
C2 = 14388;
T = 5780;

% Fractions
lambda1 = 0;
z1 = C2/(lambda1*T);
F1 = symsum((exp(-
m.*z1)./m).*((z1.^3)+((3.*z1.^2)./m)+((6.*z1)./(m^2))+(6.
/(m^3))),1,inf);
F1 = (F1.*15)./(pi.^4);

lambda2 = 0.3;
z2 = C2/(lambda2*T);
F2 = symsum((exp(-
m.*z2)./m).*((z2.^3)+((3.*z2.^2)./m)+((6.*z2)./(m^2))+(6.
/(m^3))),1,inf);
F2 = (F2.*15)./(pi.^4);

lambda3 = 3;
z3 = C2/(lambda3*T);
F3 = symsum((exp(-
m.*z3)./m).*((z3.^3)+((3.*z3.^2)./m)+((6.*z3)./(m^2))+(6.
/(m^3))),1,inf);
F3 = (F3.*15)./(pi.^4);

z4 = 0;
F4 = symsum((exp(-
m.*z4)./m).*((z4.^3)+((3.*z4.^2)./m)+((6.*z4)./(m^2))+(6.
/(m^3))),1,inf);
F4 = (F4.*15)./(pi.^4);

% Band fractions
F_uv = double(F2 - F1);
F_solar = double(F3 - F2);
F_ir = double(F4 - F3);
```

VITA

Ali Can Yelekci received his B.Sc. and his M.Sc. degrees in Mechanical Engineering from Ozyegin University in 2017 and 2021, respectively. He has attended EuroSun 2020 conference in Athens, Greece as a presenter with “Numerical Analysis of Solar Radiation Effects at indoors with Internal Partitions and External Solar Shades” paper. He is currently employed by Kale Ar-Ge (R&D) at Tuzla, Istanbul as thermal and secondary air systems engineer for development of turbojet engines. His research interest are thermal radiation in buildings and turbomachinery.